1.3μm Single-mode extended cavity GaInNAs/GaAs lasers produced using a sputtered SiO_2 quantum well intermixing technique

by John Lee Harris

Thesis submitted for the degree of
Doctor of Philosophy
to the
Department of Electronic and Electrical Engineering
Faculty of engineering
University of Glasgow
October 2005.

Abstract

The research presented in this thesis describes the realisation of single-mode extended cavity GaInNAs/GaAs lasers. The GaInNAs/GaAs material system has gained much attention recently, and has been cited as a possible replacement to the InGaAsP/InP material system due to its greater high temperature performance, which can lead to improved device efficiency and higher output power. Incorporating an extended cavity to an active laser device using selective area quantum well intermixing (QWI) can be extremely advantageous, since mirror degradation and modal instabilities at high output powers can be suppressed.

Characterisation of the GaInNAs/GaAs material used in this project was performed by fabricating oxide stripe lasers. Analysis of the lasers yielded a value of $720A/cm^2$ for the threshold current density of a device with an infinitely long cavity. Values for internal efficiency and loss were also calculated to be 62.5% and $18cm^{-1}$ respectively. Although the value for $J_{th}\infty = 720A/cm^2$ is almost twice the value for $J_{th}\infty$ of similar GaInNAs material reported by the same growers, it would prove sufficient in demonstrating the concept of the project.

The successful demonstration of QWI on GaInNAs/GaAs material was achieved using the sputtered SiO_2 intermixing technique. A differential wavelength shift of 40nm was achieved, which would prove sufficient for monolithically integrating extended cavities with GaInNAs laser devices.

Single-mode extended cavity GaInNAs lasers were realised using the sputtered SiO_2 QWI process. Only a small increase in the threshold current was measured between the extended cavity device and a standard device. From the change in the threshold current, the modal loss in the extended cavity section was calculated to be $5cm^{-1}$, indicating successful integration of the extended cavity.

Acknowledgments

There are so many people I would like to thank that it is hard to know where to begin. First of all, I would like to thank Catrina Bryce and John Marsh for their enormous support and guidance during the course of this PhD project. I'd also like to thank Olek Kowalski, as well as his alter ego "The Beast", for their immense help and advice during the project.

I would also like to thank the technical staff for their assistance and friendship, especially the cleanroom staff – Linda, Margaret, Eve, Mark and Tam. Special thanks go to the guys in dry etch – Colin Roberts and Ronnie "Depp" Rodgers.

I would like to express my gratitude to the Engineering and Physical Sciences Research Council (EPSRC) and Intense Ltd for the financial support during the project.

A huge thanks goes to all "the dudes" who kept me away from insanity, and sobriety, for the duration of the PhD project: Corrie Farmer, Iain "The Don" Eddie, Grant "The Rant" Erwin, Wei Kiong Tan, Dave Moran, the lads in AirSpiel, and the flatmates from hell, Andrew Thomson, Greig "The Ginger Pest" Anderson and the psychedelic funkster Dave Siedlecki.

Finally, I would like to send a massive thanks to my parents for their constant encouragement and support, and for putting a roof over my head during the past year.

I'd also like to thank David and Mags for their support and PhD advice, and Neil for his generosity and banter.

Last, but by no means least, I'd like to thank Zoe for her love and support. Your encouragement and support was instrumental in the completion of this project, and for that I am eternally grateful. I take my hat off to you for putting up with me over the years. You have the patience of a saint.

Publications

J.L.Harris, A.C.Bryce, O.P.Kowalski, J.H.Marsh, T.Jouhti, M.Pessa and M.Hopkinson, "Selective quantum well intermixing of 1.22 and 1.55μm GaInNAs laser material", *CLEO 2004 Conference Proceedings.*

J.L.Harris, A.C.Bryce, O.P.Kowalski and J.H.Marsh "1.3μm single-mode extended cavity GaInNAs lasers produced using a sputtered SiO_2 quantum well intermixing technique", *International Symposium on Compound Semiconductors (ISCS 2005) conference proceedings. Also to be published in Physica Status Solidi (c).*

J.L.Harris, A.C.Bryce, O.P.Kowalski and J.H.Marsh "Monothically integrated extended cavity GaInNAs lasers produced by quantum well intermixing", *Currently in production for IEEE Photonics Technology Letters.*

Contents

Chapter 1

Introduction

Semiconductor lasers have advanced tremendously since they were first demonstrated in the 1960's, and have been incorporated into our everyday life in applications ranging from CD players to medical apparatus. Due to the diversity of the lasers applications and uses, lasers have been designed and manufactured to be application specific, and therefore a great understanding of laser design, material and technology has been acquired. Nevertheless, significant improvements still need to be made to optoelectronic technology in terms of device integration. Optoelectronic integration technology is nowhere near as advanced as electronic integration technology, which allows millions of electronic components to be fabricated on a single chip. By enabling monolithic integration of many optoelectronic devices on a single chip, optoelectronic technology can reap similar benefits to that of integrated electronic technology, such as lower cost and size, with increased performance, functionality and manufacturability. Quantum well intermixing (QWI) has been recognised as a key technology in realising optoelectronic device integration, as it allows post-growth selective modification of the material bandgap. QWI has been researched extensively at Glasgow University for around the past 20 years, and has resulted in the development of a technique that is suitable for optoelectronic integration using III-V semiconductor materials.

The market for semiconductor lasers has grown rapidly from 1995 to 2005, with the largest share of the market belonging to communications, due to the mass-consumer embrace of the internet. Within the communication laser market, high power lasers have become very sought after since they enable dramatic cost reduction and performance enhancements in communication systems. High power lasers emitting light around 1.3μm or 1.55μm can be used as light sources for low-loss fibre communication systems, as well as optical amplifier pump lasers. However, such devices have several limiting factors when operating at high powers, namely mirror degradation, mode instabilities and overheating. Much of the research presently conducted into high power lasers involves overcoming these limiting factors.

At present, most of the lasers employed in communication systems are fabricated from the InGaAsP/InP material system. However, the poor temperature characteristics of this material limit the amount of power the devices can produce. Furthermore, such devices usually require thermoelectric coolers during operation, which increases the cost and size of the packaging. Recently, the GaInNAs/GaAs material system has gained much attention, and has been cited as a possible replacement to the InGaAsP/InP material system due to its greater high temperature performance, which can lead to improved device efficiency and higher output power.

This thesis describes the research and development of single-mode extended cavity GaInNAs/GaAs ridge waveguide lasers for use in telecommunication systems. Incorporating an extended cavity to an active laser device using selective area QWI can be extremely advantageous, since mirror degradation and modal instabilities at high output powers can be suppressed. By developing such devices, a good

knowledge of the intermixing characteristics of the GaInNAs/GaAs material can also be gained, which is particularly useful information for device integration purposes. A summary of the following thesis chapters is given below.

Chapter 2 – The GaInNAs material system

A brief history of the GaInNAs/GaAs material system is outlined in this chapter, along with the possible advantages offered by using the GaInNAs/GaAs material instead of InGaAsP/InP material. A detailed examination of the growth and optical properties of the GaInNAs material is also given. Characterisation of the GaInNAs material is performed by investigating the performance of GaInNAs oxide stripe lasers.

Chapter 3 – Quantum Well Intermixing

This chapter gives a detailed description of Quantum Well Intermixing (QWI), and outlines the various methods used to achieve QWI, as well as the advantages and disadvantages of each method. A detailed account of the sputtered SiO_2 intermixing technique used in this research is also presented, as well as an in depth account of the intermixing experiments conducted on 1.3μm and 1.55μm GaInNAs material.

Chapter 4 – Single Mode Ridge Waveguide Lasers

An overview of ridge waveguide laser technology is presented in this chapter, with an emphasis on the design considerations required for single mode operation. A detailed account of the fabrication and characterisation of single-mode ridge waveguide laser

devices is also given. The concepts outlined in this chapter, can be combined with the technology described in Chapter 3 to realise the devices detailed in Chapter 5.

Chapter 5 – Extended Cavity GaInNAs ridge waveguide lasers

This chapter describes the concept of single-mode extended cavity lasers, highlighting the advantages such devices have over their standard counterparts. Furthermore, a detailed account of the limitations of standard high power lasers operating in a single mode is presented in order to emphasize the importance of extended cavity laser technology. The fabrication and characterisation of extended cavity GaInNAs lasers is also detailed, highlighting the potential of using such lasers for future telecom applications, as well as emphasizing the transferability of the QWI process developed at Glasgow University to the GaInNAs material system.

Chapter 6 – Conclusions and Future Work

Chapter 6 brings the conclusion to the research and also outlines possible future work.

This research was a collaborative project with Intense Ltd. Intense is an optoelectronic solutions provider working with customers in the printing, telecoms and defence market sectors. Intense owns core intellectual property concerning optoelectronic integration and quantum well intermixing.

Chapter 2

The GaInNAs material system

2.1 Introduction

Long wavelength semiconductor lasers emitting light at 1.3μm and 1.55μm are highly desirable for use as light sources in optical fibre communication systems. Moreover, high power semiconductor lasers (>500mW) at slightly shorter wavelengths of 1.24μm and 1.45μm are highly desirable as pump lasers for the optical amplifiers to be used in dense-wavelength division multiplexing architectures. The material system InGaAsP/InP is currently used for such applications, but the limitations of this material are well documented. The aim of this chapter is to introduce GaInNAs as a possible alternative material system, since it has a greater high temperature performance, which can lead to improved device efficiency and higher output power. Section 2.2 will discuss the brief history of GaInNAs, outlining its origin and basic advantages over the InGaAsP material system. The epitaxial growth of GaInNAs will be discussed in section 2.3, before examining the spectral properties of this material in section 2.4. The progress of GaInNAs edge-emitting lasers will be discussed in section 2.5 before taking a look at how this new material will provide a means of improving long-wavelength VCSEL's in section 2.6. GaInNAs lasers are characterised and evaluated in section 2.7. Section 2.8 will conclude the chapter.

2.2 History of GaInNAs

Most long wavelength semiconductor lasers presently employed in fibre communication systems are based on the InGaAsP material system. However, as explained in chapter 1, the limitations of this material system are well known. The inability of InGaAsP to produce adequate power and temperature performance has led to an opening for GaInNAs as an alternative active-region material that can be grown on GaAs.

The GaInNAs material system was first proposed in 1996 by Kondow et al (1). This proposal was far from obvious since it did not follow the general rules of other III-V ternary and quaternary alloys, which dictate that a smaller lattice constant increases the bandgap. Kondow proposed that the large electro-negativity of N and its small covalent radius would cause a strong negative bowing parameter. Therefore, by adding N to GaAs or InGaAs, the bandgap of the resulting crystal would dramatically decrease. By combining N and In, GaInNAs would produce a rapid decrease in bandgap to reach the long wavelength emission region with simultaneous control over the bandgap and lattice match to GaAs. Kondow also pointed out that by combining GaInNAs with GaAs or other wide-gap materials that can be grown on a GaAs substrate, a type-I band lineup is achieved and thus deep quantum wells can be grown, especially in the conduction band. Figure 2.1 shows the energy band line-up between GaAs and GaInNAs. The diagram also features the energy band line-up for the InGaAsP material. Comparison of the two band diagrams clearly shows that the well created in the conduction band for the nitride material is much deeper than for InGaAsP. Since carrier leakage from the GaInNAs wells to the barrier layers at high

temperature can be suppressed, the material is highly desirable for overcoming the poor temperature characteristics of conventional long wavelength laser diodes used for optical fibre communication systems.

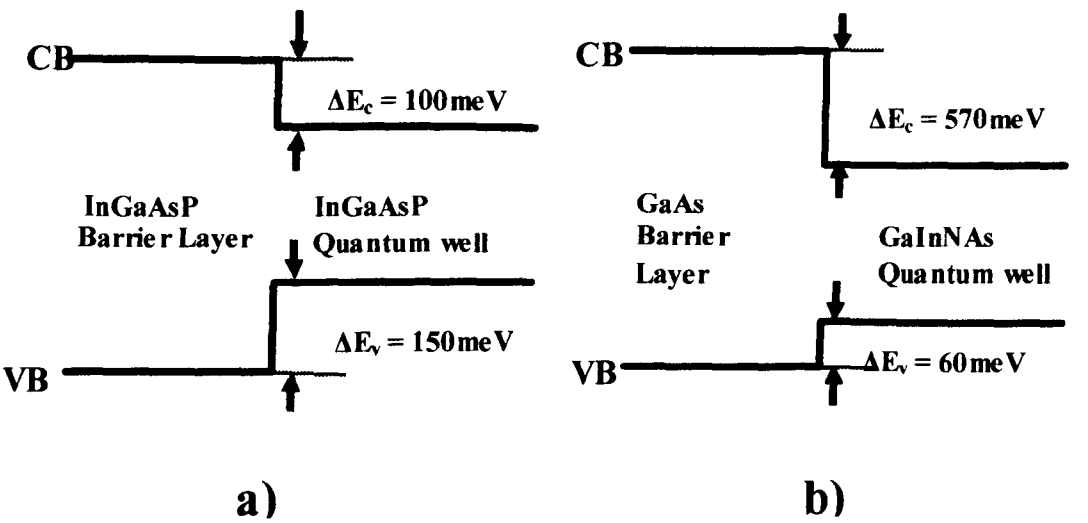

Figure 2.1: Diagrams presenting the energy bands of materials in the 1.3μm wavelength range. (a) diagram of the band lineup between a $In_{0.1}Ga_{0.9}As_{0.2}P_{0.8}$/ $In_{0.3}Ga_{0.7}As_{0.6}P_{0.4}$ barrier/ well. (b) band lineup between a GaAs/ $Ga_{0.7}In_{0.3}As_{0.99}N_{0.01}$ barrier/ well.

A schematic cross section of the first GaInNAs material structure grown by Kondow's group is shown in Figure 2.2. The material was grown by gas-source molecular beam epitaxy (GS-MBE) on a (100)-oriented n-GaAs substrate. The active layer consisted of a 7-nm-thick $Ga_{0.7}In_{0.3}N_{0.004}As_{0.996}$ compressively strained quantum well sandwiched between two 140-nm-thick GaAs unstrained waveguide layers. The cladding layers were each 1.4μm $Al_{0.3}Ga_{0.7}As$ with a carrier density of 7×10^{17} cm^{-3}. A p-GaAs contact layer with a carrier density 1×10^{19} cm^{-3} was formed to decrease the contact resistance.

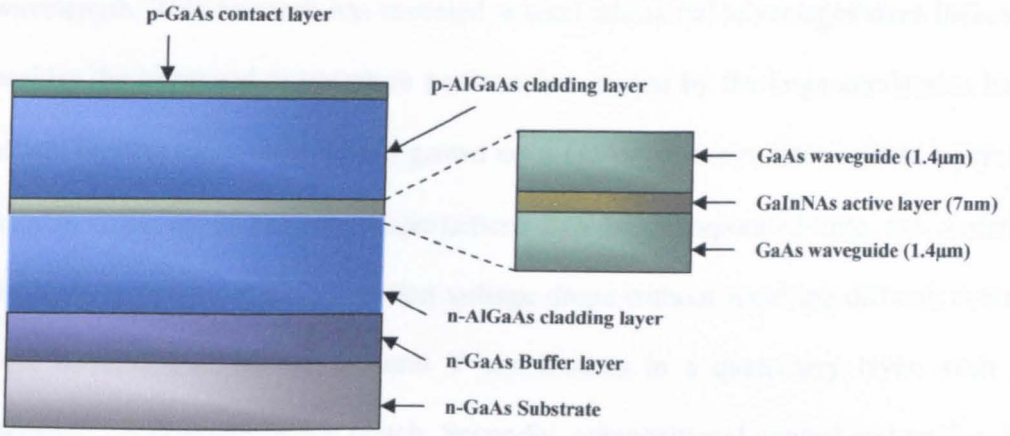

Figure 2.2: Schematic cross section of GaInNAs material grown by Kondow et al in 1995

To demonstrate the potential of the material, Kondow fabricated oxide stripe lasers and VCSEL's from GaInNAs grown from gas-source MBE. A threshold current density J_{th}= 1.4kA/cm^2 (1) was obtained from an oxide stripe laser which had a cavity length and stripe width of 1000μm and 20μm respectively. This value was four times as large as that for a similar InGaAs laser diode. This poor value was blamed on insufficient crystallinity in the GaInNAs active layer. The emission wavelength of this device at 1.1I_{th} was measured as ~1.18μm. Kondow claimed that by adding more N, the emission wavelength could be pushed out beyond 1.3μm. In VCSEL's, the group successfully obtained lasing action under RT CW conditions by photo-pumping with a low threshold pump intensity and a lasing wavelength of 1.22μm, thus demonstrating that long wavelength VCSEL's can be directly integrated with high contrast DBR's in a single epitaxial growth (1).

Since 1996, many research groups worldwide have embarked upon realising the full potential of GaInNAs. Initially, many devices were fabricated in order to establish optimum growth parameters such as growth temperature, *in-situ* annealing and alloy composition, in order to lower threshold current densities and increase emission

wavelength. This research has revealed several additional advantages over InGaAsP besides the improved temperature performance caused by the large conduction band offset. Firstly, since GaInNAs is grown on a GaAs substrate, intermediate layers of $Al_{(x)}Ga_{(1-x)}As$ or AlAs/GaAs superlattices can be incorporated into the material structure to minimise heterojunction voltage drops without requiring difficult control over both column III and column V constituents in a quaternary layer, such as InGaAsP, to maintain lattice match. Secondly, compositional control and uniformity during the growth of GaInNAs is relatively easy compared to As/P control during the growth of InGaAsP (2,3), which will provide better yield and lower production costs. Thirdly, GaInNAs VCSEL's can incorporate the well developed GaAs/AlAs mirror technology as well as AlAs oxidation layers for current and optical aperture confinement, whilst maintaining lattice match. Fourthly, GaInNAs on GaAs can be monolithically integrated with GaAs high-speed electronics, which is essential for low cost, high-speed integrated electrical drivers for direct laser modulation in high speed networks (2).

2.3 Epitaxial Growth of GaInNAs

The growth of GaInNAs is presently performed by either molecular beam epitaxy (MBE), or metal organic chemical vapour deposition (MOCVD). Much research has been conducted to find which growth technique can be used to produce the best quality material with the lowest costs.

To date, MOCVD has been the dominant growth technique for communication lasers. This is because valved P crackers did not exist during the early development of InP based material systems, which meant early attempts to grow this material by MBE were dangerous due to the fire hazard caused when the system was opened and exposed to air. MOCVD had the chemical precursors and growth parameter control to grow InP based material, therefore it became the dominant growth technique.

However, to form GaInNAs from its constituent alloys, InGaN and InGaAs, the growth temperature has to be much lower (typically between 450 and 500^0C) than for the growth of other quaternary material systems. This is due to the basic structure of InGaN and InGaAs. InGaN is a hexagonal (wurtzite) crystal, which is normally grown at relatively high temperatures, whereas InGaAs has a cubic (Zincblende) structure grown at relatively low temperatures, hence creating a miscibility gap in the alloys (4-6). This means that if either or both N and growth temperature are increased, phase segregation can occur which breaks the material up into microscopic regions of InGaN and InGaAs. This low growth temperature requirement makes growth by MOCVD far more challenging. MOCVD growth of InGaN, for example, uses ammonia as a nitrogen source. Since InGaN is grown at a relatively high temperature, reasonable cracking of ammonia can occur, hence providing N during the growth process. However, when growing GaInNAs, the growth temperature is too low to achieve the same cracking of ammonia and arsine. New N sources with difficult precursor reactions and highly non-linear incorporation ratios are therefore required, which adds to the complication of the growth process in relation to work on earlier III-V material growth. Using higher growth temperatures limit the amount of N which can be incorporated into the alloy before micro-phase segregation occurs, which

makes it difficult to achieve the N compositions needed to reach the 1.3-1.55μm lasing wavelengths.

GaInNAs has also been grown using elemental-source MBE. This process has proven to be very versatile by allowing growth at lower temperatures and giving the largest range of In and N compositions. Research carried out using MBE to grow GaInNAs has shown that the atomic sticking coefficient is near unity (4,5), which implies that the group-III growth rate controls the N concentration and N/As fraction in the film. This control is critical because it governs both bandgap and lattice constant. Moreover, background impurities in GaInNAs material grown by MBE are very low compared to the same material grown by gas-source MBE or MOCVD, because of the high purity of all the starting source elements (4). These findings indicate that using elemental-source MBE to grow GaInNAs may have advantages over MOCVD in terms of yield, growth control and reproducibility (7).

2.4 Spectral Properties of GaInNAs

Increasing the wavelength of GaInNAs has proven to be one of the greatest challenges facing the development of this material system. Since a low temperature is required during the growth of GaInNAs, many defects are generated in the material. Positron annihilation, deep level transient spectroscopy (DLTS), and the comparison of MBE and MOCVD growth have revealed a large number of N interstitials and gallium vacancies are created during the low temperature growth of GaInNAs. The most detailed study of defects in GaInNAs has been performed by Ptak et al (7) at the

National Renewable Energy Laboratory. The group studies revealed that hydrogen and carbon impurities, as well as gallium vacancies, are introduced during MOCVD growth of GaInNAs. Although the impurities and vacancies have a detrimental effect on material quality, they were found not to be the limiting defect within the material. DLTS measurements highlighted a shallow electron trap and a deep recombination centre, which appear to become more active with increased N incorporation, as possible limiting defects. However, the structures of these defects are still unknown, and much work remains to see if they can be removed.

An annealing step is normally employed to improve the quality of the material by reducing the number of non-radiative defects (9). The increase in PL of the material due to the annealing step is unfortunately accompanied by a significantly large blue shift, thus creating difficulty in reaching the wavelengths required for fibre communications whilst maintaining a high optical quality material.

At first, the simultaneous increase in PL intensity and blue shift was thought to be caused by the same microscopic process, which occurred during annealing, but has since been strongly debated. Evidence suggests that the increase in the PL intensity could purely be a consequence of the removal of non-radiative defects. However, the origin of the blue shift has been shown to possibly originate from two entirely different processes. Firstly, Ga/In/N interdiffusion induced by thermal annealing raises the quantum-confined energies in the quantum well, thus creating a blue shift in emission wavelength. The level of interdiffusion occurring has been measured by SIMS and nuclear reaction analysis measurements (4), and suggest nitrogen out-diffusion from the QW is primarily responsible for the shift. Secondly, the blue shift

may also be caused by a change in the band configuration in the local atomic clusters. It has been found that GaInNAs is not perfectly random and is supposed to contain N-centred N-In_zGa_{4-z} ($0 \leq z \leq 4$) clusters, therefore GaInNAs is not controlled by the macroscopic compositions x and y. Kim et al (8) suggested that the bandgap variation is due to a repulsion mechanism between the five energy levels of N-In_zGa_{4-z} and the alloy conduction band, which results in five different bandgaps for GaInNAs. The strength of interaction between the energy levels is increased as z is decreased. With a large z, N has mostly indium as its nearest neighbour, which is favourable for reducing local strain. When z is small, N has gallium as its predominant neighbour, which lowers cohesive bond energy. Minimising the sum of strain and bond energies gives a preferred bond configuration. Other researchers have found no diffusion in their X-ray analysis of GaInNAs and therefore attribute the blue shift solely to changes in the bond configuration (9).

2.4.1 N-Incorporation

In 1996, Kondow demonstrated the first GaInNAs lasers with an emission wavelength of 1.18μm. He claimed that by increasing the N concentration, the GaInNAs emission wavelength could be pushed out to 1.3μm and beyond. However, research has since shown that introducing more N degrades the optical properties of the material due to N related non-radiative defects (11). This is often referred to as the "nitrogen penalty", which limits the amount of N that can be incorporated into the material and thus limits the increase in emission wavelength.

In addition to the degradation in the spectral properties experienced by GaInNAs with increased N incorporation, research has also found an increase in temperature sensitivity (10). The cause of such behaviour has been attributed to the disappearance of the hole barriers with high N concentration (N> 3%).

To obtain good device quality $Ga_{1-x}\ In_x\ N_y\ As_{1-y}$ material, it has been suggested that a minimum amount of N ($y \approx 0.02$) should be introduced since larger amounts can induce large alloy fluctuations, as well as significantly reducing material gain (11). Also, by adding more indium to the alloy, compressive strain in the quantum well can be maximised in order to obtain a maximum quantum well width. However using a small amount of N in a straight-forward GaInNAs/GaAs quantum well structure will not be able to reach the longer fibre communications wavelength of 1.55μm.

2.4.2 Strain compensating layers

A novel approach to overcoming the wavelength limit imposed on a simple GaInNAs/GaAs structure with a small amount of N is to embed the quantum well in a

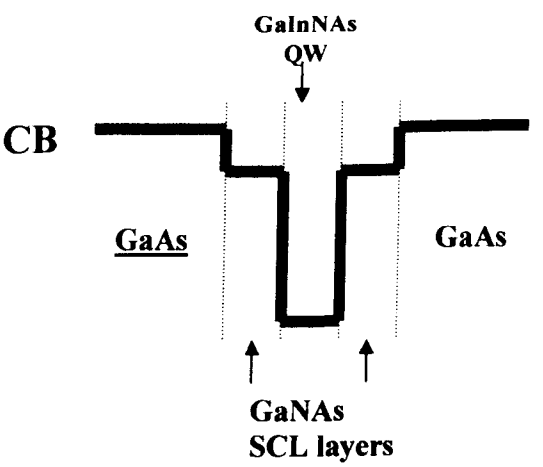

Figure 2.3: Schematic diagram of the conduction band minimum energy for GaInNAs materi GaNAs strain compensation layers.

GaNAs strain-compensating layer (SCL) or GaInNAs strain-mediating layer (SML) (12,13,14). Figure 2.3 shows the schematic diagram for the conduction band of GaInNAs material employing SCL's. These layers provide a strain compensated couple of the quantum well/barrier pair since the barrier is under tensile strain while the quantum well is under compressive strain. Strain compensation allows the growth of wider quantum wells before strain relaxation occurs, hence increasing the emission wavelength (11). The PL measured from samples employing SCL or SML layers to increase the emission wavelength has been shown not to suffer much, in comparison to the PL measured from samples that have had N added in an attempt to increase the emission wavelength. Having barriers containing N may also have the effect of decreasing the out-diffusion of N from the quantum wells during the anneal step, which helps to reduce the resulting blue shift. Furthermore, barriers containing N have the effect of decreasing the ratio $\Delta Ec/\Delta Ev$, therefore increasing the hole barrier ΔEv, which in turn reduces hole leakage and decreases the temperature sensitivity of the material.

2.4.3 GaInNAs(Sb)

A recent advance in the growth of GaInNAs, which helped increase the emission wavelength, is the addition of Sb during growth (15,16). Initially, Sb was thought only to act as a surfactant, helping to maintain the 2D layer-by-layer growth of the material with higher In and N concentrations, producing better quantum wells with smoother interfaces, as well as increasing the emission wavelength by postponing the 2D-to-3D growth. This increases the critical thickness of the quantum wells, thus allowing the growth of wider quantum wells. More recent work has shown that Sb is

actually being incorporated at levels of 6-7%, thus forming a pentenary alloy GaInNAsSb. The role Sb plays in increasing the emission wavelength is still not obvious. The addition of Sb to the alloy may simply decrease the bandgap, but it has been noticed it also helps increase the N incorporation into the alloy. While the exact mechanism for this phenomena is not clear, it is clear that alloying Sb with GaInNAs is beneficial for increasing emission wavelength, as well as improving device performance.

2.5 High Power GaInNAs edge emitting lasers

The need for low cost 1.3-1.55μm pump sources to operate at high temperature and produce high single-mode output powers has been the motivation for investigating new edge emitting laser. Livshits et al (17) were first to demonstrate high power 1.3μm GaInNAs lasers by achieving 8W (CW) from a 100 x 2000μm^2 broad area device operating at a chip temperature of 10^{0}C. As well as the encouraging output power, the lasers displayed no sign of catastrophic optical mirror damage (COMD) at a facet power density of 30mW/cm^2. Furthermore, lifetime tests carried out showed no degradation in the lasers performance over 1000 hours at a constant power of 1.5W, and a temperature of 35^{0}C.

Lowering the threshold current density and temperature sensitivity of GaInNAs is also important in the development of high power lasers. Since 1996, the threshold current density for GaInNAs devices has decreased quite considerably, with Infineon reporting one of the lowest values of J_{th} = 350 A/cm^2 (6). On the other hand, high

temperature characteristics (T_0) of GaInNAs have not shown a similar improvement with results no better than they were several years ago. It would seem that T_0 is not very high whatsoever for device quality GaInNAs. The temperature properties of 1.3μm GaInNAs were studied by Tansu and Mawst(10). He found T_0 was 80K – 140K for nitride lasers. While this value for T_0 is considerably better than InGaAsP/InP ($T_0 \approx$ 65 - 75K), it is still much less than T_0 for 1.2μm $Ga_{0.6}In_{0.4}As/GaAs$ quantum well lasers ($T_0 \approx$ 160 –200K). The reason given for the difference in T_0 in the two materials was that the injection efficiency was more temperature sensitive for GaInNAs, most probably due to the small ΔE_v , which would lead to hole leakage at elevated temperatures. However, as mentioned in section 2.4.2, the temperature sensitivity may be decreased by adding a small amount of N to the barrier layers in the active region, thus decreasing the ratio ΔEc/ΔEv. Although taking such action may increase carrier confinement in the valence band well, it will decrease carrier capture in the conduction band well. Studies will have to be performed to find the optimum ratio ΔEc/ΔEv, in order to establish a lowest threshold current density with the highest T_0. Furthermore, by adding a small amount of Sb into the GaInNAs quantum well, an increase in ΔE_v can be obtained, which would also improve T_0. It is interesting to note at this point that the Infineon group incorporated N into the barrier layers for their low threshold current density devices. Once all of the technologies mentioned have been optimised, the challenge will be to use them simultaneously to realise a truly low threshold current, high power edge-emitting laser. If this challenge can be achieved, there is a strong possibility that GaInNAs edge-emitting lasers will replace existing InP based lasers in 1.3μm short-haul communication systems.

2.5.1 Beyond 1.3μm

In order for such lasers to be appropriate for C-band Raman pumps or non-linear optical sources in channel switching, the emission wavelength must be extended beyond 1.4μm. A Raman amplifier pumped at 1.45μm will likely become a complement, or even a replacement to Er doped fibre amplifiers (EDFA's) in applications where amplifiers are far apart, provided Raman power is high enough (>20dBm). However, as discussed in section 2.4.1, increasing the wavelength of GaInNAs to 1.45μm without sacrificing optical quality is not possible by alloying more N, or by embedding the quantum wells in SCL or SML layers. Results suggest that the upper wavelength limit for antimony-free GaInNAs is approximately 1.39μm, beyond which the material will degrade too much to be of use. The research group at Stanford have obtained the best results for 1.4μm GaInNAs high power lasers by achieving 320mW of output power from a 20 x 560μm^2 device under pulsed operation conditions (18). However, the device had a high threshold current density, J_{th} = 2.1kA/cm^2, as well as a strong temperature dependence, which suggests that GaInNAs lasers beyond 1.4μm may never be a feasible alternative to InGaAsP/InP. The only plausible way of reaching the spectral range 1.4 – 1.6μm with reasonable performance characteristics may be to add Sb to GaInNAs.

Fischer et al (19) were the first to report GaInNAs lasers working at 1.5μm. This result proved lasing could be obtained in nitride material above 1.4μm, however, the threshold current density was extremely high at 50kA/cm^2. The increase in the wavelength was achieved by incorporating ~5% N into the quantum wells, this was

apparently difficult to achieve without causing micro-phase segregation and dislocations at the quantum well interfaces. As alloying more than 2% N composition in the QW is not considered beneficial to its spectral properties, adding Sb to the quantum well and N to the GaAs barrier layers is considered the most competent way of increasing the emission wavelength. Both of these technologies have been combined by the team at Stanford (20) to initially produce GaInNAsSb lasers emitting at 1.46μm, and most recently at 1.5μm. In 2002, they produced ridge waveguide lasers with 5μm x 800μm ridges from material containing three GaInNAsSb quantum wells with GaNAsSb barriers. The threshold current density obtained was 2.8kA/cm^2, which is certainly the lowest recorded threshold current density for nitride based lasers beyond 1.4μm yet this value is twice as high as the group's best 1.39μm devices. The slope efficiencies for 1.46μm devices were also twice as poor as the 1.39μm devices. However, by improving their active layer growth techniques and device structure optimisation, they were able to produce 1.5μm lasers with a threshold current density of 1.06kA/cm^2, a T_0 value of 101K and 527mW of output power (pulsed) from a single facet. For these devices, GaNAs barriers were employed instead of GaNAsSb barriers because of the superior low temperature growth morphology, strain compensation and improved electron confinement.

These results show that GaInNAsSb may indeed become a serious competitor to InP based lasers in the 1.4 –1.6μm spectral range. However, GaInNAs is a relatively new material system, which still has a long distance to go before its performance is optimised. Improvements in growth techniques, coupled with optimised laser design, have led to large improvements in device performance to date.

2.6 GaInNAs Vertical Cavity Surface Emitting Lasers (VCSEL's)

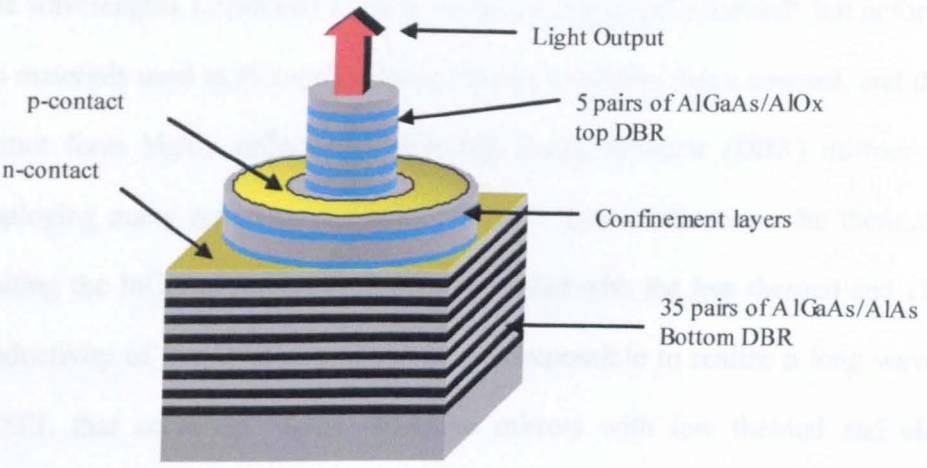

Figure 2.4: Schematic diagram of a 850nm VCSEL fabricated for research at Glasgow University. Diagram provided by I.Eddie

Although work in this project primarily deals with edge-emitting lasers, it would be inappropriate not to mention vertical cavity surface emitting lasers (VCSEL's) role in the development of the GaInNAs active layer technology. To aid in this discussion, figure 2.4 shows a cross sectional diagram of an 850nm VCSEL. GaAs based VCSELS's dominate the high performance, short-haul communications and optical networking market. The reason for VCSEL's dominance in this market is due to their low cost, ability to be easily coupled to fibre and uncomplicated fabrication of large arrays. Because of material limitations, VCSEL's have only been utilised fully at 850nm and 980nm. Operating at this wavelength limits system performance due to the dispersion and loss experienced by the signal in silica fibres. Furthermore, by using such a short wavelength, the optical power has to be kept below the power limit for eye safety regulations. To create the next generation of high-bandwidth metro

communication systems, long wavelength VCSEL's, which can be directly modulated, operated un-cooled and fabricated at low cost will be required.

The wavelengths 1.3μm and 1.55μm are accessible to InGaAsP/InP, but unfortunately the materials used in this system have limited refractive index contrast, and therefore cannot form highly reflective distributed Bragg reflector (DBR) mirrors without employing many repetitions of thick material layers. Moreover, the thermal issues limiting the InGaAsP/InP active region, coupled with the low thermal and electrical conductivity of the DBR's, make it almost impossible to realize a long wavelength VCSEL that combines highly reflective mirrors with low thermal and electrical resistance. VCSEL technology is where the GaInNAs material system will have a huge advantage over the InP based material systems. Many attempts have been made to produce VCSEL's using the InGaAsP/InP active region but with different approaches to DBR's, such as using metal mirrors, wafer-bonded AlAs/GaAs mirrors and dielectric mirrors (2). In spite of these attempts, the devices lacked the quality needed for their desired purpose. However, since the arrival of the GaInNAs/GaAs quantum well material, using this material in the active region in conjunction with the well-established DBR technology used by GaAs-based 850nm VCSEL's, seemed to provide the desired results. Improvement of GaInNAs VCSEL's follows the trend of improvement for GaInNAs edge-emitting lasers (11). This can be attributed to the improved growth techniques and optimisation of device design.

2.7 Semiconductor Laser Model

Before discussing the characterisation of the fabricated GaInNAs devices in section 2.9, it is worthwhile reviewing the theory of semiconductor lasers. The main components of a semiconductor laser diode are shown in figure 2.5. The laser diode is basically a p-i-n formation where carriers from the p and n-type regions are injected into the intrinsic quantum well region, where radiative recombination of electron/hole pairs produce photons. Light produced in the quantum well is channelled in the waveguide. Upper and lower cladding layers of lower refractive index surround the active region thus ensuring the formation of the waveguide. Two partially reflecting mirrors create feedback for the system whilst allowing some light to emit from the facets as laser output. The optical mode in the waveguide interacts with the gain region, enabling stimulated emission of radiation. The modal gain is determined by the gain of the quantum well and the overlap of the mode with the quantum well. The optical mode travels backwards and forwards along the length of the cavity during lasing. The gain provided by the quantum well to the optical mode is offset by the

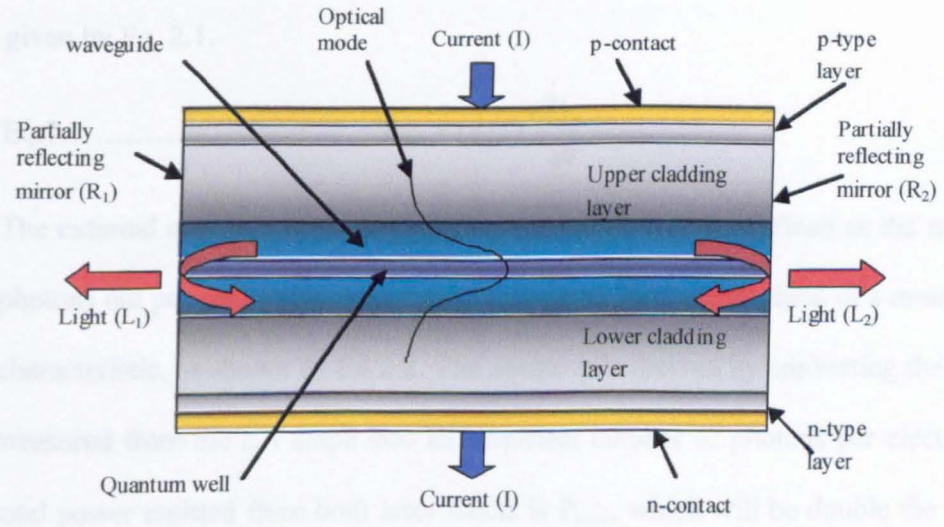

Figure 2.5: Side view schematic diagram of a simple semiconductor laser

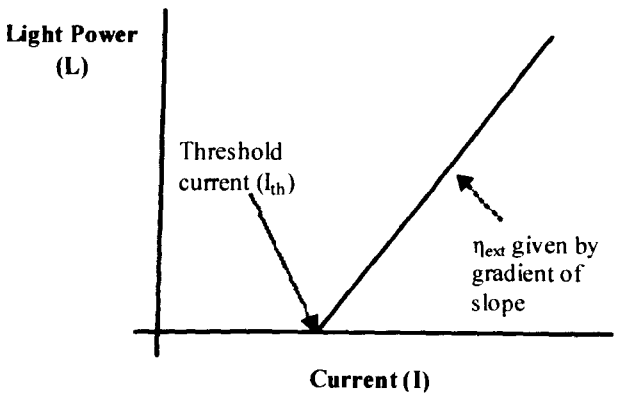

Figure 2.6: Diagram showing a typical L-I characteristic of a laser.

modal and mirror losses in the cavity. Figure 2.6 shows an illustration of a typical laser diode light-current (L-I) feature. As current injection is increased, the gain of the quantum well increases, until a point is reached where the losses are in equilibrium with laser gain. This point is known as the threshold current (I_{th}). An increase in current beyond the threshold current will result in laser emission.

By assuming the L-I plot is linear after threshold, the light power per facet (P_{out}) is given by Eq. 2.1.

Eq.2.1..... $$P_{out} = (I-I_{th})\frac{dP_{facet}}{dI}$$

The external quantum efficiency (η_{ext}) for a laser device is defined as the number of photons out per electron in, and can be calculated from the gradient of a measured L-I characteristic, as shown by Eq 2.2. The equation is derived by converting the gradient measured from the L-I slope into an empirical number of photons per electron. The total power emitted from both laser facets is P_{total}, which will be double the value of P_{out} if we assume both mirrors have the same reflectivity. In Eq 2.2. q is the electronic

charge, h is Planck's constant, v is the frequency of emitted light, which can be calculated from the speed of light, c, and the light wavelength, λ.

Eq 2.2..... $\eta_{ext} = \frac{emitted\ photons}{injected\ electrons} = \frac{q}{h\nu} \cdot \frac{dP_{total}}{dI} = 2.\frac{q\lambda}{hc} \cdot \frac{dP_{facet}}{dI}$

As light propagates through a distance (L) inside the cavity, it will be attenuated exponentially by the loss factor (α) of the material. Electrically pumping the device will amplify the light by a nominal gain factor (g). If P_2 is the light power after propagating a distance L inside the cavity, and P_1 is the initial value for light power, P_2 can be written in terms of P_1 as shown in Eq 2.3.

Eq 2.3..... $P_2 = P_1.\exp.(g-\alpha)L$

When the laser threshold is reached, the gain must be equal to the mode and mirror losses. By including the power reflectivity for both cavity mirrors, R_1 and R_2, the modal gain at threshold (g_{th}) can be obtained, as shown by Eq 2.4.

Eq.2.4..... $g_{th} = \alpha + \frac{1}{2L}.\ln\left(\frac{1}{R_1R_2}\right)$

The internal quantum efficiency (η_{int}) is another important consideration in laser analysis, and is defined as the ratio of photons created in the quantum well per electron injected. This gives a good indication of how well the material converts current into light internally. The light generated internally will suffer modal and mirror losses before being emitted. The mirror losses are related to the light output,

thus the ratio of mirror loss upon total loss gives the fraction of photons that can be emitted. This implies the external quantum efficiency can be expressed by Eq 2.5.

Eq 2.5 .... $$\eta_{ext} = \eta_{int} \cdot \frac{mirror\,loss}{total\,loss} = \eta_{int} \cdot \frac{1/2L \ln\left(1/R_1R_2\right)}{\alpha + 1/2L \ln\left(1/R_1R_2\right)}$$

By rearranging Eq 2.5, we can obtain Eq 2.6. From Eq 2.6, it is apparent that by plotting a graph of $1/\eta_{ext}$ as a function of laser length (l) will produce a straight line which allows us to estimate values for η_{int} and α from the intercept and gradient respectively.

Eq 2.6..... $$\frac{1}{\eta_{ext}} = \frac{1}{\eta_{int}} + \frac{2\alpha}{\eta_{int} \ln\left(1/R_1R_2\right)}.L$$

The calculation method commonly used to evaluate the threshold current density for a quantum well structure was based on research by McIlroy et al (21). The threshold current density (J_{th}) can be determined by relating the gain produced per quantum well to the current density per quantum well. If a multiple quantum well structure has n_w wells, each with gain G_w, experiencing a modal overlap Γ_w per well, the modal gain can be given by Eq 2.7

Eq 2.7..... $$g = n\Gamma_w G$$

The gain produced by a single quantum well as a function of applied current density can be approximated by Eq 2.8, assuming that the injected current density is split equally among the quantum wells. G_0 and J_0 are the values of gain and current density respectively, obtained from a graph of gain per QW (G_w) as a function of threshold

current density per well (J_w) at the point which the ratio G_w/J_w is maximised, hence I_{th} is minimised.

Eq 2.8..... $$G_w = G_0\left[\ln\left(\frac{J_w}{J_0}\right)+1\right]$$

By substituting Eq 2.7 and 2.8 into Eq 2.4, and rearranging, Eq 2.9 can be attained for $\ln(J_{th})$:

Eq 2.9.... $$\ln(J_{th}) = \frac{1}{L}\left[\frac{1}{2n_w\Gamma_w G_0}\ln\left(\frac{1}{R_1R_2}\right)\right]+\left[\frac{\alpha}{n_w\Gamma_w G_0}+\ln\left(\frac{n_w J_0}{\eta_{int}}\right)\right]$$

The threshold current density for an infinitely long cavity ($J_{th\infty}$) gives us important information about the material quality since it is free from mirror losses, and also from variations in facet reflectivity. By rewriting Eq 2.9 as Eq 2.10, $J_{th\infty}$ can be extracted from the intercept of the plot of $\ln(J_{th})$ as a function of inverse length.

Eq 2.10 ..... $$\ln(J_{th}) = \frac{1}{L}\left[\frac{1}{2n_w\Gamma_w G_0}\ln\left(\frac{1}{R_1R_2}\right)\right]+\ln(J_\infty)$$

2.8 GaInNAs Material Design

In view of the fact that this project was to investigate the application of selective quantum well intermixing (QWI) to the GaInNAs material system, a wafer had to be obtained which not only intermixed reasonably, but also had good lasing

characteristics. A wafer that met both of the mentioned criteria was obtained from Tampere Optoelectronic Research Centre in Finland. The layer-by-layer structure of the material is shown in Table 2.1.

Material	**Thickness**	**Layer description**
P^+ - GaAs	200nm	Contact layer
P – $Al_{0.6}GaAs$	1500nm	p- cladding
i- GaAs	176nm	Undoped waveguide
GaInNAs	6nm	Quantum well
i- GaAs	176nm	Undoped waveguide
n- $Al_{0.6}GaAs$	1500nm	n- cladding
n- GaAs	200nm	Buffer layer
n- GaAs	~	Substrate

Table 2.1: Structure of GaInNAs/GaAs material used during the project

The laser structure was grown by MBE on an n-type GaAs (001) substrate. Gallium, indium and aluminium were supplied from standard Knudsen-type effusion furnaces. Arsenic (As^2) was supplied from a solid-source valved arsenic cracker whilst N was produced from a radio-frequency N plasma source. The layer growth was monitored by reflection high-energy electron diffraction (RHEED). The GaInNAs quantum well was grown at 460^0C.

The material was grown following a lengthy period of maintenance of the MBE system. The wafer was one of the first grown after the maintenance and was, as admitted by the growers, far from perfect, as more system calibration tests were needed. However, due to project time constraints, the wafer was sent in the hope that it would be good enough to prove the concept of the project.

On receiving the material, some simple annealing tests and photoluminescence (PL) measurements were performed to see if the optical quality of the material could be improved upon, and also to saturate any associated blueshift of the peak emission wavelength (see section 2.4). However, very little improvement was observed in the PL intensity for samples annealed over a range of temperatures, and for different lengths of time. It was therefore concluded that the active region of the material had been suitably annealed *in-situ* during the high temperature growth (680^0C) of the p-cladding AlGaAs layer.

2.9 GaInNAs Laser Results

Simple oxide stripe lasers were fabricated to assess the material quality and performance. The analysis of the laser devices was performed using the theory featured in section 2.7. To test the lasers, a pulsed test setup featuring a box-car averaging system was used. An Avtech pulsed current source generating 400ns pulses at a 1kHz repetition rate was used to supply current to the devices, which were mounted in a gold plated clip. Light was collected from one laser facet by a Germanium detector. The system was controlled by a PC running the Labview program. Light-current (L-I) characteristics were obtained from a number of devices of different cavity length. Figure 2.7 shows a typical L-I curve measured from a 1000μm x 75μm GaInNAs oxide stripe laser device. The data provided by the L-I measurements were used to plot $\ln(J_{th})$ as a function of 1/(cavity length) in order to obtain a value for $J_{th}\infty$, which is the threshold current density for a device of infinite cavity length. This plot is shown in figure 2.8, and yields a value for $J_{th}\infty = 720\text{A/cm}^2$. The gradient of this plot was used to calculate the material gain $G_0 = 2414\text{cm}^{-1}$.

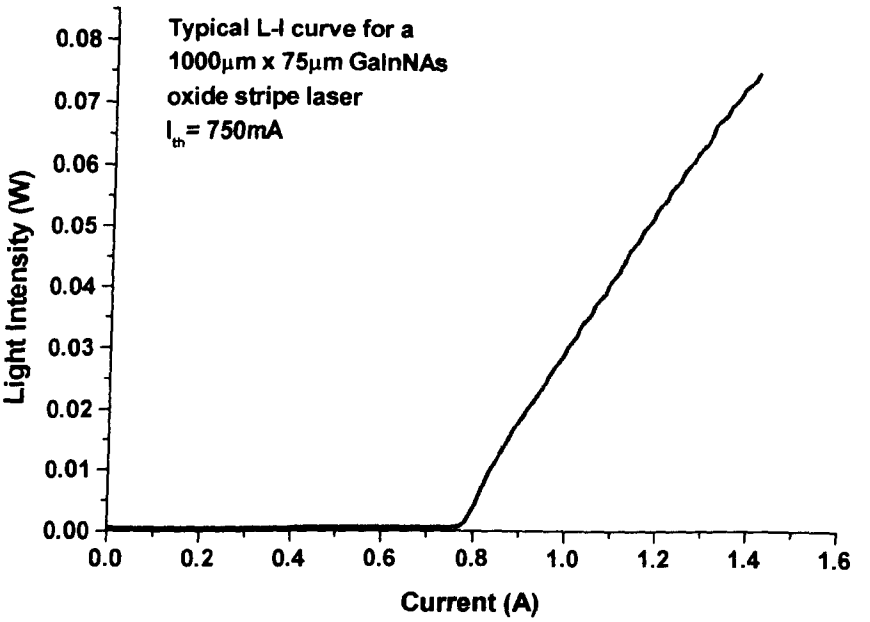

Figure 2.7: Typical L-I curve for a 1000μm x 75μm GaInNAs oxide stripe laser.

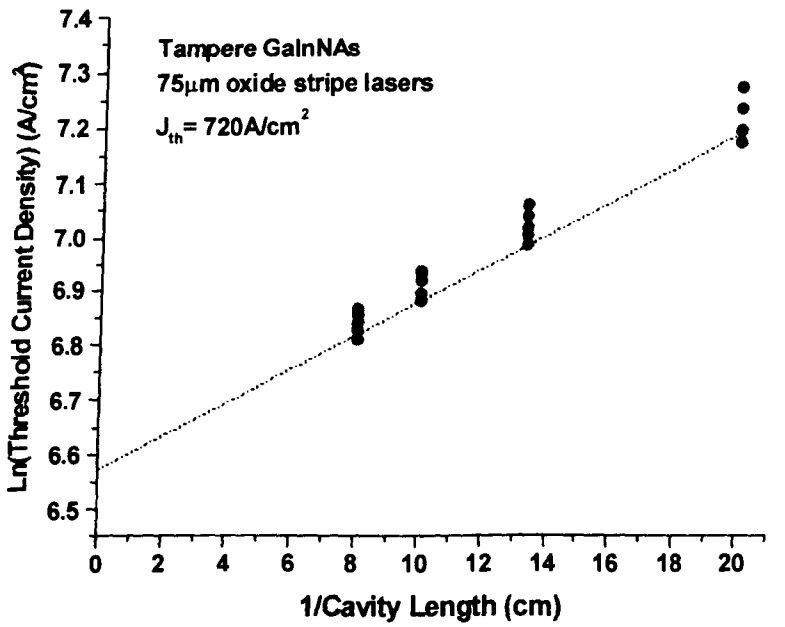

Figure 2.8: Plot of $\ln(J_{th})$ as a function of 1/cavity length for 75μm oxide stripe lasers

Figure 2.9 shows a plot of 1/external quantum efficiency as a function of cavity length, from which values for internal efficiency (η_{int}) and loss (α) are determined to be 62.5% and 18cm^{-1} respectively. Although the value for $J_{th}\infty$= 720A/cm^2 is almost twice the value for J_{th} of similar GaInNAs material reported by the same growers (13), it would prove sufficient in demonstrating the concept of the project. The higher than usual values for J_{th} and α could be attributed to the growth process, which had still to be properly calibrated, possibly introducing a higher than desired amount of non-radiative recombination centres through material defects and impurities.

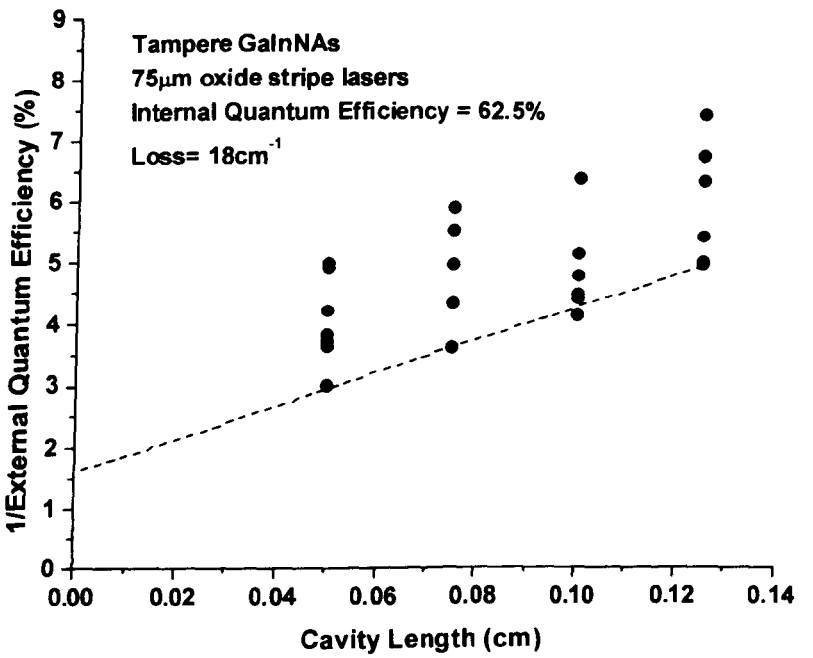

Figure 2.9: Plot of 1/external quantum efficiency as a function of cavity length for 75μm oxide stripe lasers.

Figure 2.10 shows a plot of the lasing spectrum of the measured oxide stripe laser devices, showing the peak wavelength to be~1300nm.

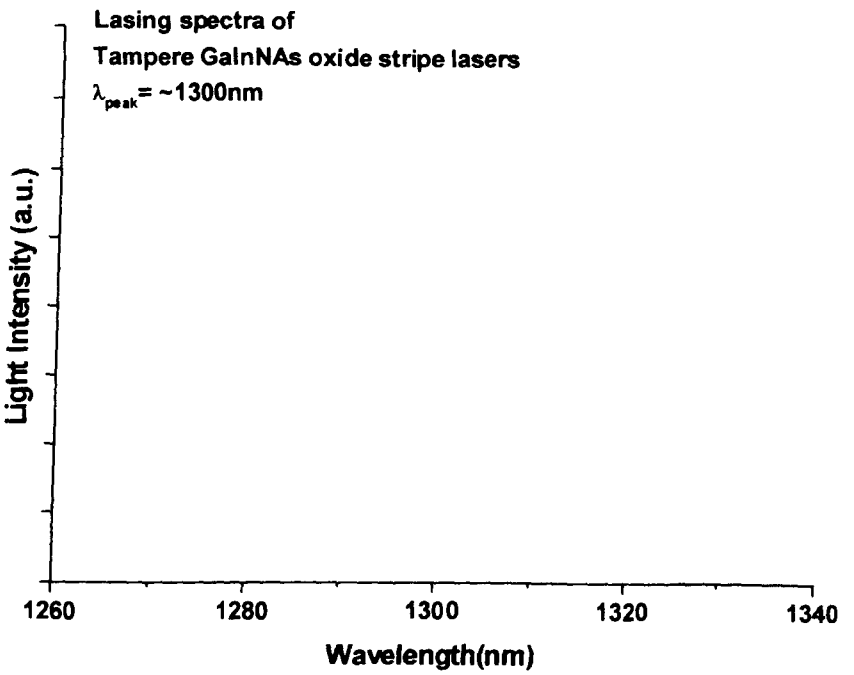

Figure 2.10: Plot of the lasing spectrum obtained from a GaInNAs oxide stripe laser

To measure the temperature characteristics of the material, several devices were mounted on a temperature controlled peltier. The devices were again tested under pulsed operation over a range of temperatures between 20^0C-90^0C. The temperature coefficient, T_0, is generally used to quantify how much the threshold current depends on temperature, and can be extracted from the plot of the threshold current as a function of temperature(T_0= 1/Gradient) ,as shown in figure 2.11. Note that devices with smaller values of T_0 have a larger dependence on temperature. For this material, a value of T_0=80K was obtained, which is 20K lower than the T_0 value reported for similar GaInNAs material produced by the same growers. Again, the smaller than desired value for T_0 could be attributed to introducing a higher than desired amount of non-radiative recombination centres through material defects and impurities caused by the non-calibrated growth conditions.

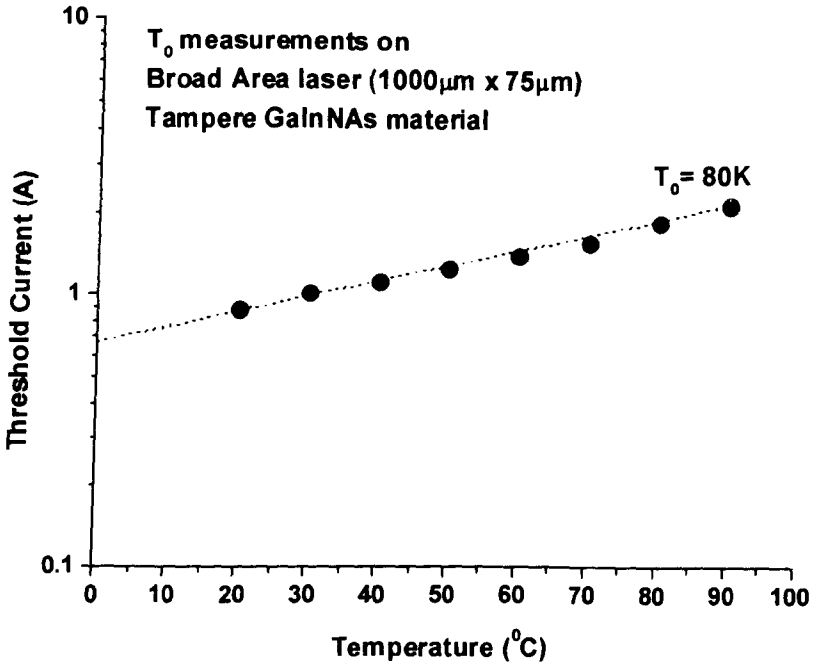

Figure 2.11: Plot of threshold current as a function of temperature for GaInNAs oxide stripe laser devices

2.10 Conclusion

The GaInNAs material system has experienced a sharp progress since it was first demonstrated in 1996. The intense interest in GaInNAs has been primarily due the inability of InGaAsP lasers to produce an adequate power and temperature performance, which is needed for Raman amplification at the telecommunication wavelengths. This chapter has given a brief history of the GaInNAs material system, and has highlighted the advantages GaInNAs may have over other material systems at the communication wavelengths, such as improved temperature performance and a relatively greater control of growth. With continued improvements to the material

system over the coming years, we may soon see GaInNAs replacing currently employed lasers in communication systems. With that in mind, it is worth exploring whether technologies currently used in other material systems, such as quantum well intermixing, can be employed by the GaInNAs material system. As this project was mainly concerned with incorporating quantum well intermixing into GaInNAs laser devices, obtaining material with decent lasing characteristics was essential. We obtained this with Tampere grown single quantum well GaInNAs material. Characterisation of the material was performed through the fabrication and testing of oxide stripe lasers. Although the results of these tests showed the material not to be of the quality the growers are capable of, it would still be sufficient to demonstrate the concept of the project.

References

1) M.Kondow, K.Uomi, A.Niwa, T.Kitatani, S.Watahiki and Y.Yazawa, "GaInNAs: A novel material for long wavelength range laser diodes with excellent high temperature performance", Jpn. J. Appl. Phys., Vol. 35, pp. 1273-1275, 1996.

2) J.S.Harris Jr "GaInNAs long wavelength lasers: progress and challenges", Semicond. Sci. Technol, Vol 17, pp 880-891, 2002.

3) G.B.Stringfellow "Organometallic Vapor-phase epitaxy: Theory and practice" (Boston:Academic), p123, 1989.

4) S.G.Spruytte, M.C.Larson, W.Wampler, C.W. Coldren, H.E. Petersen, J.S.Harris "Nitrogen incorporation in group III-nitride-arsenide materials grown by elemental source molecular beam epitaxy", Journal of Crystal Growth 227-228, pp506-515, 2001.

5) J.C.Harmand, G.Ungaro, L.Largeau, and G.Le Roux "Comparison of nitrogen incorporation in molecular-beam epitaxy of GaAsN, GaInNAs and GaAsSbN", Applied Physics Letters, Vol 77, No 16, pp 2482-2484, Oct 2000.

6) A.Yu.Egorov, D.Berklau, B.Borchert, S.Illek, D.Livshits, A.Rucki, M.Schuster, A.Kaschner, A.Hoffman, G.Dumitras, M.C.Amann, H.Riechert, "Growth of high quality InGaAsN heterostructures and their laser application" Journal of Crystal Growth, 227-228, pp545-552, 2001.

7) A.J.Ptak, S.W.Johnston, S.Kurtz, D.J.Friedman, W.K.Metzger "A comparison of MBE- and MOCVD- grown GaInNAs", Journal of Crystal Growth, 251, pp 392-398, 2003.

8) K.Kim and A.Zunger "Spatial correlations in GaInNAs alloys and their effects on band-gap enhancement and electron localization", Phys.Rev.Letters, Vol 86, pp 2609-2612, 2001.

9) V.Gambin, V.Lordi, W.Ha, M.Wistey, T.Takizawa, K.Uno, S.Friedrich, J.Harris "Structural changes on annealing of MBE grown (Ga,In)(N,As) as measured by X-ray absorption fine structure", Journal of Crystal Growth, 251, pp 408-411, 2003.

10) N.Tansu and L.J.Mawst, "The role of hole leakage in 1300nm InGaAsN quantum-well lasers", Applied Physics Letters, Vol 82, Number 10, pp 1500-1502, March 2003.

11) M.Pessa, C.S.Peng, T.Jouhti, E.M.Pavelescu, W.Li, S.Karirinne, H.Liu, O.Okhotnikov "Towards high-performance nitride lasers at 1.3μm and beyond", IEE Proceedings – Optoelectronics, Vol 150, No.1, Feb 2003.

12) E.M.Pavelescu, C.S.Peng, T.Jouhti, J.Konttinen, W.Li, M.Pessa "Effects of insertion of strain-mediating layers on luminescence properties of 1.3μm

GaInNAs/GaNAs/GaAs quantum-well structures", Applied Physics Letters, Vol 80, No 17, April 2002.

13) C.S.Peng, E.M.Pavelescu, T.Jouhti, J.Konttinen, I.M.Fodchuk, Y.Kyslovsky, M.Pessa, "Suppression of interfacial atomic diffusion in InGaNAs/GaAs heterostructures grown by molecular-beam epitaxy", Applied Physics Letters, Volume 80, No 25, June 2002.

14) M.Kawaguchi, T.Miyamoto, E.Gouardes, S.Minobe, T.Kondo, F.Koyama, K.Iga "Photoluminescence and lasing characteristics of GaInNAs quantum wells using GaInAs intermediate layers", Jpn.J.Appl.Phys, Vol 41, pp 1034-1039, 2002.

15) X.Yang, M.J.Jurkovic, J.B.Heroux, W.I.Wang "Low threshold InGaAsN/GaAs single quantum well lasers grown by molecular beam epitaxy using Sb surfactant", Electronics Letters, Vol 35, No 13, June 1999

16) H.Shimizu, K.Kumada, S.Uchiyama, A.Kasukawa "High performance CW 1.26μm GaInNAsSb-SQW ridge lasers", IEEE J.Selected topics in Quantum Electronics, Vol 7, No 2, March/April 2001.

17) D.A.Livshits, A.Y.Egorov, H.Riechert "8W continuous wave operation of InGaAsN lasers at 1.3μm", Electronics Letters, Vol 36, No 16, Aug 2000.

18) W.Ha, V.Gambin, M.Wistey, S.Bank, S.Kim, J.S.Harris "Multiple-quantum well GaInNAs-GaNAs ridge waveguide laser diodes operating out to 1.4μm", IEEE Photonics Technology Letters, Vol 14, No.5,May 2002.

19) M.O.Fischer, M.Reinhardt, A.Forchel "Room-temperature operation of GaInAsN-GaAs laser diodes in the 1.5μm range", IEEE Journal of selected topics in Quantum Electronics, Vol.7, No.2, April 2001.

20) S.R.Bank, M.A.Wistey, H.B.Yuen, L.L.Goddard, J.S.Harris "Progress towards high power 1.5μm GaInNAsSb/GaAs lasers for Raman amplifiers", 2004 Optical Fiber Communication Conference (OFC), Los Angeles, CA, Feb 2004.

21) P.W.A.McIllroy, A.Kurobe, Y.Uematsu "Analysis and application of Theoretical Gain Curves to the Design of Multi-Quantum-Well Lasers", IEEE Journal of Quantum Electronics, Vol 21, pp 1958-1963, December 1985.

Chapter 3

Quantum Well Intermixing

3.1 Introduction

As discussed in chapter 1, optical fibre systems used in both long haul and metro networks are on the verge of another revolutionary development i.e. the integration of optical and electronic components into optoelectronic integrated circuits (OEIC's) or photonic integrated circuits (PIC's). Since the vast amount of optoelectronic devices now utilise quantum wells (QW's) in their active regions, quantum well intermixing (QWI) has emerged as a strong technique for fabricating OEIC's and PIC's. During the intermixing process, the bandgap energy of the QW structures is increased in selected regions by intermixing the wells with the barriers. This technology allows low-loss waveguides, modulators, lasers and detectors to be fabricated on the same chip. This chapter gives an overview of monolithic integration techniques and QWI technologies, before discussing the QWI technique applied to the GaInNAs QW system for this research.

3.1.1Optoelectronic Integration Techniques

The main objectives of optoelectronic integration are much the same as those of electronic integration: improving performance, reliability and functionality whilst simultaneously lowering the manufacturing cost. Combining lasers, modulators and detectors with low-loss waveguides on a single epitaxially grown substrate, for the fabrication of OEIC's, requires the definition of regions with different bandgap energies. The approaches to such integration can be divided into two categories: growth techniques and intermixing techniques. In order to fully understand the

advantages and disadvantages of each integration technique, we must look at the requirements that need to be met to realise practical PIC's

3.1.2 Optoelectronic Integration Requirements

Charbonneau et al (1) stated that for any OEIC or PIC to be practical, the optoelectronic integration technique used must fulfil several requirements:

1) There must be a large, controllable bandgap energy difference between the various devices in the PIC.
2) Loss in the integrated waveguide devices must be comparable to or lower than that present in the as-grown structure.
3) The electrical properties of the various devices must suffer zero or insignificant deterioration due to the processing technique.
4) There should be no significant adverse effects on the operating lifetimes of the various devices in the PIC, after processing.
5) Any other process-initiated changes in the properties of the devices must be either neutral or advantageous to the PIC.

3.1.3 Optoelectronic Integration Using Selective Area Growth

Selective area growth (SAG) is a technique that enables control over the width of the quantum wells across a wafer during a single epitaxial step. Controlling the quantum well width allows lateral control over the bandgap. In this approach, the wafer is covered with a dielectric mask, which is then removed in small selected areas where growth is to take place. Growth cannot take place on the dielectric mask, which leads to an increase in the number of growth species available, which in turn enhances the growth rate in the regions not covered by the dielectric mask. The width of the mask

opening and the patterning of the mask therefore dictate the growth rate, and hence the width of the quantum wells.

Integrated devices containing communication lasers, modulators linked with passive sections have been achieved using this growth technique, as well as multi-wavelength DBR lasers for wavelength division multiplexing (WDM) (2). Despite this, there are still several obstacles that need to be overcome by this technology in order to compete with future integration techniques. Firstly, when growing two regions of different bandgap, two different growth rates are involved. If the growth conditions are optimised for the higher growth rate, hence higher bandgap region, the material quality and composition of the lower bandgap region will become non-uniform. Secondly, the interface between the two growth regions can be quite large (around 100μm) which can limit device miniaturisation.

3.1.4 Regrowth

Monolithic integration can also be achieved by using a regrowth technique. Firstly, a wafer is grown containing the quantum well active region for all the devices. Secondly, areas where the active region is unwanted are etched and overgrown with the same upper cladding layer everywhere on the wafer. This ensures that a virtually constant optical waveguide propagation coefficient is maintained across the wafer. This approach does inflict limitations on device performance due to the poor interface between the original and regrown material. This poor interface is caused by material mismatch, as well as imperfections in etching and regrowth, which subsequently leads to poor device characteristics and low yield. Moreover, the additional etch and regrowth stages are expensive. Such factors render regrowth methods unsuitable in the development of optoelectronic integrated circuits.

3.2 Principle of QWI

Quantum well intermixing permits post growth modification to the bandgap of QW material. During the intermixing process, atoms from the QW's move into the barriers and vice versa. This interdiffusion changes the composition of the wells and barriers,

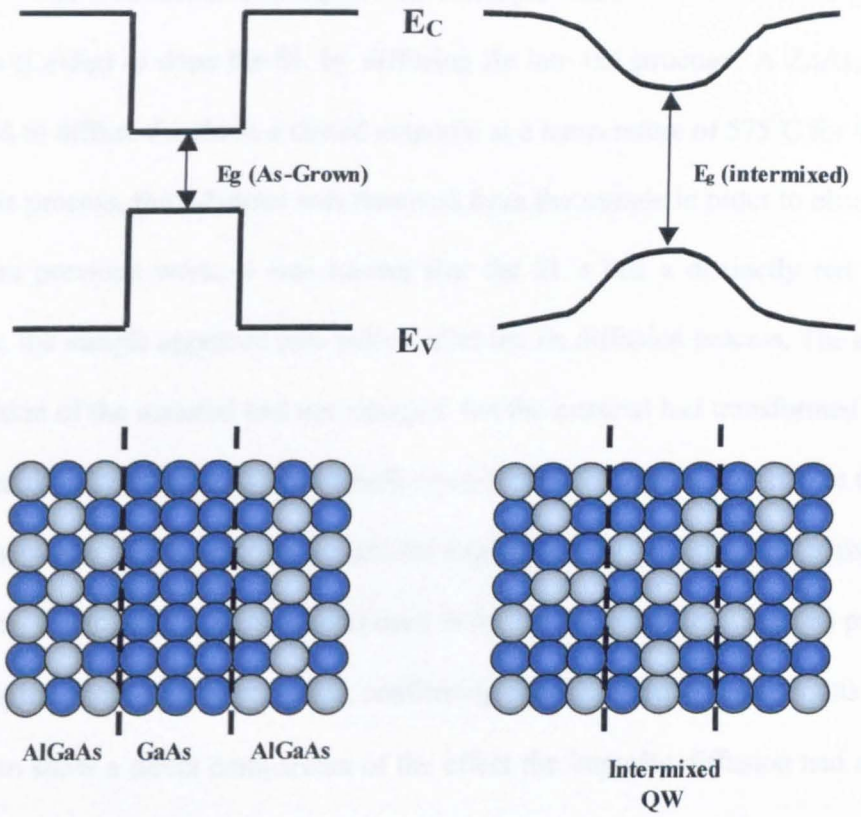

Figure 3.1: Diagram showing the effect of QWI on the $Al_{0.5}Ga_{0.5}As$ QW system

which changes the profile of the QW, and results in associated changes to the bandgap energy and refractive index. To illustrate the principle of QWI, figure 3.1 shows the change experienced by the GaAs/AlGaAs QW system during intermixing. During intermixing, the QW becomes disordered, resulting in a smoother QW profile, which increases the bandgap energy of the intermixed well.

3.2.1 Discovery of QWI

QWI was somewhat a surprise discovery for the research group at the University of Illinois in 1980. A detailed account of this discovery is given by Holonyak (3) and Laidig (4). Whilst performing research into AlAs-GaAs super-lattices (SL's) and quantum well heterostructures (QWH's), Holonyak instructed one of his graduate students (Laidig) to dope the SL by diffusing Zn into the structure. A $ZnAs_2$ source was used to diffuse the Zn in a closed ampoule at a temperature of 575^0C for 4 hours. After this process, the substrate was removed from the sample in order to observe the SL. From previous work, it was known that the SL's had a distinctly red colour, however, the sample appeared pale yellow after the Zn diffusion process. The average composition of the material had not changed, but the material had transformed from a structured SL layer form (red) into a bulk crystal form (yellow). To be certain that the Zn impurity was the cause of the result, the experiment was repeated under the same conditions, except only excess As was used in the sealed ampoule. After this process, the SL region was observed to be red, confirming the role of Zn in the previous result. In order to show a direct comparison of the effect the impurity diffusion had against simple annealing, another sample containing the same SL structures was prepared with Si_3N_4 masking stripes on the surface. After repeating the 575^0C for 4 hour annealing using the $ZnAs_2$ source in the sealed ampoule, stripes of red and yellow were observed on the sample regions that were masked and unmasked respectively. These results demonstrated the ability to selectively intermix QWH's and SL's, as well as the practical implications of the process, prompting the researchers to patent the discovery shortly afterwards. Since an impurity source was used to promote disordering, the technique was named impurity induced layer disordering (IILD), or otherwise known as impurity induced disordering (IID).

3.2.2 Disordering Mechanisms

Heterostructure disordering requires point defects to assist the movement of atoms at elevated temperatures. Without such defects, the atoms would be unable to move around. In order to understand heterostructure disordering, it is helpful to be aware of the nature of the defects involved in the process.

3.2.3 Point Defects

The three main point defects found in III-V semiconductors are vacancies, interstitials and antisites. Table 3.1 gives a short overview of point defects in GaAs, showing that each atom involved in the crystal structure has three possible associated point defects.

Defect	Description
Vacancy	**Empty site in the crystal lattice. Group III and V vacancies are notated as V_{Ga} and V_{As} respectively.**
Interstitial	**Atom in the crystal lattice located in between lattice atoms. Group III and V interstitials are notated as I_{Ga} and I_{As} respectively.**
Antisite	**Ga atom located on an As site, As_{Ga}, or an As atom located on a Ga site, Ga_{As}.**

Table 3.1: Containing a short description of point defects associated with GaAs

Point defects found in semiconductors can be divided into two categories: native defects and induced defects. Native defects occur during the growth of the semiconductor material whereas induced defects are created post-growth, most commonly by ion implantation, material doping or laser treatment.

3.2.4 Native Point Defects

The key to controlling bandgap shifts via heterostructure disordering in III-V QW structures is to control the number of point defects in the crystal that are responsible for interdiffusion. Having too few point defects in the crystal will give insufficient interdiffusion, whereas having too many point defects can lead to immobile extended defects that will also hinder interdiffusion (5). During the growth of III-V QW structures, native point defects are created by variations in the crystal stoichiometry. Gebauer et al (6) investigated the control of native point defects during MBE growth of GaAs by using the fact that the crystal stoichiometry is dependant on the growth temperature. Gebauer et al measured the concentration of defects (V_{Ga}) in the crystal following growth at temperatures between 200^0C and 350^0C. It was found that growth of low temperature (200^0C) GaAs produced a crystal with defect concentrations of around $1x10^{18}cm^3$, which would be a suitable amount to enhance the interdiffusion rate of the group III atoms. By incorporating a low temperature cap layer on top of a AlGaAs/GaAs superlattice, Tsang et al (7) demonstrated an enhancement in compositional disordering during annealing. Furthermore, they found that the enhancement in interdiffusion was due to an increase in gallium vacancies. From these results it was clear that by growing a low temperature GaAs cap layer on top of a QW structure, and subsequently patterning and etching the layer, selective area disordering of the QW structures could be achieved.

3.2.5 Induced Defects

Research into inducing point defects in QW structures has involved the scrutiny of many different methods. This section of the chapter will discuss the most common methods used.

3.2.6 Impurity Induced Layer Disordering (IILD)

As mentioned in section 3.2.1, Laidig et al (4) were the first to discover IILD by demonstrating heterostructure disordering using Zn as a dopant. Since then, many research groups have involved themselves in this intermixing technology. There have been many electrically active elements introduced to AlGaAs/GaAs QW structures that have proven to cause IILD, such as Si, Ge, Se, S and Sn as donors, and Zn, Be and Mg as acceptors (8). Laidig et al and VanVechten (9) each attempted to explain the mechanism behind IILD, however, subsequent experimental results were found not to be in accordance with these models. The problem with the models proposed by Laidig and Van Vechten were that they failed to accurately explain the effect of IILD on both group III and group V interdiffusion, and also failed to explain the effects of other dopants besides Zn. On inspection of the experimental data and the weaknesses of the proposed IILD models previously given, Tan and Gosele (10) proposed the *Fermi-level* effect as a means of explaining the phenomena. It was well known that the concentrations of point defects in silicon were dependant on the position of the *Fermi*-level, and hence on the concentration of dopants. Since such point defects are used as diffusion vehicles, the diffusivity of elements is dependent on the doping. Since the *Fermi*-level effect is a charge effect, it is the doping level and type of doping which are of primary importance. It is also noted that it is mainly the presence of the dopant that is important, not its diffusion in the crystal. For that reason, the

same effect should be observed if the same material is doped by a different dopant species to the same level and type.

IILD has been effectively applied to various devices to take advantage of the bandgap widening effects. Suzuki et al (11) used IILD successfully to incorporate non-absorbing mirrors (NAM's) to high power lasers to suppress catastrophic optical mirror damage (COMD), while Deppe et al (12) employed IILD to realise buried heterostructure devices for improved current confinement. Although this process has proven successful in the mentioned cases, it is still far from ideal due to the high concentrations of electrically active dopants. For successful IILD, impurity concentrations in the order of $10^{18}/cm^3$ are required, which can lead to large free carrier absorption losses (>43dB) (13), and hence be severely detrimental to the devices. Furthermore, the change in device resistivity associated with the electrically active impurities can be detrimental to devices requiring good electrical isolation.

3.2.7 Implantation Induced Disordering

Another method that has been used to disorder QW structures is implantation induced disordering. The ion beam used in the implantation process damages the crystal, hence creating point defects, which can sequentially promote intermixing during annealing. Annealing the crystal after the damage process also seems to be adequate in restoring crystallinity (1). Early research into this disordering mechanism by Gavrilovic et al (14) revealed that any ion can be relatively effective in disordering an AlGaAs/GaAs QW heterostructure or AlAs/GaAs superlattice via damage induced disordering. This conclusion was drawn after using many different ions to promote crystal damage, including electrically active impurities Zn, Si, and S, the lattice

constituent Al, and inert ion Kr. It was shown that all ions could effectively disorder the heterostructures, with the electrically active ions being the most effective due to the addition of the Fermi-level effect.

Charbonneau et al (1) stated that the number of point defects introduced to heterostructures during the implantation process depended on the following factors:

1) dose or fluence (i.e.number of ions/cm^2)
2) masses of the ions (ion species)
3) implantation angle
4) ion energy
5) ion flux or current density (A/cm^2)
6) temperature of the substrate during implantation

By taking all these factors into account, the implantation process can be used very accurately to induce an optimum amount of point defects for QW disordering. Furthermore, implantation induced damage can be suppressed in selected areas by using a suitably thick mask layer, such as 2μm SiO_2, thus allowing selective area intermixing.

O'Neill et al (15) demonstrated the effectiveness of implantation induced disordering in the AlGaAs/GaAs system using fluorine and boron, which are both electrically neutral at room temperature. Samples were implanted with either fluorine or boron, using a range of different implantation doses and energies. The samples were then annealed in a conventional furnace at temperatures up to 890^0C to promote disordering. Large blue shifts in the PL of up to 100meV were observed. Further experiments by O'Neill et al (16) confirmed the effectiveness of this disordering

technique to produce low loss waveguides by demonstrating a propagation loss of 4.7dB/cm in AlGaAs/GaAs waveguides that had been disordered using fluorine. The dopant concentration for the implantation disordering (around $10^{14}cm^{-3}$) was much less than that of electrically active IILD (typically around $10^{18}cm^{-3}$), hence the loss value was much lower than the approximate loss value of 43dB/cm associated with electrically active IILD (13).

Implantation induced disordering has been employed by many research groups to produce an assortment of devices from different material systems. Charbonneau et al (1) produced lasers with a range of wavelengths on the same 1.5μm InP-based wafer using P implantation disordering. Different levels of intermixing were controlled using different thickness of SiO_2 mask layer to suppress implantation damage. Such devices are particularly relevant to WDM systems. Other devices fabricated using this disordering technique included low loss waveguides, modulators and superluminescent diodes. The disordering of InGaAs/AlGaAs material using implantation of As ions was employed by Piva et al (17) to realise passive extended cavity sections to laser devices. Similarly, Hashimoto et al (18) used the implantation of N ions to disorder GaInAs/GaInP material to form non absorbing mirrors (NAM's) on high power 980nm lasers. Although this process has proved successful in the discussed cases, carrier traps associated with the implanted species and residual damage from the implantation process can cause problems with device performance and lifetimes (13). Also, the equipment required to perform implantation is complex, as well as expensive.

3.2.8 Laser Induced Disordering

Laser induced disordering (LID) is an intermixing technique which uses a laser beam to promote a shift in the bandgap edge of QW material. Initially the laser beam was used to melt the QW material to cause disordering, but more recently has been used to create defects in the QW region that can promote intermixing using a subsequent annealing step. LID was first demonstrated by Epler et al (19) by using a focussed Ar^+ laser beam to selectively disorder localised regions on an AlGaAs/GaAs superlattice. The laser beam (λ=488nm) was absorbed by the whole crystal and effectively melted the material, which afterwards recrystallised into nearly bulk form AlGaAs. A computer controlled scanning table was used in order to use the laser as a localised heat source capable of disordering the layers on a micron scale. However, the spatial resolution for this process is limited due to the conduction of heat within the material. Furthermore, the process requires high laser power densities in order to melt the material, and melting the material results in complete intermixing, which implies that the process cannot be used to create partial bandgap shifts (13). An alternative LID process was developed by McLean et al (20), in which the laser beam was only absorbed in the active region of the material by using an incident laser wavelength above the bandedge of the active region, but below the bandedge of the cladding layers. A 1064nm Nd:YAG laser was used by McLean to generate heat in the InGaAsP/InP active region, which caused intermixing between the wells and the barriers. PL measurements recorded a shift of 123meV between the intermixed and as-grown material, showing the potential for this process in the fabrication of OEIC's. This process was named photo-absorption induced disordering (PAID), and had the advantage of being an impurity free process that relied on native point defects to aid intermixing. McKee et al (21) successfully applied PAID to realise extended cavity

lasers, low loss waveguides, bandgap tuned lasers and electroabsorption modulators from InGaAsP/InP material. A more recent form of PAID, known as pulsed-PAID (P-PAID), has been used to create point defects in the QW region of the material, which can then diffuse during annealing and promote QW disordering. Since there is no large generation of heat in this process, the spatial resolution of P-PAID is much better than that of other LID techniques. Although LID has many advantageous features such as being impurity free and having direct write capability, as well as potentially being able to do parallel processing, the techniques require some improvement before they can be appealing to industry.

3.2.9 Impurity Free Vacancy Disordering (IFVD)

Impurity free vacancy disordering (IFVD) is an intermixing technique that makes use of a dielectric cap deposited on the top of the material structure to create vacancies on the group III lattice sites. In this technique, a dielectric cap layer, typically SiO_2, is deposited on the structure, which then undergoes a rapid thermal annealing (RTA) step. At elevated temperatures, some atomic species, such as Ga, become soluble and have a high diffusion coefficient in SiO_2. Therefore, during the annealing stage, Ga atoms dissolve into the SiO_2 cap layer leaving behind vacancies. These vacancies then diffuse down to the QW region to enhance disordering. The number of Ga atoms that diffuse into the cap layer is dependent on the thickness and porosity of the cap layer. The dependence on the cap layer thickness has been ascribed to the outdiffusion species reaching its solubility limit in the dielectric cap (Ooi et al (22)), therefore a thicker cap layer will allow more solubility.

IFVD was first demonstrated by Deppe et al (23), within the AlGaAs/GaAs material system. By utilizing a SiO_2 cap layer as a defect source and a Si_3N_4 masking layer, both chemical vapour deposited (CVD), a differential PL shift of 90meV was obtained following an anneal of 850^0C for 6h. Since that time, research has found Si_3N_4 to be unsuitable as a masking cap layer since it is very rarely pure, and usually contains a considerable amount of SiO_2 (13). A considerable amount of SiO_2 in the Si_3N_4 layer can be enough to promote disordering of the quantum wells covered by the layer, albeit to a smaller degree than the quantum wells covered by SiO_2. Still, the differential shift in PL wavelength between the areas chosen for disordering and those not chosen for disordering is reduced. Furthermore, Si_3N_4 layers have a highly strained interface with the QW material, which when heated can cause large differential strain effects to occur, which can create defects, and promote disordering beneath the cap.

An alternative to the Si_3N_4 cap layer that has been proved to effectively inhibit disordering is SrF_2. Beauvais et al (24) used the SrF_2 cap layer to suppress disordering is GaAs/AlGaAs heterostructures, however, it was found that the caps suffered substantial damage during the annealing stage, which made them difficult to remove. Even so, this masking layer has been used alongside SiO_2 in the IFVD process to produce promising results. Gontijo et al (25) used the SiO_2/SrF_2 method to fabricate ridge waveguide lasers with disordered (passive) extended cavities from GaAs/AlGaAs. The disordered passive sections had a measured loss value of 3.6dB/cm, which visibly demonstrated the ability to use this process for fabrication of low loss waveguides. Ooi et al (22) used the SiO_2/SrF_2 process to realise multiple wavelength laser arrays and multi-channel wavelength division multiplexers from

GaAs/AlGaAs. The bandgap tuning of the lasers was performed by varying the SrF_2 layer coverage in selected areas, with areas having most coverage experiencing the least amount of disordering. This technique allowed the fabrication of lasers with different wavelengths on the same chip.

Since there are no impurities involved in IFVD, the electrical properties of the material remain largely unaltered. Furthermore, free carrier losses associated with electrical dopants are not applicable to this process, making it possible to fabricate long lengths of low attenuation passive waveguides, which are required by OEIC's. The process also avoids the problems associated with implantation techniques, such as residual damage and changes in material resistivity. Most importantly, IFVD is simple and inexpensive, as well as relatively easy to control and reproduce.

3.3 Intermixing research at Glasgow University

Research on intermixing at Glasgow University was started by John Marsh around 1987. Early research involved implantation induced disordering of GaAs/AlGaAs, GaInAs/AlGaInAs and GaInAs/GaInAsP material systems using fluorine and boron as the implantation species. Since then, several different intermixing technologies have been investigated, such as photoabsorption induced disordering (PAID) as well as its successor pulsed-PAID (P-PAID). IFVD studies using SiO_2/Si_3N_4 and SiO_2/SrF_2 were conducted during the mid-nineties. However, since the late nineties the focus in research has been diverted to an intermixing process that involves a sputtered SiO_2 cap layer.

3.3.1 Sputtered SiO_2 Intermixing Process

In an attempt to overcome problems associated with PECVD SiO_2 cap layers, researchers tried using sputtered SiO_2 cap layers as an alternative. This led to the discovery of the sputtered SiO_2 intermixing process. During this process, a layer of sputtered SiO_2 is deposited onto the surface of the sample, which is then annealed at high temperature to promote intermixing in the QW region beneath. McDougall et al (26) reported the intermixing of several material systems using the sputtered SiO_2 process. The sputtering of the SiO_2 cap layer was performed using a Nordiko RF sputterer. Areas in which intermixing was to be suppressed were masked with PECVD SiO_2, whereas areas in which intermixing was to be promoted were covered with sputtered SiO_2. This patterning of dielectric coatings on the sample allowed selective area control of the intermixing technique. Early investigations into the disordering mechanism seemed consistent with the idea of point defect generation at the material surface caused by the energetic bombardment on the surface during the deposition of SiO_2, followed by the subsequent diffusion of the defects into the QW region during an annealing step, causing the QW's and barriers to intermix. The deposition process was thought to be responsible for breaking atomic bonds on the material surface, thus creating vacancies and interstitials.

An increase in research into the intermixing mechanism followed from the formation of a Glasgow University spin-off company Intense Photonics Ltd, due to its commercial importance. From this research, it appears that the disordering mechanism is an intricate result of several factors. The initial understanding of damage caused to the material surface during the deposition of sputtered SiO_2 promoting point defects is thought to be partly responsible for intermixing, following an annealing step.

Furthermore, the IFVD intermixing mechanism is also thought to be somewhat accountable since the sputtered SiO_2 allows improved in-diffusion of atomic species with respect to PECVD SiO_2, thus enhancing intermixing. In addition, from close inspection of the sputtered SiO_2 cap layer composition, it was revealed that it contained a small quantity of Cu impurities, which was also found to enhance intermixing. Because of the small amount of Cu impurities involved, the free-carrier losses associated with impurity induced layer disordering (IILD) are circumvented.

The sputtered SiO_2 intermixing process is still being investigated in order to fully understand the mechanism. However, the process has already been used to realise a number of devices. McDougall et al (26) used the sputtered SiO_2 process to fabricate bandgap tuned lasers, extended cavity lasers and multimode interference couplers from InGaAs/InGaAlAs and InGaAs/InGaAsP material, whilst Bubke et al (27) demonstrated low loss intermixed waveguides (~6dB/cm) using InGaAs/InGaAlAs material, thus demonstrating the potential of the intermixing technique for monolithic integration.

3.3.2 Sputtered SiO_2 QWI process

For the sputtered SiO_2 intermixing process to be useful, the designation of areas where intermixing was to occur, and where intermixing was not to occur is necessary. From work performed by McDougall et al (26) and Liu et al (28), it was found that 200nm PECVD SiO_2 was insufficient for suppressing intermixing during this process, however a 500nm thick PECVD SiO_2 layer was found to be suitable. Areas designated for intermixing could therefore be selected by opening regions in the 500nm PECVD SiO_2 cap layer, then depositing sputtered SiO_2. Fig 3 illustrates the

step process for selective area intermixing using the sputtered SiO_2 process. The first step in the process is to deposit 500nm PECVD SiO_2 onto the QW sample. From there, photolithography can be used to expose the regions of PECVD SiO_2 that are to be etched. After etching the PECVD SiO_2 layer using HF acid, regions of the semiconductor surface are left exposed. SiO_2 is then sputtered over the whole sample. A subsequent annealing step allows intermixing in the QW's below the selected

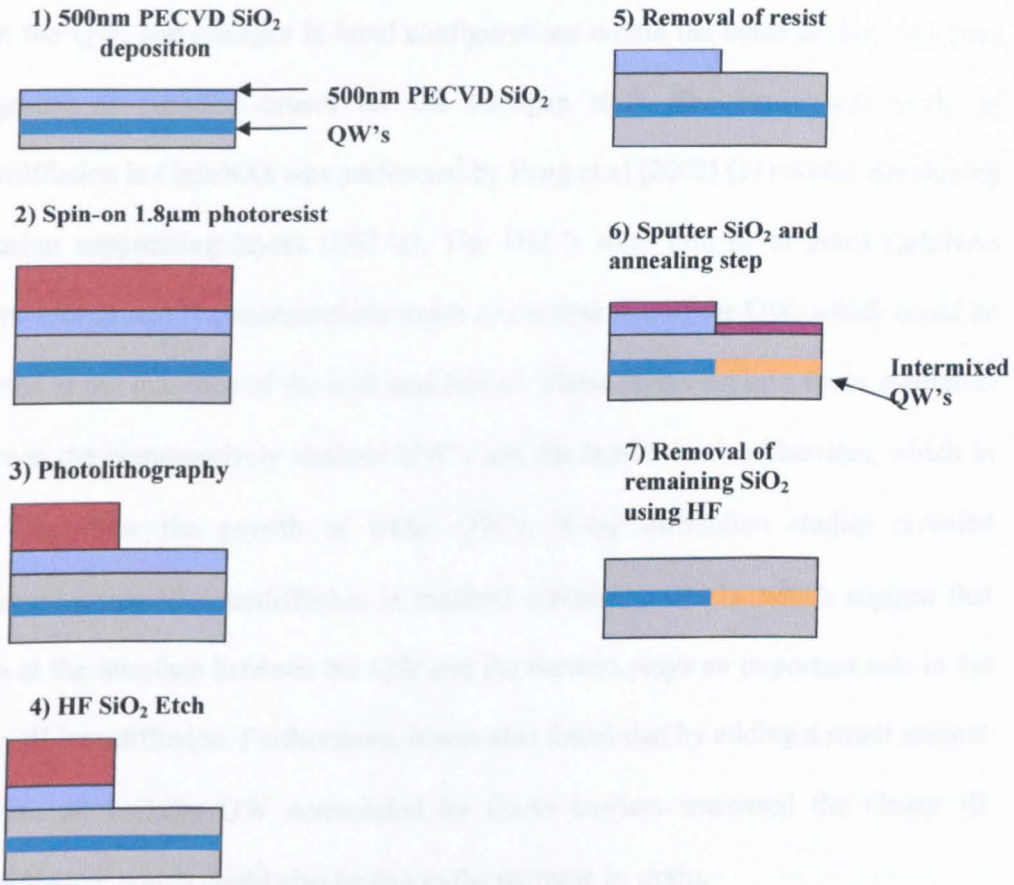

Fig 3.2: Diagram showing the step-by-step process of the sputtered SiO_2 intermixing technique

regions. Intermixing is suppressed in the QW's beneath the PECVD SiO_2 mask layer. Finally, all remaining SiO_2 can then be removed using HF acid.

3.3.3 GaInNAs intermixing

Research into QWI technology using the GaInNAs/GaAs material system has been limited to date. However, due to the inherent blue shift in the PL intensity peak associated with annealed GaInNAs (chapter 2, section 2.4), a great deal of research has focussed on the interdiffusion mechanisms involved. Research teams worldwide fail to have a common explanation for the cause of the PL blue shift. Explanations such as group III interdiffusion between the wells and barriers, nitrogen out-diffusion from the QW, and changes in bond configurations within the material, have all been suggested as possible causes for the bandgap shift. The inadvertent study of interdiffusion in GaInNAs was performed by Peng et al (2002) (31) whilst developing diffusion suppressing layers (DSL's). The DSL's were thin (2 to 3nm) GaInNAs layers with In and N concentrations much lower than that of the QW, which could be inserted at the interface of the well and barrier. These layers act as a strain mediators between the compressively strained QW's and the tensile strained barriers, which in turn can allow the growth of wider QW's. X-ray diffraction studies revealed decreased group III interdiffusion in material containing DSL's, which suggest that strain at the interface between the QW and the barriers plays an important role in the group III interdiffusion. Furthermore, it was also found that by adding a small amount of N to an InGaAs QW surrounded by GaAs barriers increased the Group III interdiffusion, which could also be due to the increase in strain.

Macaluso et al (29) are the only team to have studied selective QWI on GaInNAs material. Using the sputtered SiO_2 intermixing process detailed in section 3.8, controlled differential bandgap shifts of over 200nm were obtained from GaInNAs/GaAs MQW structures, which had been annealed to "saturate" the inherent

blue shift beforehand. Secondary Ion Mass Spectrometry (SIMS) analysis revealed that the intermixing mechanism was the result of In and Ga interdiffusion between the QW's and the barriers.

3.4 GaInNAs Intermixing Results

Intermixing experiments were performed using the method detailed in section 3.3.2. From earlier work performed in the department by Walker et al (30), it was found that 50nm thick layers of sputtered SiO_2 produced suitably reliable bandgap shifts, with 500nm thick layers of PECVD SiO_2 found suitable for inhibiting intermixing. The sputtered SiO_2 deposition process was kept constant for the duration of the project. Since intermixing is primarily a diffusion process, the anneal temperature and anneal time are the two most important control parameters. Samples covered with sputtered SiO_2 and PECVD SiO_2 were annealed simultaneously in a rapid thermal annealer (RTA). To control the experiment, only the anneal temperature was varied, with the anneal time remaining constant (1min). The annealing was performed under a nitrogen atmosphere with the samples placed p-side down onto the RTA's Si susceptor. A piece of Si was also placed on top of the sample to inhibit desorption. The samples were typically annealed at temperatures ranging between 650^0C-900^0C. To measure the differential wavelength shift between the samples, a photoluminescence (PL) setup was used. The PL spectra of the samples were measured by attaching the samples to the end of an optical fibre using an acetone/glue mixture. The sample was then immersed in liquid nitrogen to reduce its temperature to 77K in order to reduce phonon scattering effects and hence provide an improved PL signal. Optical excitation of the samples was performed using an Nd:YAG laser

emitting at 1064nm. The PL spectrum emitted by the samples following optical excitation was measured using a monochromator and a cooled Ge detector (77K).

3.4.1 Tampere 1.3μm GaInNAs laser material intermixing results

Figure 3.3 shows the differential shift of the PL spectra for GaInNAs/GaAs samples using the sputtered SiO_2 selective area intermixing technique (see chapter 2, Table 2.1 for material structure). Annealing the samples at 850^0C for 60s provided a 40nm differential wavelength shift. From work previously performed in the department by Walker et al (30), it was found that a 40nm differential shift was sufficient for producing low loss passive intermixed waveguides.

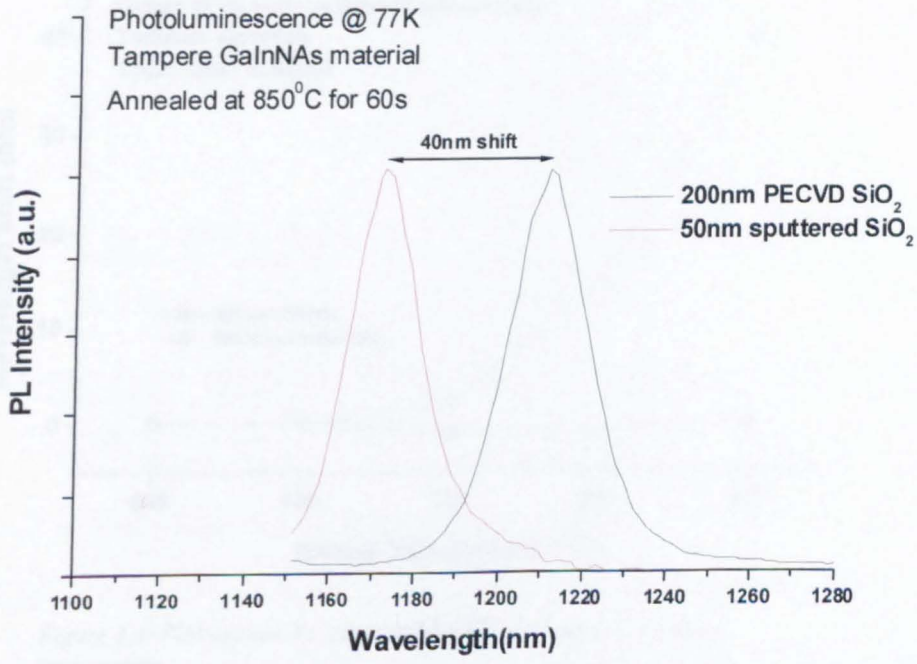

Figure 3.3: Photoluminescence spectra of Tampere 1.3 μm GaInNAs laser material. A differential shift of 40nm is obtained between samples covered with 50nm sputtered SiO_2 and 200nm PECVD SiO_2. Both samples annealed simultaneously at 850^0C for 60s.

Figure 3.4 shows the PL peak wavelength shift as a function of the anneal temperature. From this plot, it can be seen that the samples capped with 50nm sputtered SiO_2 start to intermix above an anneal temperature of 750^0C, whereas the samples capped with 200nm PECVD SiO_2 suppress intermixing for the full range of temperatures investigated. This plot allows the selection of a suitable anneal temperature that can be used in the intermixing process to integrate low loss passive waveguide sections with active laser sections. The ideal condition for intermixing would be to obtain as large a differential shift as possible without intermixing or degrading the active laser section. By annealing the samples at 850^0C for 60s, a differential wavelength shift of 40nm is obtained without causing the active section to intermix.

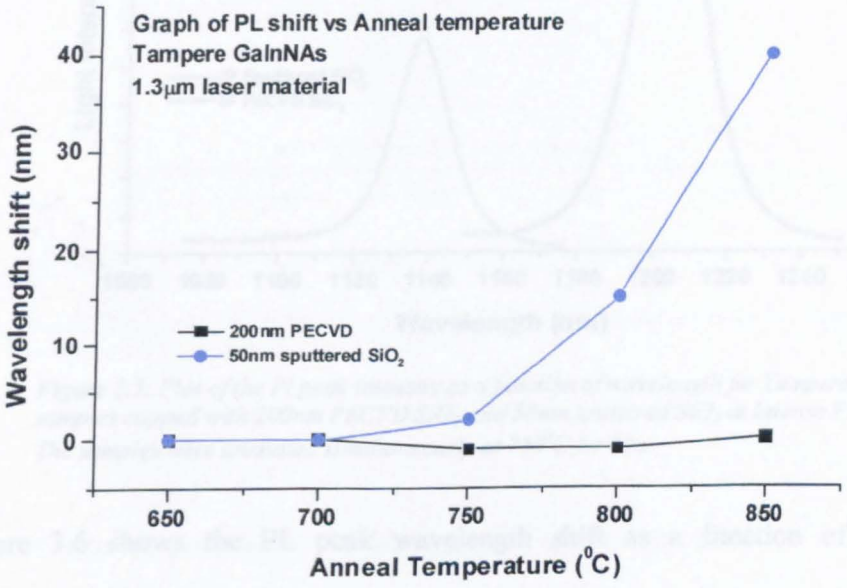

Figure 3.4: Plot of peak PL wavelength shift as a function of anneal temperature.

3.4.2 Intense Intermixing of Tampere 1.3μm GaInNAs material

Intermixing experiments were also performed on the Tampere 1.3μm GaInNAs material at Intense Ltd. Since Intense use the intermixing process for commercial purposes, much of their efforts have involved optimising the intermixing process, particularly the quality of the sputtered SiO_2 film in order to achieve better control of the process. Figure 3.5 shows the differential shift of the PL spectra for GaInNAs/GaAs samples using the sputtered SiO_2 selective area intermixing technique. Annealing the samples at 750^0C for 60s provided a 70nm differential shift.

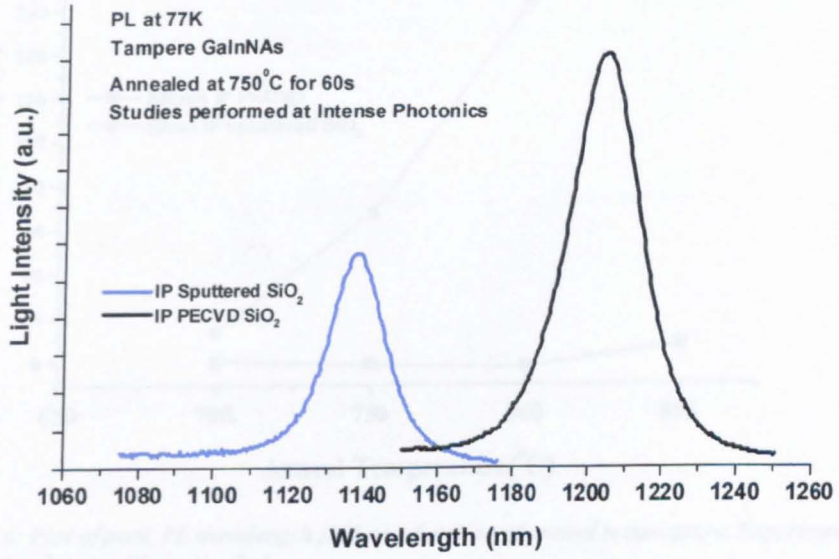

Figure 3.5: Plot of the Pl peak intensity as a function of wavelength for Tampere GaInNAs samples capped with 200nm PECVD SiO_2 and 50nm sputtered SiO_2 at Intense Photonics Ltd. The samples were annealed simultaneously at 750^0C for 60s.

Figure 3.6 shows the PL peak wavelength shift as a function of the anneal temperature. From this plot, it can be seen that the samples capped with 50nm sputtered SiO_2 start to intermix above an anneal temperature of 700^0C, whereas the samples capped with 200nm PECVD SiO_2 suppress intermixing up to an anneal temperature of 800^0C, after which, intermixing starts to occur, presumably due to IFVD taking place. Furthermore, it can be seen that a very large differential

wavelength shift of ~170nm is obtained after annealing the samples at 800^{0}C for 60s, which is much larger than the differential shift obtained at Glasgow University for the same material. Due to the commercial sensitivity of Intense Ltd intermixing process, details of the intermixing process are very limited. However, these results demonstrate the potential of using the sputtered SiO_2 intermixing process on GaInNAs laser material for commercial purposes.

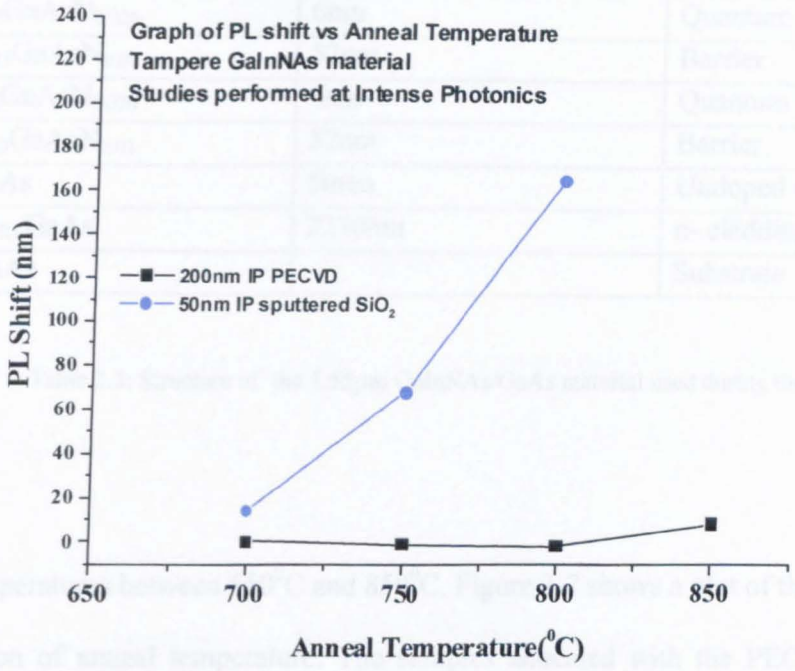

Figure 3.6: Plot of peak PL wavelength shift as a function of anneal temperature. Experiment performed at Intense Photonics Ltd

3.4.3 Intermixing of Sheffield 1.55μm GaInNAs laser material

The sputtered SiO_2 intermixing experiments were also performed at Glasgow University on a prototype 1.55μm GaInNAs material grown by Sheffield University. The material structure is detailed in Table 3.2. Samples of the 1.55μm laser structure were capped with either 50nm sputtered SiO_2 or 200nm PECVD SiO_2, and annealed

Material	Thickness	Layer description
P^+ - GaAs	300nm	Contact layer
P – $Al_{0.6}GaAs$	2250nm	p- cladding
i- GaAs	50nm	Undoped waveguide
$In_{0.023}GaAsN_{0.01}$	52nm	Barrier
$In_{0.38}GaAsN_{0.026}$	6nm	Quantum well
$In_{0.023}GaAsN_{0.01}$	52nm	Barrier
$In_{0.38}GaAsN_{0.026}$	6nm	Quantum well
$In_{0.023}GaAsN_{0.01}$	52nm	Barrier
$In_{0.38}GaAsN_{0.026}$	6nm	Quantum well
$In_{0.023}GaAsN_{0.01}$	52nm	Barrier
i- GaAs	50nm	Undoped waveguide
n- $Al_{0.6}GaAs$	2250nm	n- cladding
n- GaAs	~	Substrate

Table 3.2: Structure of the 1.55μm GaInNAs/GaAs material used during the project

at temperatures between 650^{0}C and 850^{0}C. Figure 3.7 shows a plot of the PL shift as a function of anneal temperature. The samples annealed with the PECVD SiO_2 cap showed negligible shifts up to annealing temperatures of 800^{0}C. However, the samples capped with the sputtered SiO_2 exhibited blueshifts at 750^{0}C. A differential shift of 93nm was measured at 800^{0}C. This was the first report of selective intermixing on GaInNAs quantum wells emitting at 1.55μm.

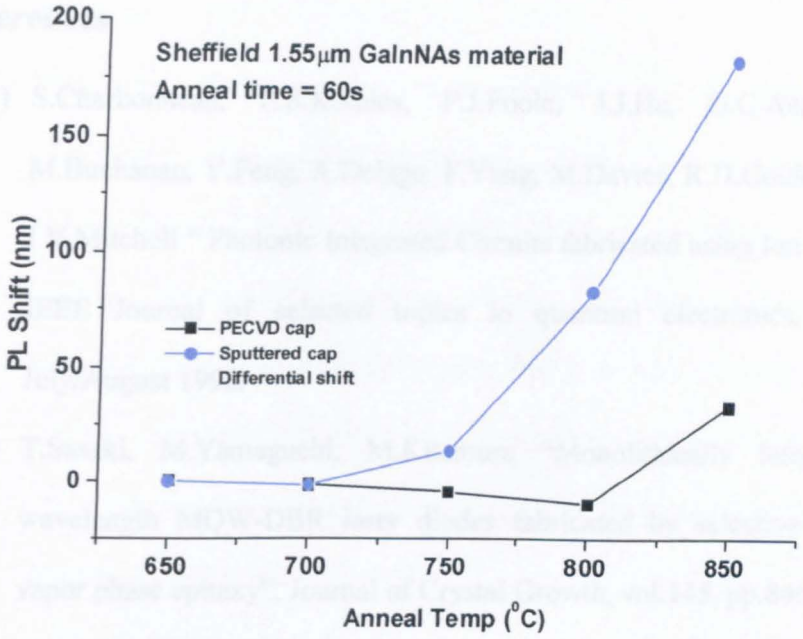

Figure 3.7: Plot of PL shift as a function of anneal temperature for 1.55μm GaInNAs material

3.5 Conclusion

This chapter has given an overview of QWI, explaining the history of QWI, and detailing the techniques used to achieve intermixing. The sputtered SiO_2 intermixing technique that was developed at Glasgow University was detailed, as well as its possible applications. Since this project is primarily concerned with applying the sputtered SiO_2 intermixing technique to GaInNAs in order to monolithically integrate low loss passive sections with active laser sections, intermixing experiments were conducted to confirm the possibility of using the process on GaInNAs material. Suitably large differential wavelengths shifts were obtained from 1.3μm and 1.55μm GaInNAs material.

References

1) S.Charbonneau, E.S.Koteles, P.J.Poole, J.J.He, G.C.Aers, J.Haysom, M.Buchanan, Y.Feng, A.Delage, F.Yang, M.Davies, R.D.Goldberg, P.G.Piva, I.V.Mitchell " Photonic Integrated Circuits fabricated using Ion Implantation", IEEE Journal of selected topics in quantum electronics, vol.4, No.4, July/August 1998.

2) T.Sasaki, M.Yamaguchi, M.Kitamura "Monolithically integrated multi-wavelength MQW-DBR laser diodes fabricated by selective metalorganic vapor phase epitaxy", Journal of Crystal Growth, vol.145, pp.846-851, 1994.

3) N.Holonyak Jr "Impurity induced layer disordering of quantum well heterostructures: Discovery and prospects", IEEE Journal of selected topics in Quantum Electronics, Vol.4, No.4, pp. 584-594, July/August 1998.

4) W.D.Laidig, N.Holonyak Jr, J.M.Brown, M.A.Nixon, P.Gavrilovic, R.D.Burnham, "Disorder of an AlAs-GaAs superlattice by impurity diffusion", Applied Physics Letters, Vol.45, pp. 776-778, May 1981.

5) T.K.Ong, Y.C.Chan, Y.L.Lam, B.S.Ooi, "Wavelength tuning in InGaAs/InGaAsP quantum well lasers using pulsed-photoabsorption-induced disordering", Applied Physics Letters, Vol 78, No 18, April 2001.

6) J.Gebauer, R.Krause-Rehberg, S.Eichler, M.Luysberg, H.Sohn, E.R.Weber,"Ga vacancies in low-temperature-grown GaAs identified by slow positrons", Applied Physics Letters, Vol 71, No.5, pp 638, August 1997.

7) J.S.Tsang, C.P.Lee, J.C.Fan, K.L.Tsai, H.R.Chen, "Compositional disordering of AlGaAs/GaAs superlattices by using the low temperature grown GaAs",

Journal of Vacuum Science & Technology B, Vol 13, No.4, pp1536-1538, July/August 1995.

8) D.G.Deppe, N.Holonyak Jr, "Atom diffusion and impurity-induced layer disordering in quantum well III-V semiconductor heterostructures", Journal of Applied Physics, Vol 64, No.12, pp 93-112, December 1988.

9) J.A.Van Vechten, "Intermixing of an AlAs-GaAs superlattice by Zn diffusion", Journal of Applied Physics, Vol 53, p 7082, October 1982.

10) T.Y.Tan, U.Gosele, "Destruction mechanism of III-V compound quantum well structures due to impurity diffusion", Journal of Applied Physics, Vol 61, No.5, pp 1841-1845, March 1987.

11) Y.Susuki, Y.Horikoshi, M.Kobayashi, H.Okamoto, "Fabrication of GaAlAs window stripe multi-quantum-well heterostructure lasers utilising Zn diffusion-induced alloying", Electronics Letters, Vol.20, No.9, pp 383-384, April 1984.

12) D.G.Deppe, K.C. Hsieh, N.Holonyak Jr, "Low-threshold disorder-defined buried heterostructure $Al_xGa_{1-x}As$-GaAs quantum well lasers", Journal of Applied Physics, Vol 58, No.12, pp 4515-4520, December 1985.

13) J.H.Marsh, "Quantum Well Intermixing", Semiconductor Science Technology, Vol 8, pp 1136-1155, February 1993.

14) P.Gavrilovic, D.G.Deppe, K.Meehan, N.Holonyak Jr, J.J.Coleman, "Implantation disordering of $Al_xGa_{1-x}As$ superlattices", Applied Physics letters, Vol 47, No.2, pp 130-132, July 1985

15) M.O'Neill, A.C.Bryce, J.H.Marsh, R.M.De La Rue, "Multiple quantum well optical waveguides with large absorption edge blue shift produced boron and

fluorine impurity-induced disordering", Applied Physics Letters, Vol 55, No.14, pp 1373-1375, October 1989.

16) M.O'Neill, J.H.Marsh, R.M.De La Rue, "Reduction of the propagation losses in impurity disordered quantum well waveguides", Electronics Letters, Vol 26, No 19, pp 1613-1615, September 1990.

17) P.G.Piva, R.D.Goldberg, I.V.Mitchell, "Reduced 980nm laser facet absorption by bandgap shifted extended cavities", Journal of Vacuum Science Technology B, Vol 16, No.4, pp 1790-1793, Jul/Aug 1998.

18) J.Hashimoto, N.Ikoma, M.Murata, T.Katsuyama, "A highly reliable GaInAs-GaInP 0.98μm window laser", IEEE Journal of Quantum Electronics, Vol.36, No.8, pp 971-977, August 2000.

19) J.E.Epler, R.D.Burnham, R.L.Thorton, T.L.Paoli, M.C.Bashaw, "Laser induced disordering of GaAs-AlGaAs superlattice and incorporation of Si impurity", Applied Physics Letters, Vol 49, No.21, pp 1447-1449, November 1986.

20) C.J.McLean, J.H.Marsh, R.M.De La Rue, A.C.Bryce, B.Garrett, R.W.Glew, "Layer selective disordering by photoabsorption-induced thermal diffusion in InGaAs/InP based multiquantum well structures", Electronics Letters, Vol 28, No.12, pp 1117-1119, June 1992.

21) A.McKee, C.J.McLean, G.Lullo, A.C.Bryce, R.M.De La Rue, J.H.Marsh, "Monolithic integration in InGaAs-InGaAsP multiple quantum well structures using laser intermixing", IEEE Journal of Quantum Electronics, Vol 33, No.1, pp 45-55, January 1997.

22) B.S.Ooi, K.McIlvaney, M.W.Street, A.S.Helmy, S.G.Ayling, A.C.Bryce, J.H.Marsh, J.S.Roberts, "Selective quantum well intermixing in GaAs-

AlGaAs structures using impurity free vacancy diffusion", IEEE Journal of Quantum Electronics, Vol 33, No 10, October 1997.

23) D.G.Deppe, L.J.Guido, N.Holonyak, K.C. Hsieh, R.D.Burnham, R.L.Thornton, T.L.Paoli, "Stripe geometry quantum well heterostructure $Al_xGa_{1-x}As$-GaAs lasers defined by defect diffusion", Applied Physics Letters, Vol 49, No.9, pp 510-512, Sept 1986.

24) J.Beauvais, J.H.Marsh, A.H.Kean, A.C.Bryce, C.Button, "Suppression of bandgap shifts in GaAs/AlGaAs quantum wells using strontium fluoride caps", Electronics Letters, Vol 28, No.17, pp 1670-1672, August 1992.

25) I.Gontijo, T.Krauss, R.M.De La Rue, J.S.Roberts, J.H.Marsh, "Very low loss extended cavity GaAs/AlGaAs lasers made by impurity-free vacancy diffusion", Electronics Letters, Vol 71, No 5, August 1997.

26) S.D.McDougall, O.P.Kowalski, C.J.Hamilton, F.Camancho, B.Qiu, M.Ke, R.M.De La Rue, A.C.Bryce, J.H.Marsh, "Monolithic integration via a universal damage enhanced quantum well intermixing technique", IEEE Journal of selected topics on Quantum Electronics, Vol 4, No.4, pp 636-646, July/August 1998.

27) K.Bubke, M.Sorel, F.Robert, A.C.Bryce, J.M.Arnold, J.H.Marsh, "Loss measurements in intermixied InGaAs/AlGaInAs Multiple-Quantum-Well Ridge Waveguides", IEEE WFOPC conference, Glasgow, 2002.

28) X.F.Liu, B.C.Qiu, M.Ke, A.C.Bryce, J.H.Marsh, "Control of Multiple Bandgap shifts in InGaAs-AlInGaAs Multiple-Quantum-Well material using different thickness of PECVD SiO_2 protection layers", IEEE Photonics Technology Letters, Vol 12, No.9, pp 1141-1143, September 2000.

29) R.Macaluso, H.D.Sun, M.D.Dawson, F.Robert, A.C.Bryce, J.H.Marsh, H.Riechert, "Selective modification of bandgap in GaInNAs/GaAs structures by quantum well intermixing", Applied Physics Letters, Vol 82, No.24, pp 4259-4261, June 2003.

30) C.L.Walker, A.C.Bryce, J.H.Marsh, "Improved catastrophic optical damage level from laser with Nonabsorbing Mirrors", IEEE Photonics Technology Letters, Vol 14, pp 1394-1396, October 2002.

31) C.S.Peng, T.Jouhti, P.Laukkenen, E.M.Pavelescu, J.Kontinnen, W.Li, M.Pessa, "1.32μm GaInNAs/GaAs laser with low threshold current density". IEEE Photon.Tech.Lett, 14, pp.275-277 (2002)

Chapter 4

Single Mode Ridge Waveguide Lasers

4.1 Introduction

Single mode ridge waveguide lasers are highly desirable for applications that require efficient coupling of the laser beam to an optical fibre. However, obtaining single mode operation from an edge-emitting laser is far from trivial. This chapter outlines the main issues involved in achieving single mode laser operation by focussing on the design, fabrication and characterisation of single mode edge emitting lasers. Single mode operation in semiconductor lasers and single mode waveguiding regimes are discussed in section 4.2. The design and simulation of single mode ridge waveguide lasers are featured within section 4.3, after which a detailed account of the fabrication process used during this research is given in section 4.4. Section 4.5 discusses the results obtained from the single mode laser devices fabricated during the project. Section 4.6 concludes the chapter.

4.2 Single mode laser operation

As discussed in chapter 1, single mode edge-emitting lasers are essential for applications that require efficient coupling of the laser beam to an optical fibre. Achieving single mode output from an edge-emitting laser requires careful consideration of the material and device design, in order to maintain single mode operation in both the vertical and lateral directions. Confinement of the optical mode in the vertical direction is achieved by the discontinuity in the refractive index

between the cladding layers and the active region in heterostructure lasers. Since epitaxial growth allows accurate control over layer refractive index (via composition) and thickness, the waveguide can be designed to support only the fundamental mode. Moreover, the typically central location of the QW's in the core waveguide ensures that the fundamental mode receives significantly greater modal gain than higher order modes, which also assists single mode operation. Modal confinement in the lateral direction can be achieved by three different guiding methods: gain guiding, index guiding, or combined gain and index guiding.

4.2.1 Gain guiding lasers

In gain-guided lasers, the current injection is limited to a narrow stripe along the cavity length providing a narrow region of optical gain in the lateral direction. Waveguiding of light occurs in this region of high gain. Away from this region, light will experience a high amount of loss and will not be guided. Due to their relatively simple fabrication process, gain-guided lasers were investigated in the early development of edge emitting lasers. However, it was thereafter realised that gain-guided lasers were not without their problems. Research conducted on gain-guided lasers revealed a strong dependence between the optical mode, gain, refractive index, and carrier density, which can lead to hole burning and filamentation effects at high current injection levels, which in turn can cause lateral mode instabilities and excitation of higher order waveguide modes (1,2). These problems prevent gain-guided lasers from being useful for achieving high power single mode operation.

4.2.2 Index guiding lasers

Index-guided lasers use a change of refractive index in the lateral direction to guide the optical mode. The change in refractive index can be achieved by lateral changes in material or doping. An example of a device with an index guiding system is the buried heterostructure laser. To fabricate such a device, a ridge structure is etched into the material, etching all the way through the active region. Following the etch process, a new material of lower refractive index is grown around the ridge, thus forming a rectangular dielectric waveguide. By careful choice of the device dimensions and materials (i.e. refractive index), maximum preference to single-mode operation can be achieved. As lateral mode confinement in index-guided lasers does not vary with current injection, variations of gain in the device should not have detrimental effects on the guided mode, therefore circumventing the gain associated problems experienced by the guided mode in gain-guided lasers. However, by employing strong index guiding for device fabrication, a very narrow waveguide is required to ensure single-mode operation, which is difficult to fabricate, as well as difficult to inject current into. Moreover, an undesirable regrowth stage is required to realise index-guided devices, which adds further to the difficulty of the fabrication.

4.2.3 Ridge Waveguide lasers

Some index-guiding can be induced in gain-guided lasers by making the upper cladding layer non-uniform. The ridge waveguide laser (RWL) shown in figure 4.1 is an example of such a device. The guiding mechanisms involved in a RWL are generally quite complex, and can exhibit varying degrees of gain or index guiding, depending on the choice of the device parameters. Since RWL's operate in the waveguiding regime between that of gain-guiding devices and strong index-guided

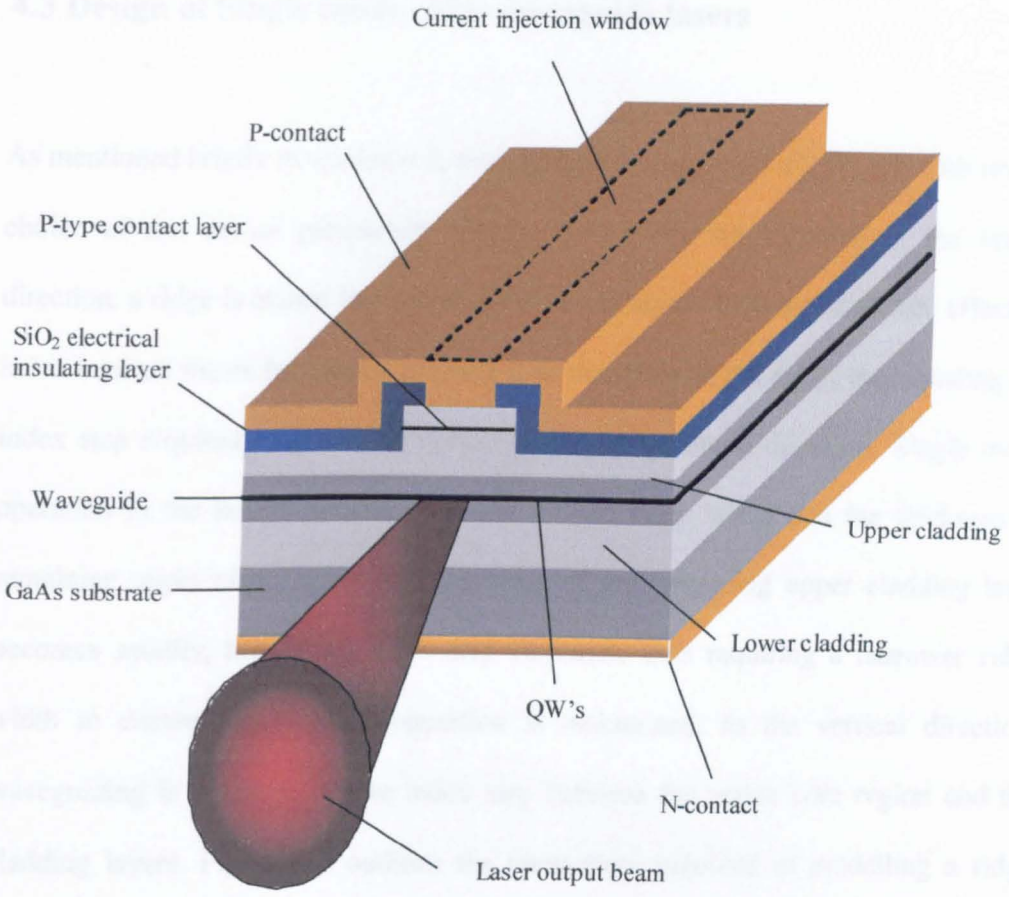

Fig 4.1: Diagram of typical ridge waveguide laser.

devices, the problems associated with both guiding systems can be alleviated to a certain extent, allowing laser devices to be easily fabricated that can achieve stable lateral mode operation at reasonable injection levels. Because of the ease of fabrication, RWL's are employed in this research. Furthermore, RWL's are suitable structures to be used in conjunction with quantum well intermixing, allowing the integration of active and passive waveguides, where both waveguides use the same guiding mechanism. This ensures minimum disruption to the mode profile in passing from the active to the passive waveguide sections and vice versa.

4.3 Design of Single mode ridge waveguide lasers

As mentioned briefly in section 4.2, the guiding mechanism of a RWL depends on the choice of the device parameters. Firstly, to achieve waveguiding in the lateral direction, a ridge is etched into the upper cladding layer of the material. The effective index beneath the etched region is lower than that beneath the ridge, thus creating the index step required to guide the optical mode in the lateral direction. Single mode operation in the lateral direction depends on the ridge width and the thickness of remaining upper cladding. As the thickness of the remaining upper cladding layer becomes smaller, the lateral index step increases, thus requiring a narrower ridge width to ensure single mode operation is maintained. In the vertical direction, waveguiding is achieved by the index step between the active core region and the cladding layers. Figure 4.2 outlines the parameters involved in modelling a ridge waveguide. Because of the mathematical difficulty involved in solving the wave equation for such structures, a computer program was used to model the device. The modelling of the ridge waveguide was performed using a program called FIMMWAVE.

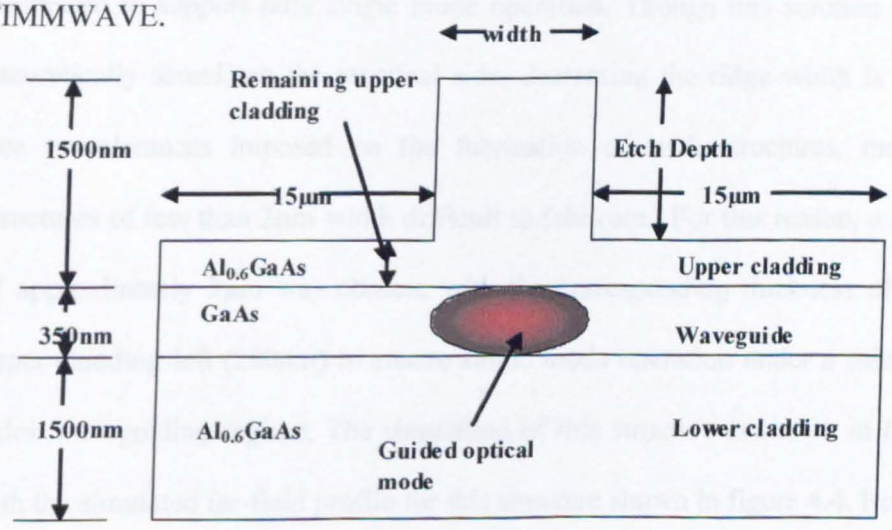

Figure 4.2: Diagram showing the ridge waveguide structure modelled using FIMMWAVE

The program requires information on the layer thickness and refractive index, as well as ridge width and upper cladding etch depth. From the information provided, the program can simulate the modal profile, and establish whether only the fundamental mode is supported by the waveguide. The waveguide structure and parameters displayed in figure 4.2 were modelled for this research. The value of refractive index for each layer in the material were calculated using programs based on papers by Adachi (3) and Marple (4). The QW's were not included in the model since the modal overlap with these layers is very small and would have little effect on the waveguiding characteristics. Different values for ridge width and thickness of remaining upper cladding were selected and simulated to achieve single mode operation. Figure 4.3 shows the results of several simulations. As it is important to have a strong index guiding mechanism, the lateral index step must be as large as possible. This can be achieved by decreasing the thickness of remaining upper cladding in the etched regions. However, decreasing the thickness of remaining upper cladding can result in the ridge waveguide structure supporting higher order modes, as shown in figure 4.3a. To combat such behaviour, the ridge width would need to be decreased to support only single mode operation. Though this solution may appear theoretically sound, on the practical side, decreasing the ridge width is undesirable due to tolerances imposed on the fabrication of such structures, making ridge structures of less than 2μm width difficult to fabricate. For this reason, a ridge width of approximately 3μm was chosen, with the corresponding thickness of remaining upper cladding left (200nm) to ensure single mode operation under a suitably strong index waveguiding regime. The simulation of this structure is shown in figure 4.3c, with the simulated far-field profile for this structure shown in figure 4.4. Both of these results clearly show single-mode operation.

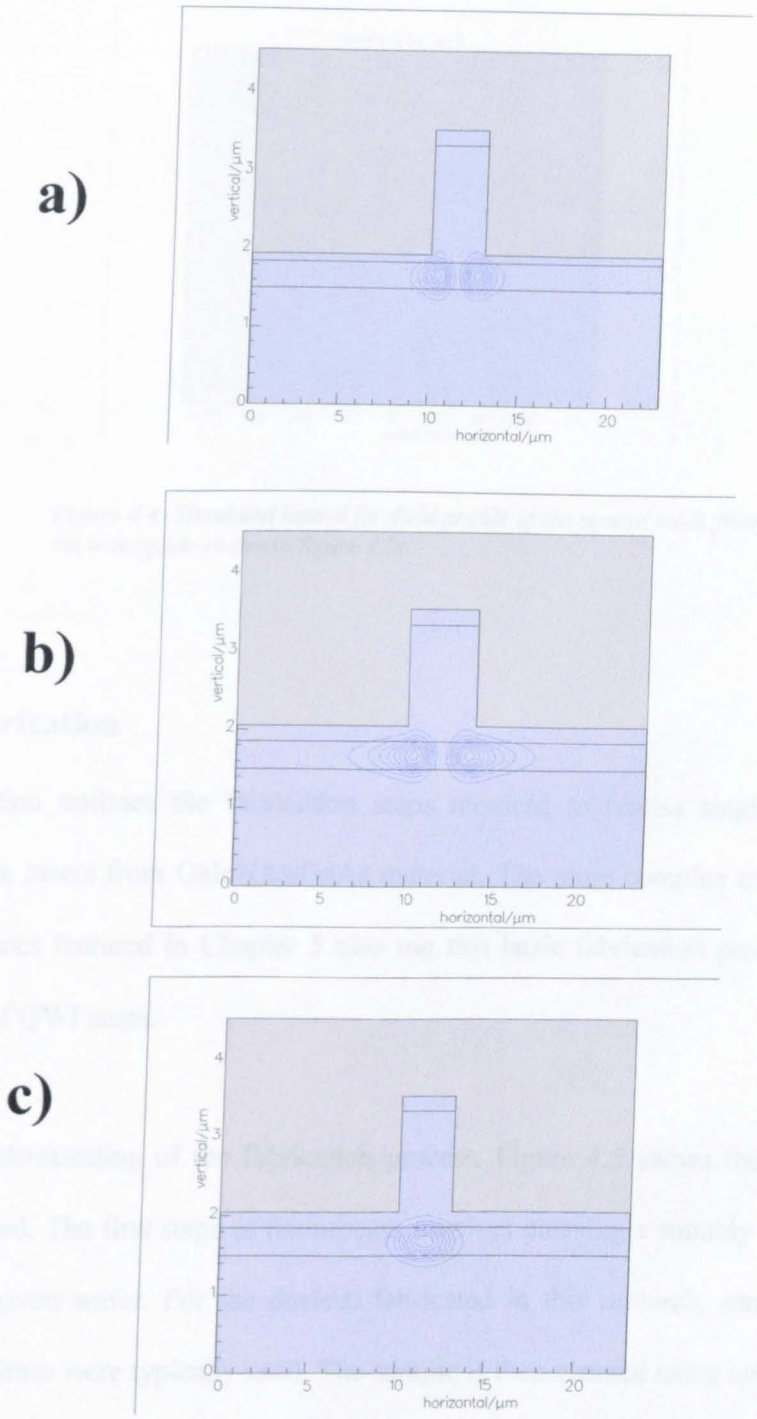

Figure 4.3: Diagram showing the results of various simulations performed using FIMMWAVE. a) Simulation result of a 3µm ridge with 100nm of upper cladding remaining. The deeper etch depth results in multi-mode operation. b) Simulation result of a 4µm ridge with 200nm of upper cladding remaining. The wider ridge width clearly allows multi-mode operation. c) Simulation result of a 3µm ridge with 200nm remaining upper cladding. This structure clearly shows single mode operation. .

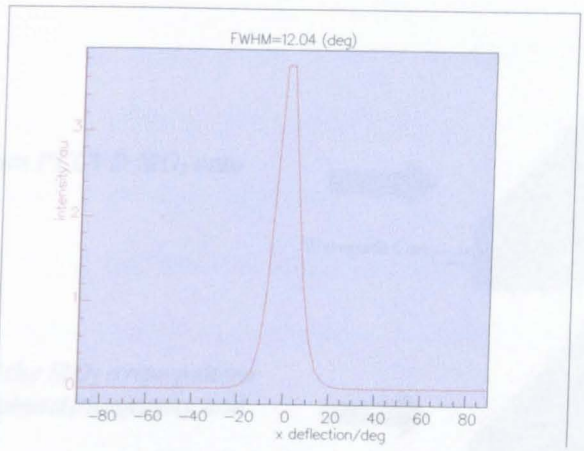

Figure 4.4: Simulated lateral far-field profile of the optical mode from the waveguide shown in figure 4.3c.

4.4 Fabrication

This section outlines the fabrication steps required to realise single mode ridge waveguide lasers from GaInNAs/GaAs material. The more complex extended cavity laser devices featured in Chapter 5 also use this basic fabrication process, with the addition of QWI steps.

To aid understanding of the fabrication process, Figure 4.5 shows the step-by-step process used. The first stage of the process involves cleaving a suitably sized sample from the given wafer. For the devices fabricated in this research, samples of size 12mm x 10mm were typically used. The sample is then cleaned using acetone (5mins in ultrasonic bath), methanol (5mins in ultrasonic bath), followed by a rinse in reverse osmosis (R.O.) water for 5mins. The sample is then blow-dried using a nitrogen airgun and inspected under a microscope to ensure that a suitable level of cleanliness has been achieved in order to continue the fabrication process.

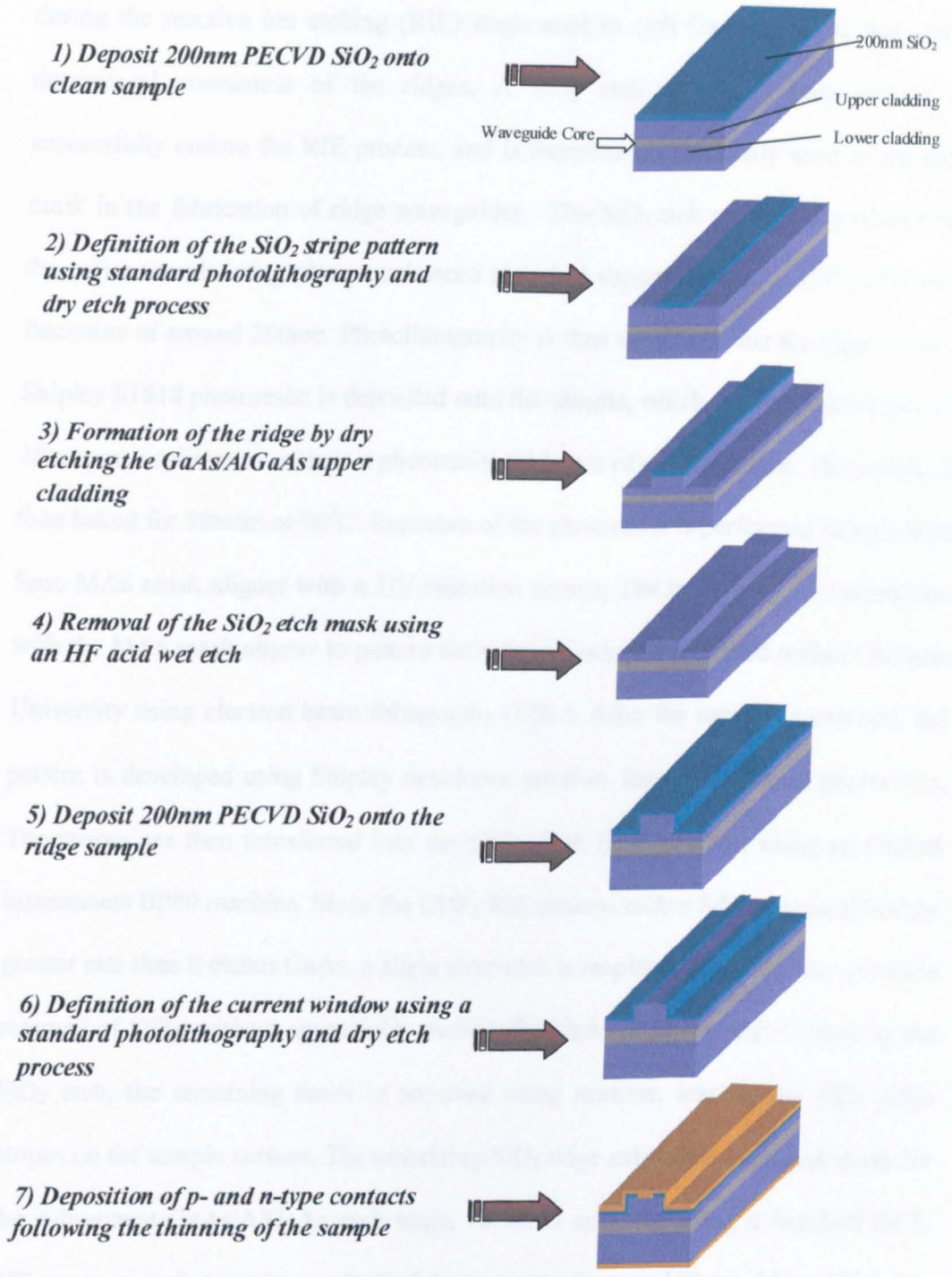

Fig 4.5: Diagram outlining the step process used to fabricated ridge waveguide lasers

In order to etch ridges onto the sample, a suitable etch mask is necessary. Using photoresist as an etch mask is possible, however deterioration of this mask can occur during the reactive ion etching (RIE) stage used to etch GaAs/AlGaAs, and cause detrimental coarseness of the ridges. A SiO_2 etch mask has been proven to successfully endure the RIE process, and is therefore preferentially used as the etch mask in the fabrication of ridge waveguides. The SiO_2 etch mask is deposited over the entire sample using plasma enhanced chemical vapour deposition (PECVD), to a thickness of around 200nm. Photolithography is then used to define the ridge stripes. Shipley S1818 photoresist is deposited onto the sample, which is spun at 4000rpm for 30secs on a spinner to achieve a photoresist thickness of around 1.8μm. The sample is then baked for 30mins at 90^0C. Exposure of the photoresist is performed using a Karl Suss MA6 mask aligner with a UV radiation source. The mask used in conjunction with the MA6 mask aligner to pattern the ridge stripes was produced within Glasgow University using electron beam lithography (EBL). After the sample is exposed, the pattern is developed using Shipley developer solution, leaving stripes of photoresist. The stripes are then transferred into the SiO_2 mask by CHF_3 RIE using an Oxford instruments BP80 machine. Since the CHF_3 RIE process etches SiO_2 at a considerably greater rate than it etches GaAs, a slight over-etch is employed to ensure the complete removal of SiO_2, without appreciably etching the GaAs layer beneath. Following the SiO_2 etch, the remaining resist is removed using acetone, leaving the SiO_2 ridge stripes on the sample surface. The remaining SiO_2 ridge stripes act as an etch mask for the subsequent GaAs/AlGaAs etch stage, which is achieved using a standard $SiCl_4$ RIE process performed by an Oxford Instruments System 100 machine. Since the thickness of remaining upper cladding has a large influence on the single mode operation of the ridge waveguide, laser interferometry is employed within the System

100 machine to ensure an etch accuracy of within 50nm is reached (5). Afterwards, the SiO_2 mask stripes are removed using HF acid etch. The next stage in the fabrication is to create an opening on top of the ridge through which current can flow. This is achieved by depositing a 200nm PECVD SiO_2 layer over the sample, which covers the entire ridge, followed by a photolithography step to define a window on top of the ridge. The photoresist pattern is then etched into the 200nm PECVD SiO_2 layer using the CHF_3 RIE process. The remaining photoresist is then removed using acetone. The remaining PECVD SiO_2 provides sufficient electrical isolation at the ridge sidewalls and other etched regions. With the current injection window opened, the p-type metal contact can be deposited. To make sure there are no unfavourable native oxides on the sample surface before the contact deposition, the sample is deoxidised by placing it in a solution of 4:1 H_2O/HCl acid for 30s. Following deoxidation, the sample is loaded into an e-beam evaporator, within which it has the following metal layers sequentially evaporated: Ti (33nm)/ Pd (33nm)/ Au (240nm). This evaporation process provides poor coverage of the ridge sidewalls, which can seriously impede current injection into the device. Because of this, a further metallisation stage (NiCr (15nm)/ Au (100nm)) is performed in an e-beam evaporator at an angle of 45^0 from two opposite directions to ensure full coverage of both the sidewalls. After the p-type contact evaporation, the sample is thinned to make the sample easier to cleave into individual devices, as well as decrease the substrate resistance. The sample is mounted on a glass coverslip with photoresist p-side down, before being mounted onto a metal chuck using wax. The glass coverslip is used to prevent the sample from coming into contact with the wax during this process, as wax is difficult to remove. The sample is then ground down by using a glass plate and alumina grit, until a measured thickness of between 150μm and 200μm is reached.

Following this process, the sample can be removed from the coverslip using acetone and thoroughly cleaned. Before the n-type contact is deposited, the sample must once again be deoxidised using the 4:1 H_2O/HCl acid solution. Resembling the p-contact process, the n-contact is deposited using an e-beam evaporator, which sequentially deposits the following metals: Au(11nm)/Ge(11nm)/Au(11nm)/Ni(14nm) /Au(240nm). Once the n-contact process has been completed, the sample is annealed at 360^0C for 60s in a rapid thermal annealer, in order to form the ohmic contacts. Individual laser devices can then be cleaved from the sample, with special attention being paid to the cleaved facets, to ensure the creation of good quality mirrors.

4.5 GaInNAs Ridge Waveguide Laser Results

The scanning electron microscope (SEM) image of a fabricated GaInNAs ridge waveguide laser is shown in figure 4.6. These devices were fabricated simultaneously on the same laser chip as the extended cavity devices featured in Chapter 5.

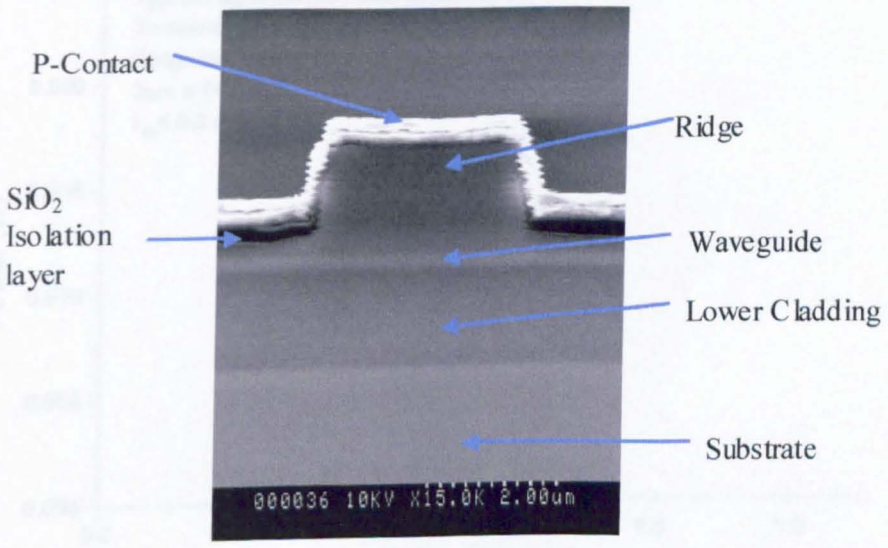

Figure 4.6: SEM image of a GaInNAs ridge waveguide laser

As intended, the ridge is approximately 3μm wide, with a remaining upper cladding thickness between 150-200nm. These device dimensions are close to those used to simulate the modal properties of the device in section 4.3, and should therefore be sufficient for supporting single mode operation.

A pulsed test setup featuring a box-car averaging system was used to measure the light-current (L-I) characteristics of the laser. An Avtech pulsed current source generating 400ns pulses at a 1kHz repetition rate was used to supply current to the devices, which were mounted in a gold plated clip. Light was collected from one laser facet by a Germanium detector. Figure 4.7 shows the L-I characteristic of the 1000μm long GaInNAs ridge waveguide laser featured in figure 4.6. From this plot, a threshold current of 300mA and an external quantum efficiency of ~14% are obtained.

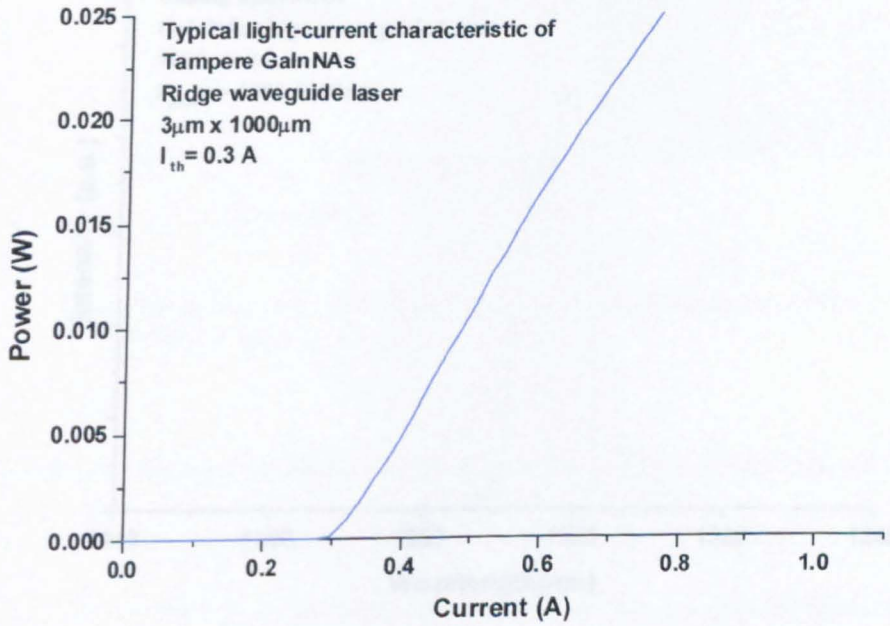

Figure 4.7: Light –current (L-I) characteristic of a 3μm x 1000μm GaInNAs ridge waveguide laser.

As explained in Chapter 2, section 2.7.1, the lasing characteristics for this material are far poorer than similar GaInNAs material grown previously by the same growers (6). However, since the project concerns relative comparison of intermixed and non-intermixed laser devices, these results will be sufficient to prove the concept of device integration using GaInNAs material.

The lasing spectrum of the device operating above threshold is shown in figure 4.8, indicating that the laser emission wavelength lies in the region of 1295-1300nm. Figure 4.9.a) shows the far-field beam profile of the laser. The far-field lateral beam profile was also measured using the pulsed test setup. The laser clip was mounted on a computer controlled rotational stage, at the centre of rotation, and the photodiode detector was placed around 10cm away from the device facet with a narrow slit immediately in front of it.

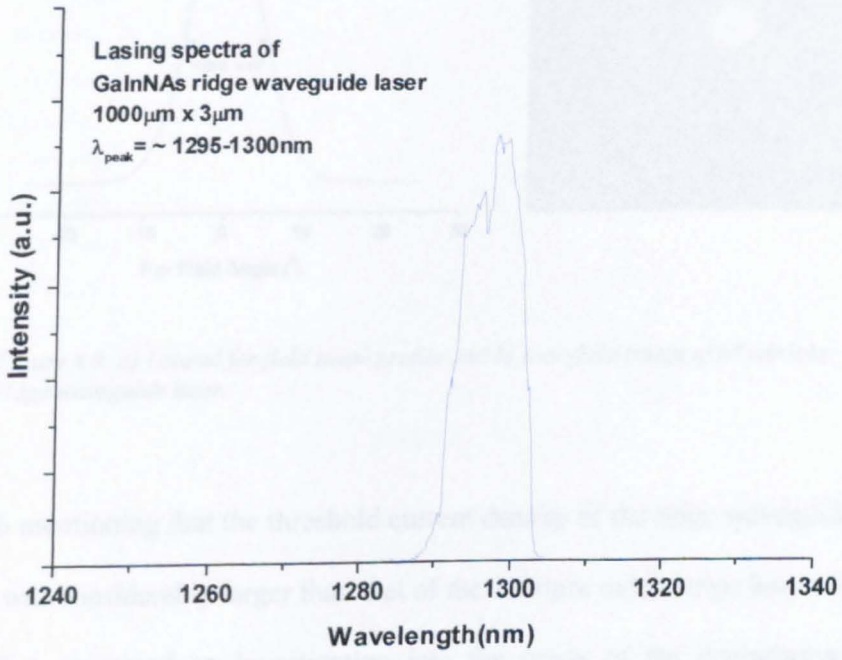

Figure 4.8: Lasing spectrum of a GaInNAs ridge waveguide laser

By rotating the laser device across the fixed detector/slit combination, the beam profile could be determined. From figure 4.9.a) it can be clearly seen that the laser is operating in a single lateral mode, and is in good agreement with the far-field simulation conducted in section 4.3. A near-field measurement was also performed in order to confirm single mode operation in both the lateral and vertical directions. The near-field image was captured by focussing a 40x microscope lens onto the facet of the ridge waveguide laser during operation. The beam image was then collected by a Hamamatsu camera, which subsequently sent the image to a computer using image capture software. Figure 4.9.b) shows the beam image captured, showing single mode operation in both the lateral and vertical directions.

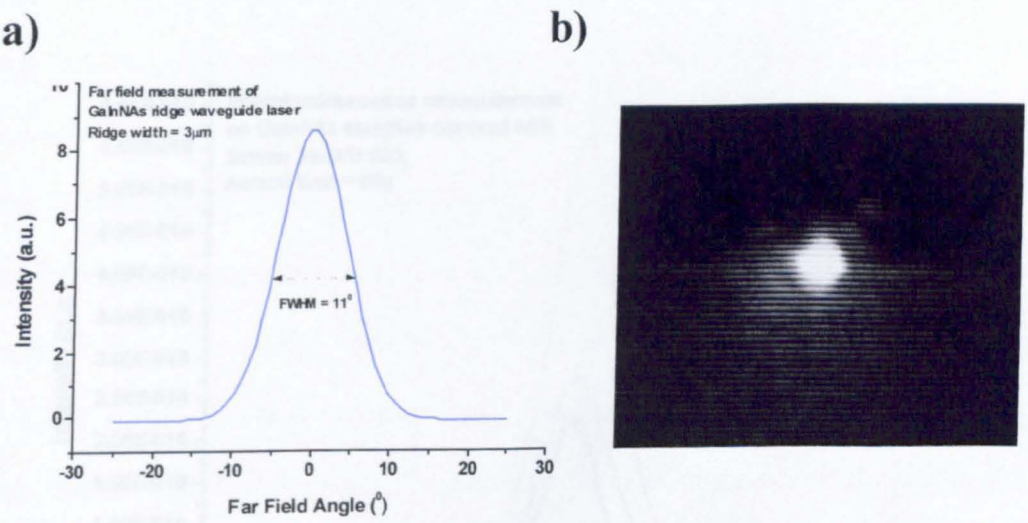

Figure 4.9: a) Lateral far-field beam profile and b) near-field image of a GaInNAs ridge waveguide laser.

It is worth mentioning that the threshold current density of the ridge waveguide lasers (RWL's) was considerably larger than that of the 1000μm oxide stripe lasers (OSL's). This finding prompted an investigation into the cause of the degradation in the performance of the RWL's. The only major difference in the fabrication process

between the OSL's and the RWL's was the addition of the annealing process to the RWL fabrication, and therefore the annealing step was investigated foremost. As shown in figure 4.10, the PL intensity of GaInNAs samples capped with PECVD SiO_2 was measured at Intense. Interestingly, the PL intensity more than doubled in the GaInNAs samples annealed at 750^0C for 60s. However, the PL intensity decreased by a factor of 4 in the GaInNAs samples annealed at 850^0C for 60s. Since the RWL's and the extended cavity lasers (ECL's) were fabricated simultaneously on the same chip (see chapter 5, section 5.5), the material was annealed at 850^0C for 60s in order to create intermixed sections for the ECL's, thus explaining the degradation in threshold current density between the RWL's and the OSL's. The degradation itself could be attributed to the activation of non-radiative defects caused by the high temperature

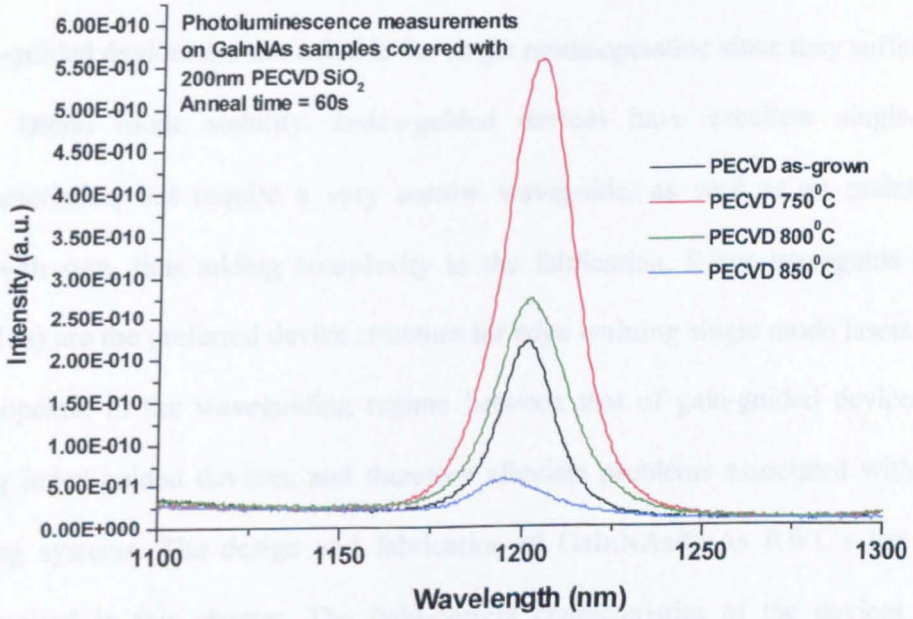

Figure 4.10: Graph showing the variation of PL intensity measured from GaInNAs with anneal temperature.

anneal required in the intermixing process. Although this seems like a problem for incorporating the quantum well intermixing process at Glasgow University to the

GaInNAs material, the superior intermixing process used by Intense enabled intermixing to occur in this material at much lower temperatures (chapter 3, section 3.4.2) , thus alleviating the problem of device degradation with high anneal temperatures. By carefully choosing the annealing conditions for the Intense intermixing process, it may be possible to simultaneously create low-loss intermixed passive sections whilst improving the optical quality of the active sections in GaInNAs laser devices.

4.6 Conclusion

Single mode edge-emitting lasers are essential for applications that require efficient coupling of the laser beam to an optical fibre. Achieving single mode output from an edge-emitting laser requires careful consideration of the material and device design. Gain-guided devices are not suitable for single mode operation since they suffer from poor lateral mode stability. Index-guided devices have excellent single-mode characteristics, but require a very narrow waveguide, as well as an undesirable regrowth step, thus adding complexity to the fabrication. Ridge waveguide lasers (RWL's) are the preferred device structure for edge emitting single mode lasers since they operate in the waveguiding regime between that of gain-guided devices and strong index-guided devices, and therefore alleviate problems associated with both guiding systems. The design and fabrication of GaInNAs/GaAs RWL's has been summarised in this chapter. The light-current characteristics of the devices were measured, showing good laser operation. Near and far-field measurements confirmed single-mode operation in both the vertical and lateral directions. These results were shown to be in good agreement with the simulations performed.

4.9 References

1. K.Kobayashi "Optoelectronic and Lightwave Communication Systems-Transverse Mode control in Semiconductor lasers" published by Van Nostrand Reinhold, New York, 1989.
2. N.W.Carlson "Monolithic Diode Laser Arrays", published by Springer, 1994.
3. S.Adachi "GaAs, AlAs, $Al_xGa_{1-x}As$ material parameters for use in research and device applications", Journal of Applied Physics, Vol 58, No 3, pp 1-30, August 1985.
4. D.T.F.Marple "Refractive Index of GaAs", Journal of Applied Physics, Vol 35, No.4, pp 1241-1242, April 1964.
5. S.E.Hicks, W.Parkes, J.A.H.Wilkinson, C.D.W.Wilkinson "Reflectance modelling for in situ dry etch monitoring of bulk SiO_2 and III-V multilayer structures", Journal of Vacuum Science & Technology, B , Vol 12, No.6, pp 3306-3310, Nov/Dec 1994.
6. C.S.Peng, N.Laine, J.Konttinen, T.Jouhti, M.Pessa "Low Threshold, High Power and Long Lifetime InGaAsN/GaAs lasers", IEE Proceedings-Optoelectronics, Vol 151, No 5, 426-428, October 2004.

Chapter 5

Extended Cavity GaInNAs Ridge Waveguide Lasers

5.1 Introduction

Single mode laser operation under high drive current is limited mainly by facet degradation. By incorporating a passive extended cavity to the output facet of such devices, the factors that limit the single mode operation at high power can be suppressed. This chapter describes the incorporation of extended cavities to the GaInNAs ridge waveguide lasers described in chapter 4, using the sputtered SiO_2 QWI technique mentioned in chapter 3. Fig 5.1 shows a schematic diagram of the extended cavity laser device investigated for this research. Section 5.2 discusses the limiting factors of high power single mode laser operation, and an overview of the suppression of such limiting factors is detailed in section 5.3. Extended cavity lasers are introduced in section 5.4. The design and fabrication of the extended cavity lasers investigated is described in section 5.5. The results and discussion are explained in section 5.6, before the conclusion in section 5.7.

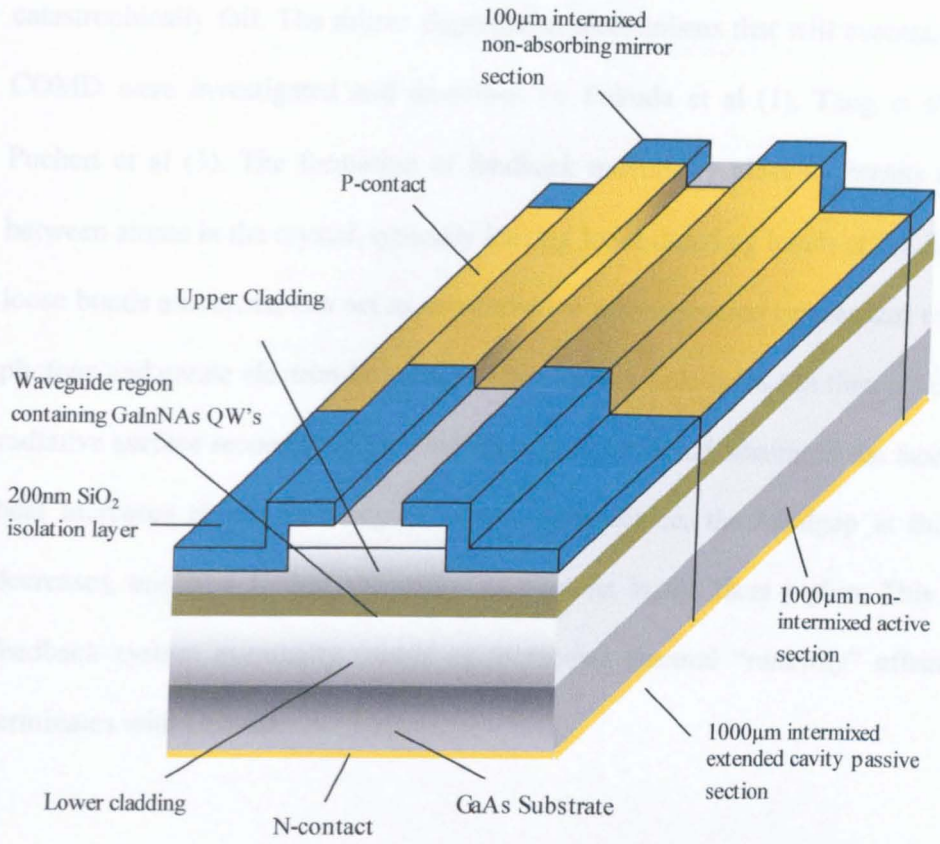

Figure 5.1: Schematic diagram of a 3μm ridge waveguide laser with an intermixed extended cavity passive section and non-absorbing mirror section.

5.2 High Power Single Mode Laser limitations

In order to fully understand the functionality of the extended cavity laser, this section will address in detail the main factors that cause detriment to high power single mode lasers.

5.2.1 Catastrophic Optical Mirror Damage (COMD)

Catastrophic optical mirror damage (COMD) occurs when heating at the laser facet becomes too high and causes the facet to melt. The melting of the facet causes the laser feedback system to be disrupted, which in turn causes the device to

catastrophically fail. The mirror degradation mechanisms that will eventually lead to COMD were investigated and described by Fukuda et al (1), Tang et al (2), and Puchert et al (3). The formation of feedback mirrors by cleaving breaks the bonds between atoms in the crystal, typically leaving loose dangling bonds at the facet. Such loose bonds and atoms can act as non-radiative recombination centres that can absorb photons and create electron-hole pairs. The electron-hole pairs can then undergo non-radiative surface recombination, which results in localised heating at the facet. As the heat increases at the facet region of the laser device, the bandgap at this region decreases, enabling further absorption of photons in the facet region. This positive feedback system eventually causes an increasing thermal "runaway" effect, which terminates with COMD.

Facet oxidation is also a source of non-radiative recombination centres, which further promote the mirror degradation mechanism. The loose bonds and atoms that are exposed following cleaving are subject to water vapour and other oxidising agents contained in the air, thus promoting facet oxidation. The facet oxides can absorb photons, which leads to localised heating at the facet region. The localised heating at the facet not only reduces the bandgap in this area, but also promotes further oxidation to occur at the facet. This causes more non-radiative recombination centres on the facet, which can in turn cause greater absorption of photons, and enhance heating at the facet. It is clear that this process is also a positive feedback mechanism that contributes to mirror degradation. The problems caused by facet oxidation are more significant for lasers containing AlGaAs. Tang et al (2) investigated mirror degradation in AlGaAs ridge waveguide lasers, and provided useful information about

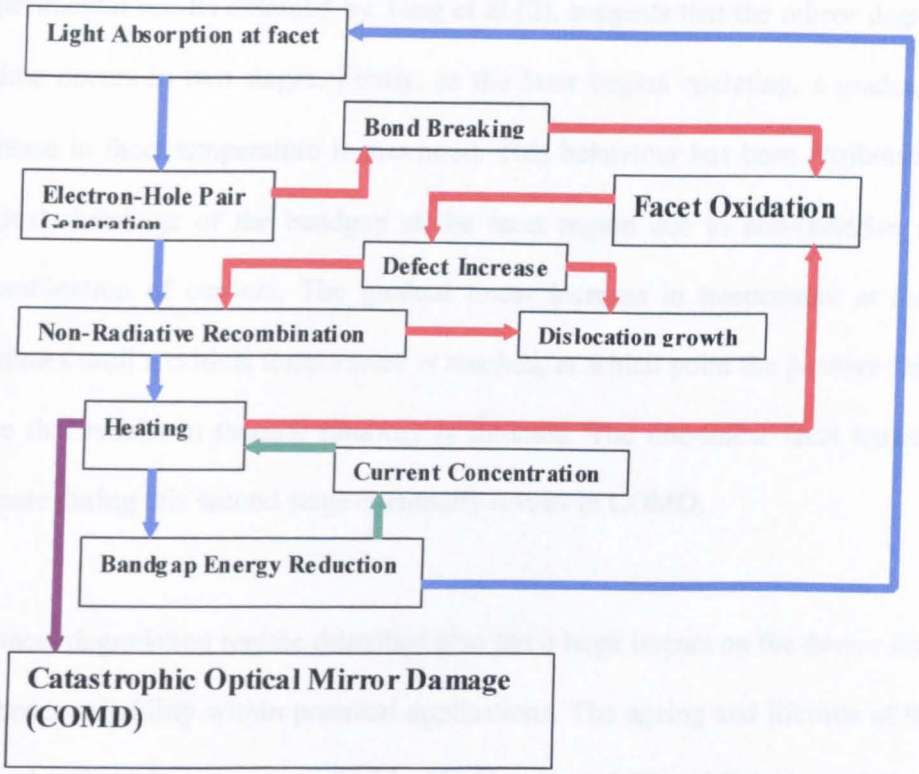

Fig 5.2: Diagram showing the positive feedback loop effect of facet degradation mechanisms. The positive feedback loops will lead to thermal runaway and ultimately COMD.

how the atmosphere in which the laser is operating plays an important role in the mirror degradation process. It was found that lasers operating in air tend to have faster mirror degradation than the same lasers operating in a helium or nitrogen atmosphere. This behaviour was attributed to facet oxidation occurring when operated in air, hence promoting facet heating. Tu et al (4) increased the COMD level of similar AlGaAs lasers by cleaving the devices and depositing facet coatings under vacuum conditions. This process suppressed facet oxidation and showed that reducing facet oxidation can reduce the amount of mirror degradation in a device during lasing, and therefore can increase the COMD level for the laser.

Experimental results obtained by Tang et al (2), suggests that the mirror degradation regime occurs in two stages. Firstly, as the laser begins operating, a gradual linear increase in facet temperature is measured. This behaviour has been attributed to the gradual shrinkage of the bandgap at the facet region due to non-radiative surface recombination of carriers. The gradual linear increase in temperature at the facet continues until a critical temperature is reached, at which point the positive feedback cycle that results in thermal runaway is initiated. The non-linear facet temperature increase during this second stage eventually results in COMD.

The facet degradation regime described also has a large impact on the device lifetime, and hence reliability within practical applications. The ageing and lifetime of 980nm strained InGaAs lasers were studied by Hashimoto et al (5) and Fukuda et al (1). Both research groups used a stress-strength model to explain the lifetime characteristics of the devices under study. In this model (shown in fig 5.3), the critical power level (CPL) of the laser is the measure of the lasers strength. The CPL is the minimum power level required for a device to undergo instantaneous COMD at the first moment of operation (t = 0s). The output power level of the device is termed stress. For devices operating at power levels below the CPL, the device ageing process will be initiated, causing the CPL to gradually decrease. COMD will occur at the point where the CPL becomes lower than the output power level of the laser i.e. the stress in the device becomes greater than the strength. The rate of the decrease in CPL with respect to ageing time of the device depends on the power level of the device, with higher power devices suffering from the earlier onset of COMD due to the high stress level and rapidly degrading strength. For lower output laser devices, the stress level is

lower, and the strength degrades less rapidly, therefore increasing the lifetime of the device.

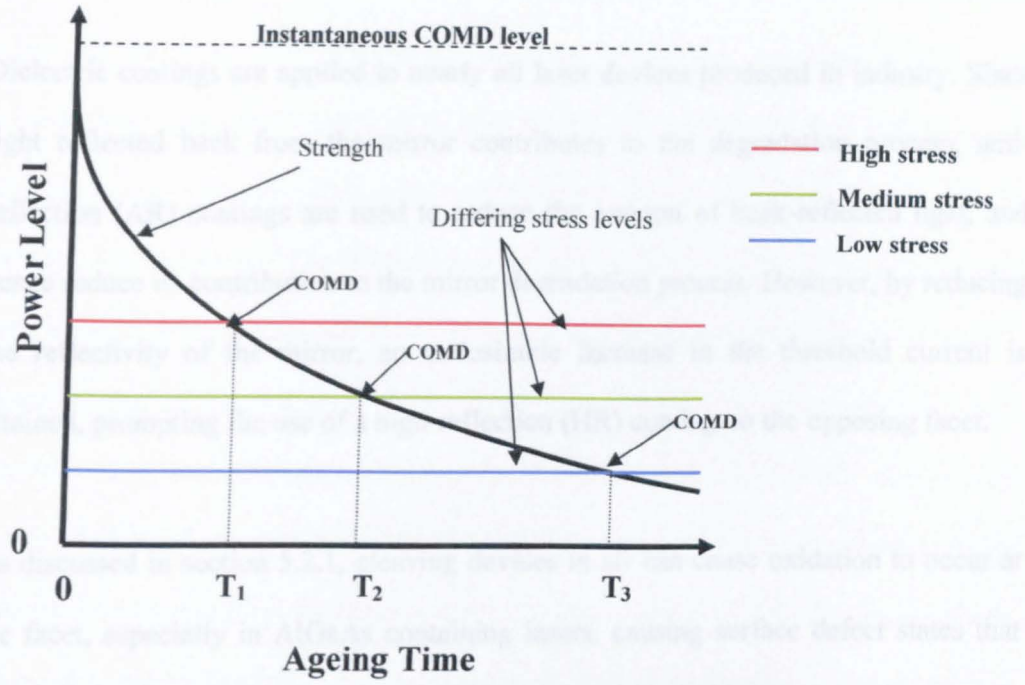

Figure 5.3: A stress-strength model for COMD occurrence in an edge-emitting laser. The stress levels indicate the output power under ageing, and the strength plot relates to the endurance level of the device against COMD.

5.3 COMD suppression techniques

Many methods have been devised to suppress COMD in laser devices. Most of these facet degradation methods involve either the reduction of non-radiative surface states at the facet, or the reduction of light absorption at the facet. The three most common methods employed are described in this section.

5.3.1. Defect Reduction Using Facet Passivation and Dielectric coatings

Dielectric coatings are applied to nearly all laser devices produced in industry. Since light reflected back from the mirror contributes to the degradation process, anti-reflection (AR) coatings are used to reduce the amount of back-reflected light, and hence reduce its contribution to the mirror degradation process. However, by reducing the reflectivity of the mirror, an undesirable increase in the threshold current is attained, prompting the use of a high-reflection (HR) coating on the opposing facet.

As discussed in section 5.2.1, cleaving devices in air can cause oxidation to occur at the facet, especially in AlGaAs containing lasers, causing surface defect states that can absorb light at the facet, causing localised heating. Although AR coatings can reduce mirror degradation by reducing back-reflected light, AR coatings usually contain oxygen (e.g. SiO_2 and Al_2O_3), which can oxidise the facet. Because of this, a thin (~30Å) passivation layer, typically Si or ZnSe, is deposited on the facet prior to AR/HR coating deposition. Although the thin passivation layer prevents the AR/HR coatings oxidising the facet, the initial surface states on the facet caused by oxidation following cleaving in air still exist, and can promote mirror degradation. This problem prompted IBM (Zurich), now part of Bookham Technology, to develop a process in which the cleaving and deposition of the thin passivation layer is performed under ultra-high vacuum (UHV). By cleaving devices under UHV, the possibility of surface oxidation occurring prior to facet passivation is reduced.

The cleaving and passivation under UHV process has shown to be a very capable technology for producing reliable high power laser devices. Tu et al (4) demonstrated the process on single mode AlGaAs/GaAs lasers operating at λ= 860nm. The devices were cleaved under UHV conditions. The facets were then passivated with Si, and subsequently deposited with SiO_2 and Al_2O_3 to form HR and AR coatings respectively. It is worthwhile to note that the whole process was performed in a multi-chamber UHV system. The devices treated under UHV conditions were compared with standard devices that had been cleaved in air and coated with the same AR/HR coatings. The standard devices failed from COMD at an output power of around 220mW, while the devices processed under UHV did not suffer COMD for an output power of $\leq$270mW (which was the highest power achievable with the current supply used in the experiments (0-500mA range)). This clearly shows the improvement achieved by using the UHV process to suppress facet oxidation, and prevent surface contamination, which both promote facet degradation.

Although the cleaving and passivation under UHV process has been shown to be very capable technology for producing reliable high power laser devices, the process is quite complex and expensive, and thus reduces productivity. A promising alternative to the UHV process has recently been researched and perfected by Comlase, with patents pending (Silfvenius et al (6)). In this process, native-nitride ion beam epitaxy (N^2-IBE) is used to remove oxides and other contaminants from the facet surface, as well as to generally smooth the facet surface. By using the correct parameters for the N^2-IBE process (i.e. ion beam energy, ion beam density, exposure time and composition of the background gas mixture) the nitrogen ions can also bond with the exposed group III atoms at the facet surface, and eliminate dangling bonds by creating

chemically stable nitrides. If the facets of the treated devices are thereafter exposed to air or moisture, or coated with AR/HR coatings containing oxygen, there are no group III atoms or dangling bonds to combine with, thus facet oxidation cannot take place. Since the N^2-IBE process does not require a capital-intensive UHV cleaving system, costs for eliminating facet oxidation are reduced. Furthermore, optical coatings can be produced in the same load-locked vacuum chamber as used for the N^2-IBE process, thus reducing process complexity, device handling and production time. Single mode InGaAlAs lasers operating at λ= 806nm tested under pulsed conditions displayed an increase in the COMD threshold by around 46% following the N^2-IBE process. Lifetime tests performed on the lasers operating at a constant power density of 15mW/μm showed an average degradation rate of 0.1%/1000h for the lasers treated by N^2-IBE, compared to an average 46%/1000h for standard devices. These results clearly show the benefits of employing the N^2-IBE process, which may become a main rival to the UHV cleaving/passivation process, and NAM technologies.

5.3.2. Non-Absorbing Mirrors (NAM's)

From inspection of figure 5.2, it can be seen that light absorption and current concentration at the facet increases facet heating and mirror degradation. By employing non-absorbing mirrors (NAM's) at the facet regions, the mirror degradation caused by both light absorption and current concentration can be suppressed (7). NAM's are formed by widening the bandgap of the material at the facet region using QWI. The widened bandgap at the facet prevents incident photons from being absorbed and causing further heating, hence reducing mirror degradation.

The problem of current concentration at the facet is easily suppressed by simply not allowing current injection in the NAM region. This is commonly achieved by using a contact pattern and subsequent lift-off stage during fabrication to define active and non-active regions. The concept of NAM's is illustrated in figure 5.4. A simple bandgap diagram of a standard laser is shown in figure 5.4.a. Since the whole of the standard laser cavity is injected with current, there is a high carrier density in the facet region, thus causing a large amount of non-radiative recombination via surface states on the laser facet, which in turn causes a large amount of facet heating and degradation. Figure 5.4.b shows a simple bandgap diagram of a laser incorporating NAM's. Since the facet region of the laser with NAM's are not injected with current, non-radiative recombination via surface states on the laser facet is dramatically reduced, causing less facet heating and degradation. Futhermore, the increased bandgap in the NAM region makes the region transparent to light emitted from the lasers active region, thus reducing the light absorption which also contributes to heating at the laser facet.

NAM's have previously been incorporated into single-mode 980nm InGaAs/GaAs laser material using the sputtered SiO_2 intermixing process by Walker et al (7). In this work, NAM's were shown to sufficiently suppress the onset of COMD when compared to standard lasers.

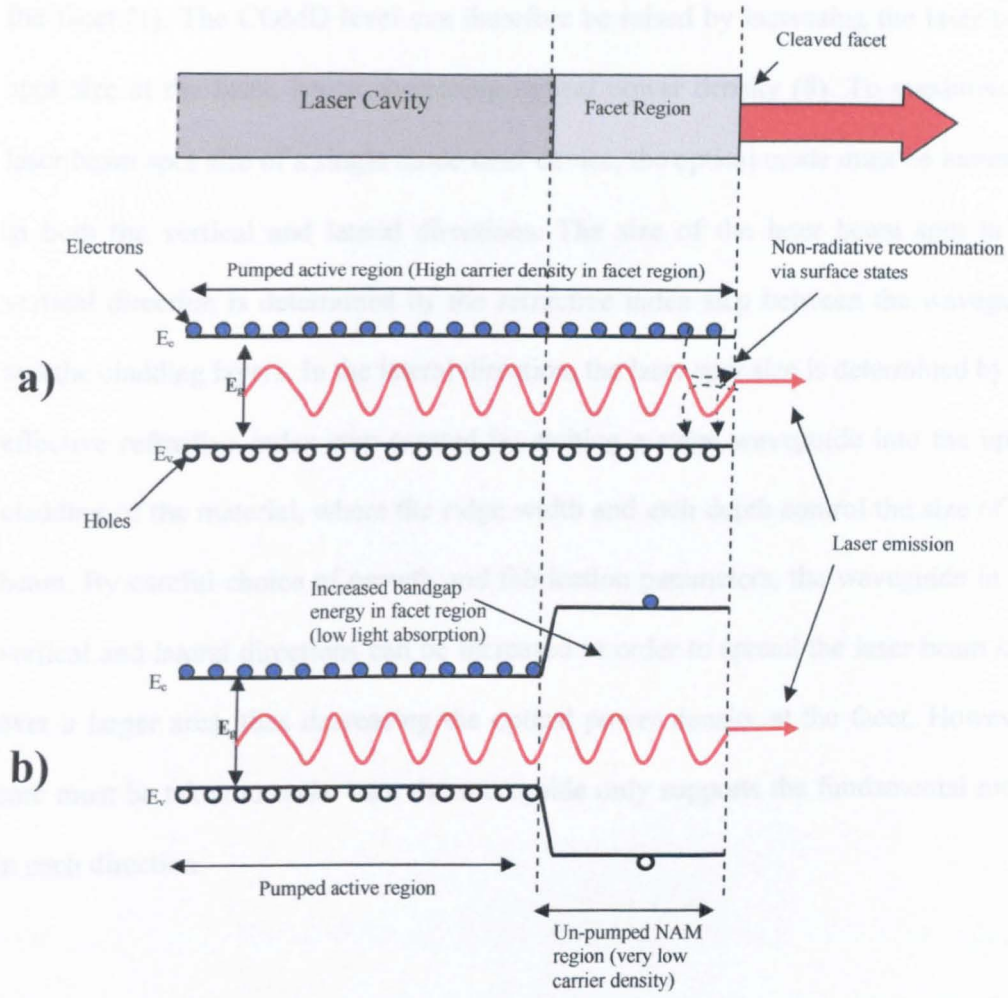

Figure 5.4: Simple diagram illustrating the concept of non-absorbing mirrors (NAM's). ***a)*** *Simple band diagram of a standard laser device* ***b)*** *band diagram of a laser device with a NAM incorporated to the facet region.*

5.3.3 Large Optical Cavities (LOC's)

COMD is also determined by the optical power density at the facet. Since COMD is known to be generated by the loop reaction between light absorption and active layer heating at the facets where the optical power density and the density of defects states at the facet are high, a higher optical power density will cause a higher amount of localised heating, due to increased non-radiative recombination over a fixed area of

the facet (1). The COMD level can therefore be raised by increasing the laser beam spot size at the facet, hence decreasing optical power density (8). To maximise the laser beam spot size of a single mode laser device, the optical mode must be increased in both the vertical and lateral directions. The size of the laser beam spot in the vertical direction is determined by the refractive index step between the waveguide and the cladding layers. In the lateral direction, the laser spot size is determined by the effective refractive index step created by etching a ridge waveguide into the upper cladding of the material, where the ridge width and etch depth control the size of the beam. By careful choice of growth and fabrication parameters, the waveguide in the vertical and lateral directions can be increased in order to spread the laser beam spot over a larger area, thus decreasing the optical power density at the facet. However, care must be taken to make sure the waveguide only supports the fundamental mode in each direction.

5.4 Extended Cavity lasers

Extended cavity lasers work on the same principle as non-absorbing mirrors (NAM's), where the bandgap of the material is widened at the facet region using quantum well intermixing. However, extended cavities are generally longer (>500μm) than NAM regions. Like NAM's, extended cavities also suppress COMD, but have the further advantage of being able to filter out the unwanted higher order optical modes that can occur at high drive currents. This is an attractive feature for use in high power lasers where LOC's have been employed to enhance the power performance (see section 5.3.3). By widening the optical cavity in the vertical and

lateral directions for a single mode laser, the optical cavity parameters become closer to those which can support higher order optical modes. Therefore, any increase in the refractive index in the core of the waveguide beneath the ridge structure, caused by a high drive current, could easily swing the optical cavity parameters from a single-mode regime to an undesirable multi-mode regime. However, since the extended cavity is not injected with current during laser operation, the optical cavity parameters remain unchanged in this section, therefore making it physically impossible for higher order modes produced in the active section to propagate the length of the extended cavity section. Since the higher order optical modes are not guided by the extended cavity, they will be "filtered" out as they move through the extended cavity section, and will not be fed back into the active cavity. This process assists stable single-mode operation.

Broad oxide stripe InGaAlP/InGaP lasers with monolithically intermixed passive waveguides on either side of the active laser section have previously been shown to lead to significant improvements in the near and far-field patterns (9,10). The intermixing in the study was performed using the sputtered SiO_2 process. The improvement in the beam characteristics was supposedly due to suppression of filamentation by the diffraction of higher-order transverse modes within the slab waveguides.

5.5 Fabrication of extended cavity lasers

By applying the sputtered SiO_2 intermixing process described in chapter 3 to the ridge waveguide laser technology outlined in chapter 4, extended cavity lasers can be realised. To define intermixed passive regions on the GaInNAs sample, standard photolithography was used. However, since it is not clear where the intermixed sections are on the sample after performing the intermixing step, alignment markers were required to ensure proper alignment of the ridges and contacts during subsequent photolithography steps. The alignment markers were etched into the sample before the intermixing process using $SiCl_4$ RIE. The sample was then intermixed using the process described in chapter 3, section 3.3.2. Following the intermixing step, all the SiO_2 was removed from the sample surface. Ridge waveguides were then formed on the sample using the process outlined in chapter 4, section 4.5. However, before the p-contact layer was deposited, an additional photolithography step was used to form a contact pattern on the sample surface. The contact pattern enabled the "lift-off" of the p-contact in selected regions (i.e. the intermixed regions), and ensured that no current was injected into the facet regions of the devices.

The layout of the processed sample is shown in fig 5.5.a. In order to compare extended cavity lasers with standard ridge waveguide lasers, both sets of devices were fabricated simultaneously on the same chip. Furthermore, intermixed ridge waveguide lasers, also known as bandgap shifted lasers, were fabricated on the same chip in order to establish how successful the intermixing step was. A photograph of a fabricated extended cavity laser is featured in figure 5.5.b.

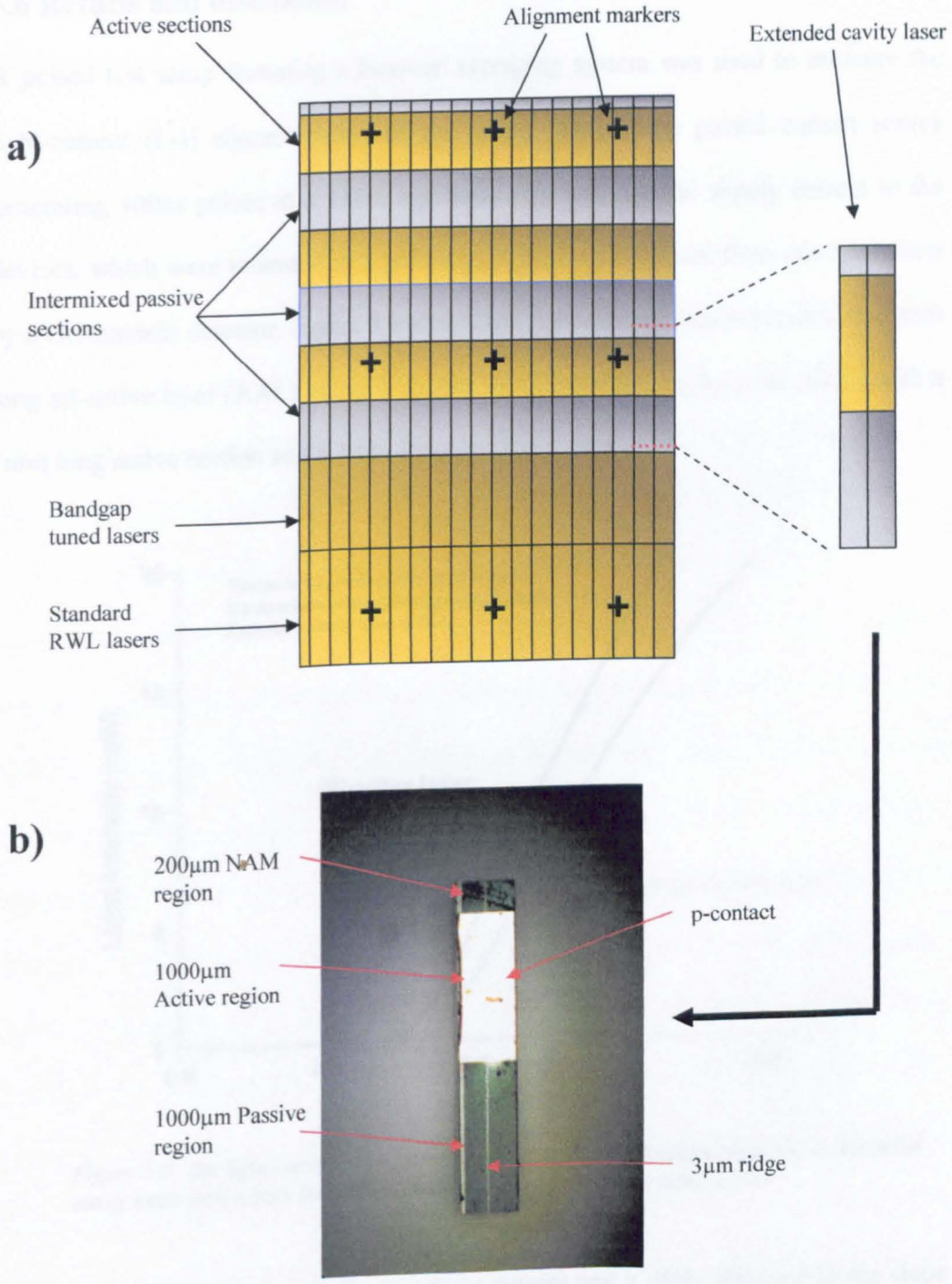

Figure 5.5.a) Schematic diagram of the device layout on the 12mm x 10mm GaInNAs laser chip. b) Photograph of a fabricated extended cavity GaInNAs laser.

5.6 Results and discussion

A pulsed test setup featuring a box-car averaging system was used to measure the light-current (L-I) characteristics of the lasers. An Avtech pulsed current source generating 400ns pulses at a 1kHz repetition rate was used to supply current to the devices, which were mounted in a gold clip. Light was collected from one laser facet by a Germanium detector. Figure 5.6 shows the light-current characteristics of a 1mm long all-active laser (AAL) along with that of an extended cavity laser (ECL) with a 1mm long active section and a 1mm long passive section.

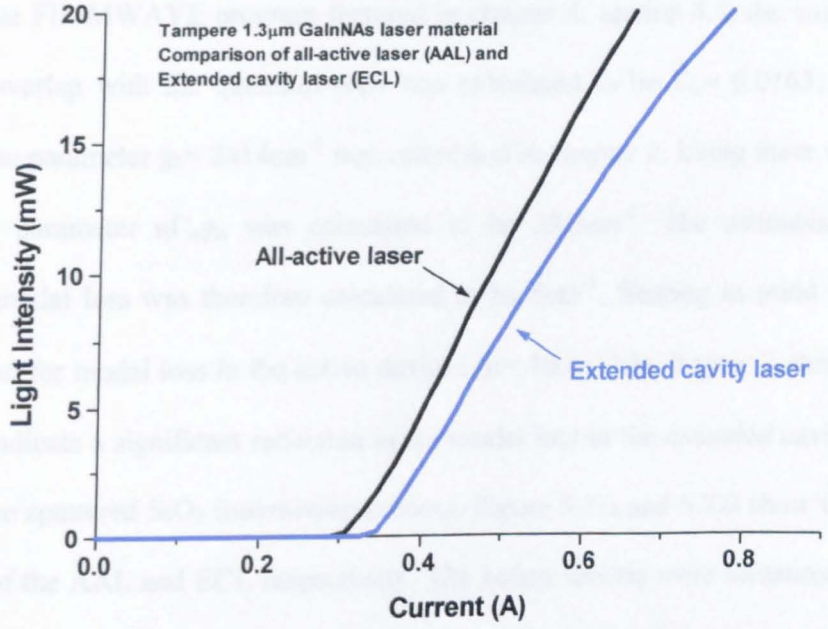

Figure 5.6: The light-current characteristics of a 1mm long all-active laser and an extended cavity laser with a 1mm long active section and a 1mm long passive section

There was a small increase in the threshold current and a slight decrease in the slope efficiency of the ECL compared to the AAL. From the change in the threshold current, it was possible to calculate the modal loss in the passive section using equation 5.1,

Equation 5.1 ..... $$\frac{I_{ECL}}{I_{AAL}} = \exp\left(\frac{\alpha_p L_p}{n\Gamma_w g_0 L_a}\right)$$

where α_p is the modal loss in the passive section, n is the number of quantum wells, Γ_w is the modal overlap with the quantum wells , and g_0 is the gain saturation parameter. L_p and L_a are the lengths of the passive and active cavity respectively. The threshold current of the AAL and ECL are represented by I_{AAL} and I_{ECL} respectively. The equation 5.1 assumes a zero reflection at the active/passive boundary, and that the logarithmic gain/current density relationship for quantum wells is effective (9,11). Using the FIMMWAVE program featured in chapter 4, section 4.4, the value for the modal overlap with the quantum well was calculated to be Γ_w= 0.0163. The gain saturation parameter g_0= 2414cm^{-1} was calculated in chapter 2. Using these values the material parameter $n\Gamma_w g_o$ was calculated to be 39.3cm^{-1}. The estimated passive section modal loss was therefore calculated to be 5cm^{-1}. Bearing in mind the value calculated for modal loss in the active devices (α= 18cm^{-1}) in chapter 2, these results clearly indicate a significant reduction in the modal loss in the extended cavity region due to the sputtered SiO_2 intermixing process. Figure 5.7.a and 5.7.b show the lasing spectra of the AAL and ECL respectively. The lasing spectra were measured using a threshold current of approximately 1.3-1.6Ith. Evidently, there are no significant differences between the spectra of the AAL and the ECL. A comparison of the near-field and far-field characteristics of a standard and extended cavity laser was also performed, confirming no significant differences. These results demonstrate the ability to incorporate the sputtered SiO_2 intermixing technology to GaInNAs/GaAs quantum well laser devices without significantly degrading the device performance.

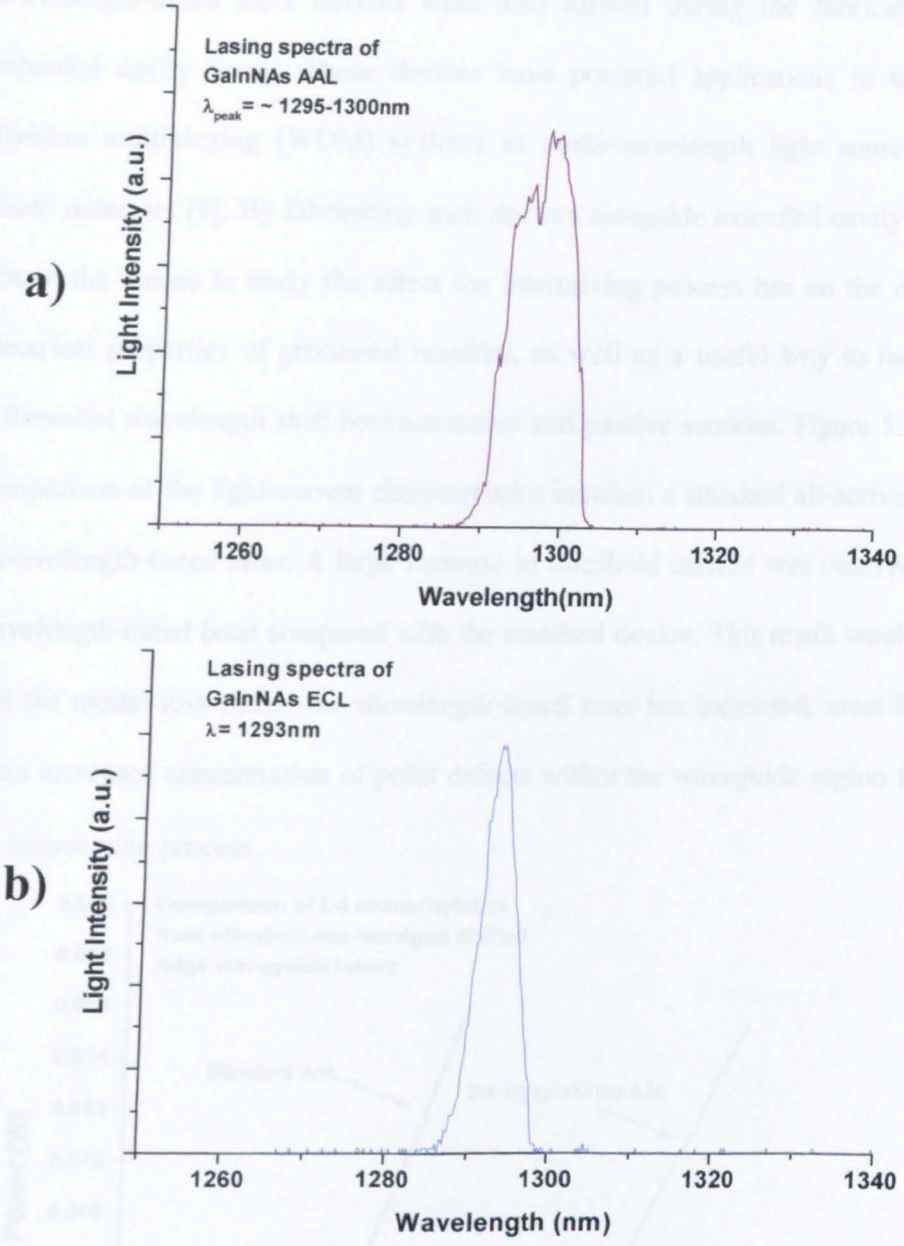

Figure 5.7: Lasing spectra of a) GaInNAs all-active ridge waveguide laser b) GaInNAs extended cavity ridge waveguide laser

5.6.1 Wavelength-tuned lasers

Wavelength-tuned laser devices were also formed during the fabrication of the extended cavity lasers. These devices have potential applications in wavelength-division multiplexing (WDM) systems as multi-wavelength light sources, and as photo detectors (9). By fabricating such devices alongside extended cavity lasers, we obtain the means to study the effect the intermixing process has on the optical and electrical properties of processed material, as well as a useful way to measure the differential wavelength shift between active and passive sections. Figure 5.8 shows a comparison of the light-current characteristics between a standard all-active laser and a wavelength-tuned laser. A large increase in threshold current was observed for the wavelength-tuned laser compared with the standard device. This result would suggest that the modal loss within the wavelength-tuned laser has increased, most likely due to an increased concentration of point defects within the waveguide region following the intermixing process.

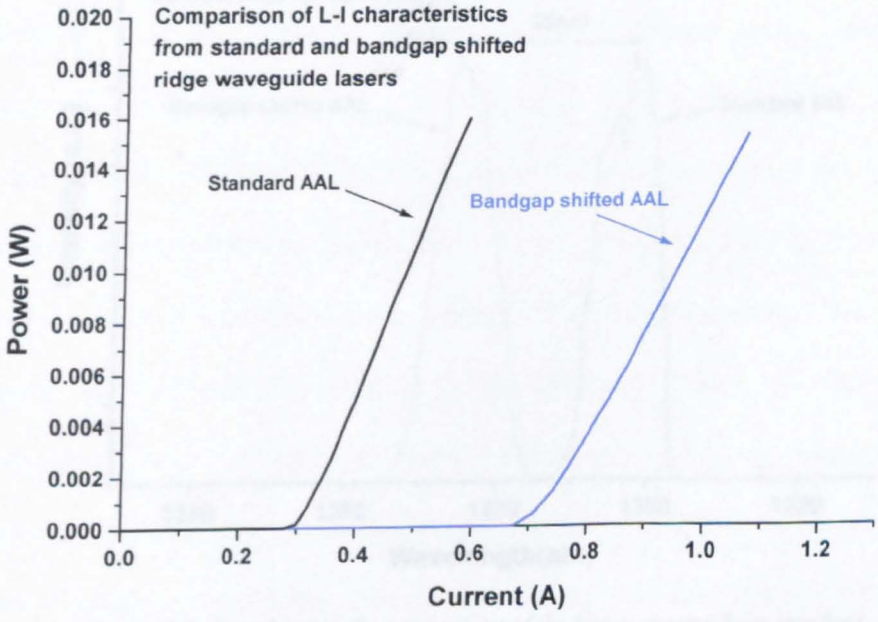

Figure 5.8: Plot showing a comparison of the light-current characteristics from standard and bandgap shifted GaInNAs ridge waveguide lasers

The small decrease in the slope efficiency of the wavelength tuned laser can be attributed to a decrease in the internal quantum efficiency, caused by the change in the shape and barrier height of the quantum well following the intermixing step. A decrease in the internal quantum efficiency would also have the effect of increasing the threshold current of the device.

Figure 5.9 shows a comparison of the lasing spectra between the standard and wavelength-tuned lasers. A 25nm blue-shift was observed for the wavelength-tuned laser. This result shows that the differential shift obtained during fabrication was not as successful as the differential shift previously obtained during intermixing experiments (see chapter 3, section 3.4.1), indicating that there may be inconsistencies with the intermixing process at Glasgow University, such as unwanted variation in the

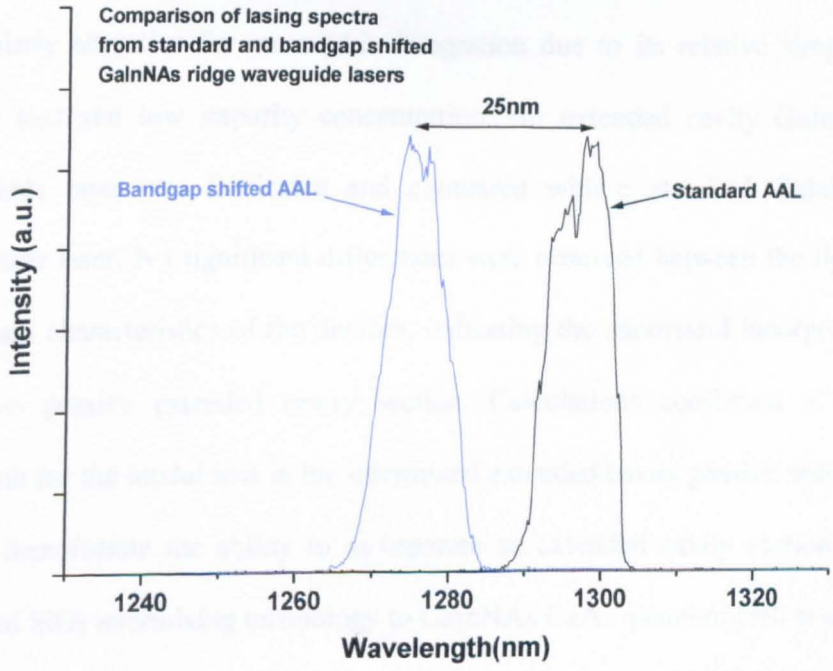

Figure 5.9: Plot showing the comparison of the lasing spectra from standard and bandgap shifted GaInNAs ridge waveguide lasers

anneal temperature or sputtered SiO_2 film composition. However, even with this smaller degree of intermixing, extended cavity lasers were still realised, showing that a 25nm differential wavelength shift between active and passive sections is sufficient to fabricate such devices. With further improvements to the intermixing process, larger differential wavelength shifts will be obtainable, and will reduce the loss in the intermixed passive sections even further. The undesirable deterioration of the optical and electrical properties of the material after intermixing may also be minimised with future development. Even so, the differential wavelength shifts required to realise light sources for WDM systems are considerably smaller than 25nm, and hence may not incur the same level of deterioration.

5.7 Conclusion

This chapter successfully demonstrated monolithically integrated GaInNAs devices using the sputtered SiO_2 intermixing technology. This intermixing technology is particularly attractive for monolithic integration due to its relative simplicity, low optical loss and low impurity concentration. An extended cavity GaInNAs ridge waveguide laser was fabricated and compared with a standard GaInNAs ridge waveguide laser. No significant differences were observed between the light-current and beam characteristics of the devices, indicating the successful incorporation of a low loss passive extended cavity section. Calculations confirmed a significant reduction for the modal loss in the intermixed extended cavity passive section. These results demonstrate the ability to incorporate an extended cavity section using the sputtered SiO_2 intermixing technology to GaInNAs/GaAs quantum well laser material without causing significant detrimental effects to the device performance. Wavelength-tuned GaInNAs lasers were also fabricated and compared against

standard lasers. These devices have potential applications in wavelength-division multiplexing (WDM) systems as multi-wavelength light sources, and as photo detectors. The differential wavelength shift obtained between the emission spectra of the devices demonstrated the potential of wavelength tuning GaInNAs material using the sputtered SiO_2 intermixing process.

5.8 References

1) M.Fukuda. M.Okayasu, J.Temmyo, J.Nakano "Degradation behaviour of 0.98μm strained quantum well InGaAs/AlGaAs lasers under high-power operation", IEEE Journal of Quantum Electronics, Vol 30, No.2, pp 471-476 February 1994.

2) W.C.Tang, H.J.Rosen, P.Vettinger, D.J.Webb "Evidence for current-density-induced heating of AlGaAs single-quantum-well laser facets" Applied Physics Letters, Vol 59, No.9, pp 1005-1007 August 1991.

3) R.Puchert, A.Barwolff, U.Menzel, A.Lau, T.Elsaesser "Facet and bulk heating of GaAs/AlGaAs high-power laser arrays studied in spatially resolved emission and micro-Raman experiments." Journal of Applied Physics, Vol 80, pp 5559-5563, November 1996

4) L.Tu, E.F.Schubert, M.Hong, G.J.Zydik " In-vacuum cleaving and coating of semiconductor laser facets using thin silicon and a dielectric", Journal of Applied Physics, vol 80, pp 6448-6451, November 1996.

5) J.Hashimoto, I.Yoshida, M.Murata, T.Katsuyama "Ageing time dependence of Catastrophic Optical Damage (COD) Failure of a 0.98μm GaInAs-GaInP

Strained Quantum-Well Laser" IEEE Journal of Quantum Electronics, Vol 33, No.1, pp 66-69, January 1997.

6) C.Silfvenius, P.Blixt, C.Lindstrom, A.Feitisch "Native-nitride passivation eliminates facet failure" Laser Focus World, November 2003.

7) C.L.Walker, A.C.Bryce, J.H.Marsh "Improved Catastrophic Optical Damage Level From Laser With Nonabsorbing Mirrors", IEEE Photonics Technology Letters, Vol 14, pp 1394-1396, October 2002.

8) D.Botez "Design considerations and analytical approximations for high continuous wave power, broad waveguide diode lasers", Applied Physics Letters, Vol 74, No 21, pp 3102-3104, May 1999.

9) S.D.McDougall, O.P.Kowalski, C.J.Hamilton, F.Camancho, B.Qiu, M.Ke, R.M.De La Rue, A.C.Bryce, J.H.Marsh, "Monolithic integration via a universal damage enhanced quantum well intermixing technique", IEEE Journal of selected topics on Quantum Electronics, Vol 4, No.4, pp 636-646, July/August 1998.

10) K.McIllvaney, J.Carson, A.C.Bryce, J.H.Marsh, R.Nicklin "Far-field behaviour of broad area lasers incorporating bandgap widened extended slab waveguides" Electronics letters, Vol 31, No 7, pp 553-554, March 1995.

11) P.W.A.McIllroy, A.Kurobe, Y.Uematsu "Analysis and application of theoretical gain curves to the design of multiquantum well lasers", IEEE Journal of Quantum Electronics, Vol 21, pp 1958-1963, 1985.

Chapter 6

Conclusions and Future work

This thesis has detailed the realisation of single-mode extended cavity GaInNAs lasers through the monolithic integration of passive sections using quantum well intermixing. In order to realise such devices, several independent technologies had to be investigated and integrated. Chapter 2 highlighted the advantageous features of the GaInNAs material system, such as improved temperature performance and greater control of growth when compared with other material systems at the communication wavelengths. GaInNAs material obtained from Tampere was characterised through the fabrication and testing of oxide stripe lasers. The results of the tests showed the material to be of sufficient quality to be able to prove the concept of the project. As well as requiring sufficiently good lasing characteristics from the GaInNAs material, it was required that the material also had controllable quantum well intermixing characteristics, in order to incorporate a low loss extended cavity passive section onto a GaInNAs laser device. Chapter 3 presented a brief history of quantum well intermixing, highlighting its ability to monolithically integrate optoelectronic devices on the same chip, and detailing the techniques used to achieve intermixing, with particular attention being paid to the sputtered SiO_2 intermixing process used in this project. Intermixing experiments were performed to confirm the possibility of using the sputtered SiO_2 intermixing process on GaInNAs laser material. Suitably large differential wavelength shifts were obtained from 1.3μm and 1.55μm GaInNAs

material, which added strength to the possibility of using the sputtered SiO_2 intermixing process to create extended cavity devices from GaInNAs material. The design considerations and fabrication of single mode lasers were discussed in Chapter 4. Computer simulations of the laser design were performed to establish appropriate device parameters for single mode operation. Single mode lasers were then fabricated from GaInNAs material and the light-current characteristics of the devices were measured, showing good laser operation. Near and far-field measurements confirmed single-mode operation in both the vertical and lateral directions. These results were shown to be in good agreement with the simulations performed. Chapter 5 discussed the limiting factors involved in the high power operation of edge emitting lasers, and highlighted the most successful techniques used to overcome such limitations. Non-absorbing mirrors (NAM's) and extended cavities were proposed as effective technologies for overcoming high power device limitations. By combining the single mode laser technology described in chapter 4 with the intermixing technology in chapter 3, single mode extended cavity GaInNAs lasers were realised. An extended cavity GaInNAs ridge waveguide laser was fabricated and compared with a standard GaInNAs ridge waveguide laser. There were no significant differences observed between the light-current and beam characteristics of the devices, which indicated the successful incorporation of a low loss passive extended cavity section. Calculations confirmed a significant reduction for the modal loss in the intermixed extended cavity passive section. These results demonstrate the ability to incorporate an extended cavity section using the sputtered SiO_2 intermixing technology to GaInNAs/GaAs quantum well laser material without causing considerable harmful effects to the device performance. Wavelength-tuned GaInNAs lasers were also fabricated and compared against standard lasers. These devices could potentially be employed in

wavelength-division multiplexing (WDM) systems as multi-wavelength light sources. The differential wavelength shift obtained between the emission spectra of the devices displayed the potential of wavelength tuning GaInNAs material using the sputtered SiO_2 intermixing process.

This research has created several openings for future work. Although the incorporation of extended cavities to laser facet regions has previously been shown to suppress catastrophic optical mirror damage (COMD) in single-mode laser devices, and to improve the beam quality of broad area lasers, it would be useful to prove both of these benefits in single-mode extended cavity GaInNAs lasers. By testing the extended cavity lasers using high drive currents, the high power capabilities of the extended cavity lasers would be established. Operating the lasers at high drive currents should activate COMD, causing the devices to fail. If the devices were fabricated in a bar, the extended cavities could then be easily cleaved off, leaving standard ridge waveguide lasers (RWL's) with newly formed mirrors. These devices could be tested under high drive currents to investigate the power level at which COMD is activated, and compared with the power level required to activate COMD in the extended cavity devices, thus determining whether adding extended cavities to GaInNAs lasers helps suppress COMD. In a similar way, the proposed improvement in the beam quality by using extended cavities can be investigated. Extended cavity laser devices which function just inside the boundary between single mode and multimode operation can be designed and fabricated. By doing so, the devices may switch from single-mode operation to multi-mode at a moderately high drive current due to changes in the refractive index in the waveguide region. By studying the near and far-field images of the output beams produced at different power levels, then

cleaving off the extended cavities, a comparison of the beam characteristics can be performed between standard and extended cavity devices.

Another future route for research could involve the addition of high quality LR/HR facet coatings to GaInNAs lasers to further suppress COMD, as well as to improve device efficiency. Moreover, careful material design and fabrication of an extended cavity which is tapered at the device facet could be utilised to increase the area of the optical mode at the facet, thus also increasing the output power level at which COMD activates.

The demonstration of quantum well intermixing using GaInNAs material in this project opens up the possibility of fabricating more advanced monolithically integrated devices on the same laser chip. Furthermore, GaInNAs can be used to fabricate other important devices that require selective quantum well intermixing, such as buried heterostructure devices and multi-mode interference (MMI) coupler laser arrays.

The GaInNAs material has still a long way to go before it reaches the maturity of the InGaAsP and InGaAlAs material systems. There may still be significant improvements made to the growth of the material that would lead to improvement at a device level. Until then, it would be unfair to compare the performance of GaInNAs devices with those fabricated from different material systems, and leaves open the debate of whether GaInNAs will ever reach the level required to become the material system of choice for communication systems applications. At the same time, GaInNAs material will have to compete against other promising material

technologies, such as quantum dot material. As discussed in chapter 2, VCSEL technology is where the GaInNAs material system will have a huge advantage over the InP based material systems. InP based VCSEL's cannot form highly reflective distributed Bragg reflector (DBR) mirrors without employing many repetitions of thick material layers. Moreover, the thermal issues limiting the InGaAsP/InP active region, coupled with the low thermal and electrical conductivity of the DBR's, make it almost impossible to realize a long wavelength VCSEL that combines highly reflective mirrors with low thermal and electrical resistance. GaInNAs VCSEL's can easily incorporate the well-established DBR technology used by GaAs-based 850nm VCSEL's.